SOAH DOCKET NO. 582-22-0844
TCEQ DOCKET NO: 2021-1000-MSW

IN THE MATTER OF THE APPLICATION BY DIAMOND BACK RECYCLING AND SANITARY LANDFILL, LP FOR NEW MSW PERMIT NO. 2404	**§**	**BEFORE THE STATE OFFICE OF ADMINISTRATIVE HEARINGS**

EXHIBIT KNOX-103

37

Geosynthetics

Jorge G. Zornberg
University of Texas at Austin

Barry R. Christopher
Independent Consultant

37.1 Introduction

Geosynthetics can be defined as planar products manufactured from polymeric material, which are used with soil, rock, or other geotechnical engineering-related material as an integral part of a man-made project, structure, or system (ASTM, 1995). Geosynthetics are widely used in many geotechnical, environmental, and hydraulic applications related to groundwater quality and control. One of the most common examples is the use of geotextile filters in trench (i.e., French) drains. Base and cover liner systems for modern landfills also make extensive use of geosynthetics with the main purpose of minimizing the potential for groundwater contamination. Furthermore, the use of geosynthetics is rapidly increasing in applications related directly to groundwater control. This is the case of high density polyethylene (HDPE) vertical barrier systems, which can be used instead of traditional soil-bentonite cutoff walls in projects involving groundwater remediation and control.

The geosynthetics market is strong and rapidly increasing due to the continued use of geosynthetics in well-established applications and, particularly, due to the increasing number of new applications that make use of these products. The strength of the geosynthetics market can be appreciated by evaluating the growth in the estimated amount of geosynthetics in North America over the years. Table 37.1 shows the estimated North American shipments of geosynthetics for 2001. While the total amount of geosynthetics

TABLE 37.1 North American Shipments of Geosynthetics Material 1995–2001 (in million m^2)

	1995	1996	1998	2001
Geotextiles	346.2	356.2	419.7	477.4
Geomembranes	62.4	64.4	74.6	86.8
Geogrids	22.4	24.3	29.1	36.8
Geosynthetic clay liners	5.0	5.4	6.1	8.2
Erosion-control products	72.7	77.8	82.8	93.6
Specialty geosynthetics	16.7	20.1	25.9	31.8

Source: Industrial Fabrics Association International (1996).

produced in North America was slightly over 83 million m^2 in 1980, the production of geosynthetics was approximately 1 billion m^2 in 2005.

Geosynthetics applications are very diverse. To fulfill different functions in the design of geotechnical-, environmental-, and hydraulic-related systems, the geosynthetic industry has developed a number of products to meet engineers' needs. In addition to the use of geotextiles as filters in trench drains, geomembranes in landfill liner systems, and HDPE vertical panels in groundwater control projects, other examples of geosynthetics applications include the use of geotextiles as filtration elements in dams and waste containment systems, the use of geocomposites as erosion control elements in channels and slopes, and the use of geogrids as reinforcement elements in soil embankments, to mention just a few.

Numerous tests have been developed to characterize the hydraulic and mechanical properties of geosynthetics. Many of these properties are important in the manufacture and quality control of geosynthetics; however, many others are also important in design. The material properties that are primarily related to the manufacture and quality control of geosynthetics are generally referred to as index properties and those related to the design are referred to as performance properties. When properly correlated to performance properties, some index properties may also be used for design. As the various geosynthetic products can perform different functions, they should be designed to satisfy minimum criteria to adequately perform these functions in a given design. The different functions performed by geosynthetics are discussed in Section 37.2. The functions that geosynthetics may provide are as follows: separation, reinforcement, filtration, drainage, barrier, and/or protection (or stress relief).

Geosynthetics are manufactured in sheet form in a factory-controlled environment. They are most often packaged in rolls for transporting to the site. They may also be folded or cut and stacked and placed in cartons. At the project site the geosynthetic sheets are unrolled on the prepared subgrade surface, overlapped to form a continuous geosynthetic blanket, and often physically joined to each other, for example, by welding (geomembranes) or sewing (geotextiles). The different types of geosynthetics are discussed in Section 37.3. They include geotextiles, geomembranes, geogrids, geosynthetic clay liners (GCLs), geocomposite sheet drains, geocomposite strip (wick) drains, geocells, erosion control products and HDPE vertical barrier systems.

Different types of geocomposite drains and HDPE vertical barriers, a special form of geomembranes, are considered separately in the list above. These geosynthetics are described separately in this chapter because of their particular relevance in groundwater-related applications.

Geotechnical, environmental, and hydraulic systems frequently incorporate several types of geosynthetics, which are designed to perform more than one function in the system. The bottom and cover liner systems of waste containment facilities are good examples of applications that make use of geosynthetics for multiple purposes. In these facilities, the different geosynthetic products are combined to create the liner system, the components fulfill the functions of infiltration barrier, filtration, separation, drainage, protection, and reinforcement. The multiple uses of geosynthetics in the design of modern landfills are described in Section 37.4. Finally, a case history illustrating the use of HDPE panels as vertical barrier in a groundwater control project is presented in Section 37.5. A glossary of relevant terms and a list of sources are also included for further information.

37.2 Geosynthetic Functions

37.2.1 Design by Function of Geosynthetics

As with other engineering materials, there are several design approaches that could be used during the selection process of geosynthetic products. The most common methods are design by experience, by specification, or by function (Koerner, 2005).

Design-by-experience is generally based on the use of manufacturer's literature and of the designer's experience and familiarity with specific geosynthetic products. An extension of design by experience is design-by-specification, which consists of selecting geosynthetic products for common application areas based on basic minimum or maximum specified property values. These methods may be acceptable for routine, repeat, non-critical applications.

Design-by-function is the preferred approach. Design-by-function should be performed as a check for applications covered by specifications and required for applications not covered by specifications or of such a nature that large property or personal damage would result in the event of a failure. A generic design process that applies to the different geosynthetic functions is summarized as follows (Koerner, 2005):

1. Evaluate the critical and severe nature of the application
2. Determine the function(s) of the geosynthetic
3. Calculate, estimate, or otherwise determine the required property value for the function(s)
4. Test or otherwise obtain the allowable property of the candidate geosynthetic material(s)
5. Calculate the factor of safety (*FS*) as follows:

$$FS = \frac{\text{allowable (test) value}}{\text{required (design) value}} \tag{37.1}$$

6. Determine if the resulting factor of safety is adequate for the site-specific situation under consideration
7. Prepare specifications and construction documents
8. Observe construction and post-construction performance

If the factor of safety is sufficiently high for the specific application, the candidate geosynthetic(s) is (are) deemed acceptable. The same process can be repeated for a number of available geosynthetics, and the final selection among acceptable products is based on availability and cost.

The design-by-function approach is the general approach to be followed in the majority of the projects. As mentioned, the primary function(s) of geosynthetics can be separation, reinforcement, filtration, drainage, infiltration barrier, or protection. However, a certain geosynthetic product can perform different functions and, similarly, the same function can often be performed by different types of geosynthetics. Geosynthetic applications are usually defined by the primary or principal function. In addition, geosynthetics can perform one or more secondary functions, which must also be considered when selecting the geosynthetic characteristics for optimum performance. For example, a geotextile can provide separation of two dissimilar soils (e.g., gravel from clay in a road), but the geosynthetic may also be required to provide the secondary function of filtration to minimize the build up of excess pore water pressure in the soil beneath the separator. The specific function(s) of the different geosynthetic(s) are presented in Table 37.2. Each of these functions is described in Section 37.2.2 to Section 37.2.7.

37.2.2 Separation Function

Separation is the introduction of a flexible, porous geosynthetic product between dissimilar materials so that the integrity and functioning of both materials can remain intact or be improved. For example, a major cause of failure of roadways constructed over soft foundations is contamination of the aggregate base course with the underlying soft subgrade soils (Figure 37.1a). Contamination occurs both due to: (1) penetration of the aggregate into the weak subgrade due to localized bearing capacity failure under

TABLE 37.2 Function of Different Geosynthetic Products

	Geotextile	Geo-membrane	Geogrid	GCL	Geocomposite sheet drain	Geocomposite strip (wick) drain	Geocell	Erosion control product	HDPE vertical barrier
Separation	X	X			X				
Reinforcement	X		X				X		
Filtration	X				X				
Drainage	X				X	X			
Barrier	X[a]	X		X					X
Protection	X			X	X		X	X	

[a]Asphalt-saturated geotextiles.

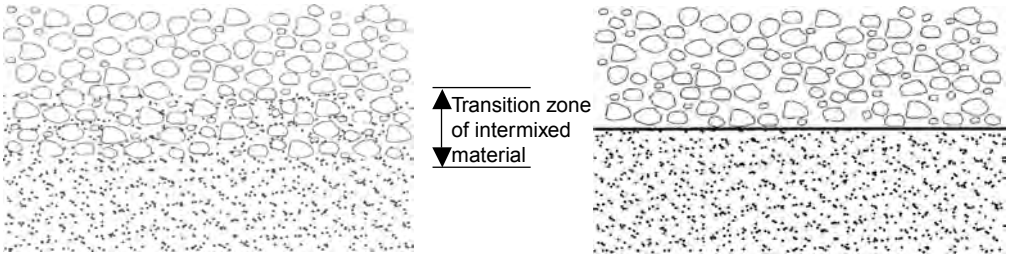

FIGURE 37.1 Separation function of a geotextile placed between road aggregate and soft saturated subgrade. (a) Without geotextile and (b) With geotextile.

stresses induced by wheel loads, and (2) intrusion of fine-grained soils into the aggregate because of pumping or subgrade weakening due to excess pore water pressure. Subgrade contamination results in inadequate structural support that often leads to premature failure of the system. A geotextile can be placed between the aggregate and the subgrade to act as a separator and prevent the subgrade and aggregate base course from mixing (Figure 37.1b).

Among the different geosynthetics, geotextiles have been the products generally used in the function of separation. Examples of separation applications are the use of geotextiles between subgrade and stone base in roads and airfields, and between geomembranes and drainage layers in landfills. In addition to these applications, in which separation is the primary function of the geotextile, it could be said that most other geosynthetic applications generally include separation as a secondary function. The design of geosynthetics for separation applications is provided by Holtz et al. (1997, 1998) and Koerner (2005).

37.2.3 Reinforcement Function

Geosynthetic inclusions within a soil mass can provide a reinforcement function by developing tensile forces that contribute to the stability of the geosynthetic-soil composite (a reinforced soil structure). Design and construction of stable slopes and retaining structures within space constrains are major economical considerations in geotechnical engineering projects. For example, when geometry requirements dictate changes of elevation for a retaining wall, or dam project, the engineer faces a variety of distinct alternatives for designing the required earth structures. Traditional solutions have been either a near vertical concrete structure or a conventional, relatively flat, unreinforced slope (Figure 37.2). Although simple to design, concrete wall alternatives have generally led to elevated construction and material costs. On the other hand, the construction of unreinforced embankments with flat slope angles dictated by stability considerations is an alternative often precluded in projects where design is controlled by space constraints. As shown in

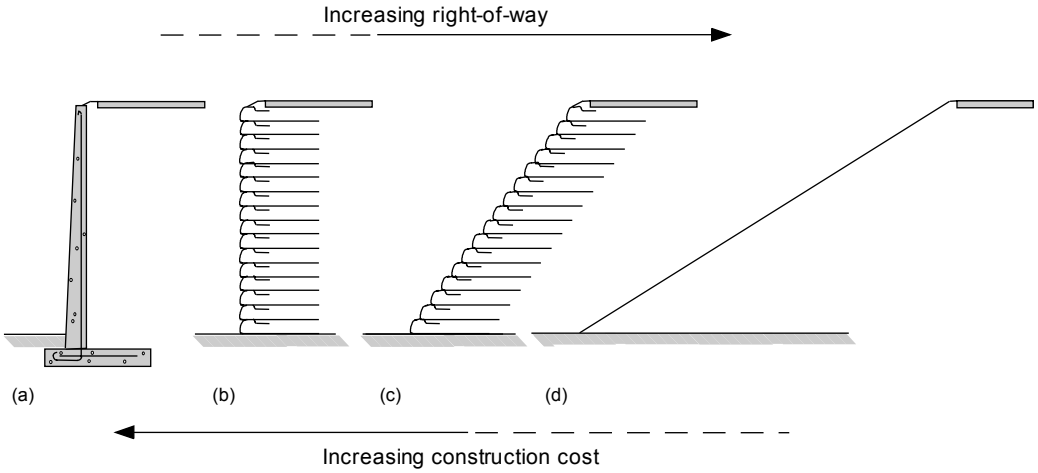

FIGURE 37.2 Reinforcement function of geosynthetics used to optimize the design of earth retaining structures: (a) concrete retaining wall; (b) reinforced wall; (c) reinforced slope; (d) unreinforced slope.

Figure 37.2, an alternative would be to place horizontal, geosynthetic reinforcing elements in the soil to allow construction of very steep embankment side slopes or a vertical reinforced soil wall. For example, vertical reinforced soil walls have been used to both construct dams for reservoirs and increase the height of existing dams.

Geosynthetic products typically used as reinforcement elements are geotextiles and geogrids. Additional products include geocells and fiber reinforcement. Reinforced soil walls generally provide vertical grade separations at a lower cost than traditional concrete walls. Reinforced wall systems involve the use of facing elements such as precast panels, cast-in-place concrete panels, or modular block systems. Alternatively, steepened reinforced slopes (with facing inclination below approximately 70°) may eliminate the use of facing elements, thus saving material costs and construction time in relation to vertical reinforced walls. As indicated in Figure 37.2, a reinforced soil system generally provides an optimized alternative for the design of earth retaining structures by combining lower cost and decreased right-of-way requirements.

The effect of geosynthetic reinforcements on the stability of slopes is illustrated in Figure 37.3, which shows a reduced scale geotextile-reinforced slope model built using dry sand as backfill material. The maximum slope inclination of unreinforced sand under its own weight is the angle of repose of the sand, which is well below the inclination of the slope face of the model in the figure. Horizontal geotextile reinforcements placed within the backfill provided stability to the steep sand slope. In fact, not only did the reinforced slope model not fail under its own weight, but its failure only occurred when the unit weight of the backfill was increased 67 times by placing the model in a geotechnical centrifuge (Zornberg et al., 1998). Figure 37.4 shows the reinforced slope model after centrifuge testing.

The use of inclusions to improve the mechanical properties of soils dates to ancient times. However, it is only within the last 35 years (Vidal, 1969) that analytical and experimental studies have led to the contemporary soil reinforcement techniques. Soil reinforcement is now a highly attractive alternative for embankment and retaining wall projects because of the economic benefits it offers in relation to conventional retaining structures. Its acceptance has also been triggered by a number of technical factors including aesthetics, reliability, simple construction techniques, good seismic performance, and the ability to tolerate large deformations without structural distress. The design of reinforced soil walls is based on earth pressure theory while the design of reinforced slopes is based on the use of limit equilibrium methods. The design process involves evaluation of the external (global), internal, and compound stability of the structure. The required tensile strength of the reinforcements is selected in design so that the margins of safety to prevent internal failure, such as that shown in Figure 37.4, are adequate. Guidance in soil reinforcement design procedures is provided by Elias et al. (2001), Holtz et al. (1997, 1998), and NCMA (1997).

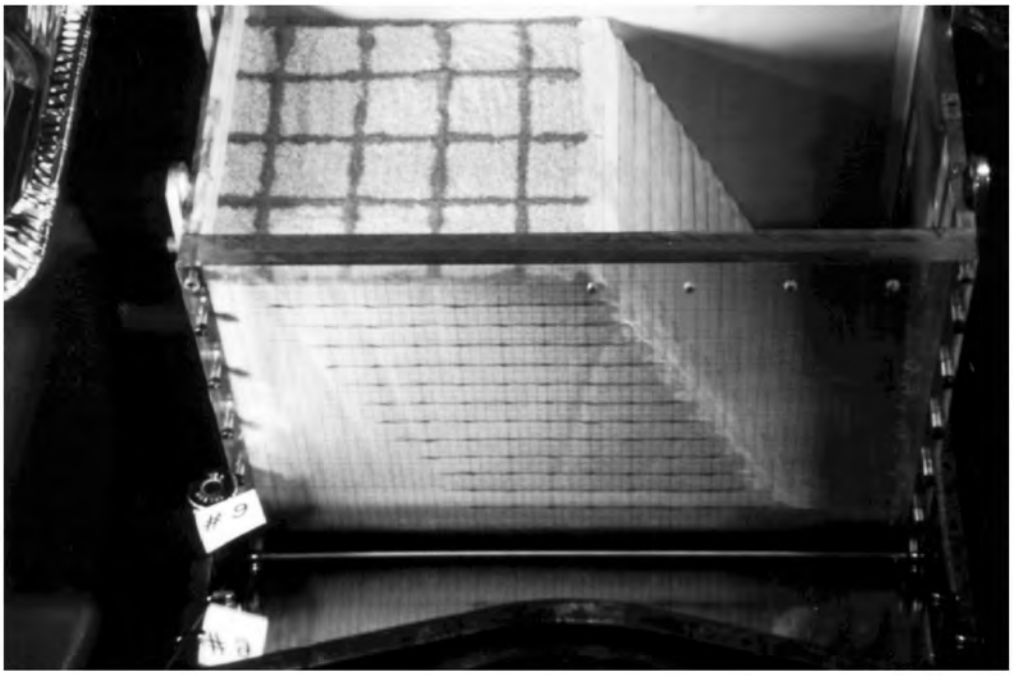

FIGURE 37.3 Model of a sand slope reinforced with geosynthetics.

FIGURE 37.4 Reinforced slope model brought to failure by increasing the unit weight of the backfill.

A special form of geosynthetic reinforcement is the mixing of fibers with the soil. Fiber reinforcement is used in applications such as stabilization of thin soil veneers, localized repair of failed slopes and increasing the seismic performance. Randomly distributed fibers can provide isotropic strength increases to the soil and avoid the existence of the potential planes of weakness that can develop on the soil-reinforcement interface. The design of fiber-reinforced soil slopes has typically been performed using composite approaches, where the fiber-reinforced soil is considered as a single homogenized material. Accordingly, fiber-reinforced soil design has required non-conventional laboratory testing of composite fiber-reinforced soil specimens, which has discouraged implementation of fiber-reinforcement in engineering practice. A new discrete approach was recently proposed (Zornberg, 2002), which predicts the "equivalent" shear strength of the fiber-reinforced soil based on the independent properties of fibers (e.g., fiber content, fiber aspect ratio) and soil (e.g., friction angle and cohesion).

37.2.4 Filtration Function

The filtration function involves movement of liquid through the geosynthetic and, at the same time, retention of soil on its upstream side. As indicated in Table 37.2, geotextiles are the product generally used for the function of filtration. Applications include geotextile filters for trench drains, blanket drains, interceptor drains, structural drains, toe drains in dams, filters for hard armor (e.g., rip-rap, gabions, fabric-form) erosion control systems, silt fences, and silt curtains. Both adequate hydraulic conductivity (provided by a geotextile with a relatively porous structure) and adequate soil retention (provided by a geotextile with a relatively tight structure) should be offered by the selected product. In addition, considerations should be made regarding the long-term soil-to-geotextile flow compatibility such that the flow through the geotextile will not be excessively reduced by clogging during the lifetime of the system. The geosynthetic-to-soil system should then achieve an equilibrium that allows for adequate liquid flow with limited soil loss across the geotextile throughout a service lifetime compatible with the application under consideration. Filtration concepts are well established in the design of soil filters, and similar concepts are used in the design of geotextile filters.

As the flow of liquid is perpendicular to the plane of the geosynthetic, filtration refers to the cross-plane hydraulic conductivity. Some of the geosynthetics used for this purpose are relatively thick and compressible. For this reason, geosynthetics are generally characterized by their permittivity, which is defined as:

$$\psi = k_n/t \tag{37.2}$$

where ψ is the permittivity, k_n is the cross-plane hydraulic conductivity, and t is the geosynthetic thickness at a specified normal pressure.

Testing procedures for geotextile permittivity follow similar guidelines used for testing the hydraulic conductivity of the soil. Some designers prefer to work directly with hydraulic conductivity and require the geotextile's hydraulic conductivity to be some multiple of the adjacent soil's hydraulic conductivity (Christopher and Fischer, 1992).

As the flow of liquid through the geotextile increases, the geotextile voids should be larger. However, large geotextile voids can lead to an unacceptable situation called soil piping, in which the soil particles are continuously carried through the geotextile, leaving large soil voids behind. The liquid velocity then increases, which accelerates the process and may lead to the collapse of the soil structure. This process can be prevented by selecting a geotextile with voids small enough to retain the soil on the upstream side of the fabric. It is the coarser soil fraction that must be initially retained. The coarser-sized particles eventually create a filter "bridge," which in turn retains the finer-sized particles, building up a stable upstream soil structure (Figure 37.5).

Several methods have been developed for soil retention design using geotextiles; most of them compare the soil particle size characteristics to the 95% opening size of the geotextile (defined as O_{95} of the geotextile). The test method used in the United States to determine the geotextile opening size is called the apparent opening size (AOS) test (ASTM D 4751).

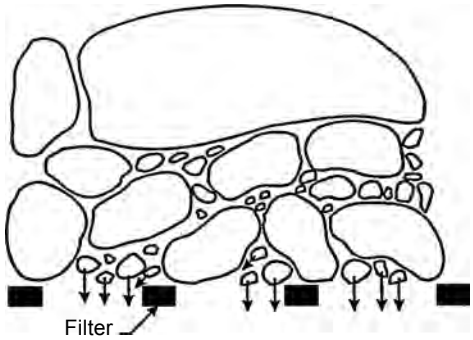

FIGURE 37.5 Geotextile providing adequate filtration through selection of adequate opening size and formation of soil filter bridge.

Some of the soil particles will rest on or embed them within the geotextile structure, and will cause a reduction in the hydraulic conductivity or permittivity of the geotextile. Although some partial clogging should be expected, the designer should ensure that the geotextile will not become excessively clogged, that is, that the flow of liquid will not be decreased to a point in which the system will not adequately perform its function. Thus, the geotextile voids should be large enough to allow the finer soil particles to pass. Clogging potential creates a special problem when geotextiles are used to wrap pipes due to the restricted area available for flow (i.e., a portion of the geotextile is covered by the pipe walls). Any clogging will significantly reduce the flow into the pipe. Either the flow capacity of the geotextile should be increased proportionally to the covered area (i.e., the total pipe area divided by geotextile area available for flow, which is usually the area of the holes in the pipe) or the geotextile should only be used to wrap gravel placed around the pipe. Design guidelines are available for clogging evaluation of non-critical, non-severe cases (Holtz et al., 1997, 1998; Koerner, 2005), but laboratory testing is strongly recommended in important applications. The gradient ratio test (ASTM D 5101), the long-term flow test (Halse et al., 1987), or the hydraulic conductivity ratio test (ASTM D 5567) should be performed. An evaluation of the filtration function of geotextiles is provided by Giroud (1996), Bhatia and Smith (1996a,b), Bhatia et al. (1996), Holtz et al. (1997, 1998), and Palmeira and Fannin (2002).

Proper construction is a critical factor in the performance of the filtration function. To develop and maintain the filter bridge, the geotextile must be placed in continuous (*intimate*) contact with the soil to be filtered such that no void spaces occur behind the geotextile. Placement granular material (e.g., gravel, drain rock, or rip rap) must also be consistent with the strength and durability of the geosynthetic to prevent damage during construction.

37.2.5 Drainage Function

Geosynthetics provide a drainage function by transmitting liquid within the plane of their structure. As shown in Table 37.2, the geosynthetics generally used for drainage purposes are geotextiles and geocomposites. The drainage function of geosynthetics allows for adequate liquid flow with limited soil loss within the plane of the geotextile over a service lifetime compatible with the application under consideration.

Thick, needle-punched nonwoven geotextiles have considerable void space in their structure and can convey liquid in their plane (on the order of 0.01 to 0.1 l/sec/m width of geotextile). Geocomposite drains can transmit one to two orders of magnitude more liquid than geotextiles. Proper design should dictate what type of geosynthetic drainage material is necessary.

The soil retention and the long-term compatibility considerations regarding the drainage function of geosynthetics are the same as those discussed in Section 37.2.4 regarding the filtration function of geosynthetics. As the geosynthetic thickness decreases with increasing normal stress, the in-plane drainage

of a geosynthetic is generally quantified by its transmissivity, which is defined as:

$$\theta = k_p \cdot t \tag{37.3}$$

where θ is the transmissivity, k_p is the in-plane hydraulic conductivity, and t is the geosynthetic thickness at a specified normal pressure. The in-plane flow capacity of geosynthetic will reduce under compression and with time (due to creep). Therefore, the transmissivity should be evaluated under normal pressures that are comparable to field conditions with a factor of safety included in the design to account for the design life of the project. Design guidance is provided by Holtz et al. (1997, 1998) and Koerner (2005).

Calculating the thickness of the liquid in or above a liquid collection layer is an important design step because one of the design criteria for a liquid collection layer is that the maximum thickness of the liquid collection layer must be less than an allowable thickness. The thickness of liquid in a liquid collection layer depends on the rate of liquid supply. A typical case of liquid supply is that of liquid impinging onto the liquid collection layer. Two examples of liquid collection layers with such a type of liquid supply can be found in landfills: (1) the drainage layer of the cover system, where the liquid that impinges onto the liquid collection layer is the precipitation water that has percolated through the soil layer overlying the drainage layer; and (2) the leachate collection layer, where the liquid that impinges onto the leachate collection layer is the leachate that has percolated through the waste and through the protective soil layer overlying the leachate collection layer. Equations are available (Giroud et al., 2000) to calculate the maximum thickness of liquid in a liquid collection layer located on a single slope with a perfect drain at the toe.

37.2.6 Barrier Function

The barrier function can be performed by geosynthetic products that have adequately low hydraulic conductivity as to provide containment to liquid or vapor. As shown in Table 37.2, the barrier function may be provided by several types of geosynthetics, namely, geomembranes and geosynthetic clay liners (GCLs). Other geosynthetic products also used as infiltration barriers include membrane-encapsulated soil layers (MESLs) used with paved or unpaved road construction, asphalt-saturated geotextiles used in the prevention of bituminous pavement crack reflection problems, and geofoam used for insulation against moisture and extreme temperatures.

Geosynthetic barriers are commonly used as liner for surface impoundments storing hazardous and nonhazardous liquids, as covers above the liquid surface of storage reservoirs, and as liner for canals used to convey water or chemicals. Geosynthetic barriers are also used as secondary containment for underground storage tanks, and in applications related to dams and tunnels. Of particular relevance for groundwater applications is the use of geosynthetic barriers for seepage control (HDPE vertical barrier systems). A common application of geosynthetics as infiltration barriers is base and cover liners for landfills. In landfill applications, infiltration barriers are typically used instead of (or in addition to) low-hydraulic conductivity soils. Base liners are placed below the waste to prevent liquids from the landfill (leachate) contaminating the underlying ground and the groundwater. Geosynthetic cover liner systems are placed above the final waste configuration to keep precipitation water from entering the waste and generating leachate. If a building or other structure is constructed on a landfill, a geosynthetic barrier may be placed under the building foundation to provide a barrier for vapors such as landfill gas. The use of geosynthetics in infiltration barriers is further described in Koerner (2005).

Dams are among the most critical hydraulic structures and stand to benefit the most from the use of geosynthetics. Deterioration and structural damage due to seepage are major concerns that have been addressed by placement of geomembrane liners. Geosynthetic systems as hydraulic barriers in dams are effective solutions to the problem of degradation. Accordingly, geosynthetics have been used in a wide range of dam types and dam sizes. The first installation of a geomembrane in a dam was in Italy in 1959. Since then, geosynthetics have been installed in dams worldwide as part of new projects and rehabilitation projects. Most recently, the Olivenhain Dam in San Diego was built with a geosynthetic system as an infiltration barrier. Significant advances have taken place in geosynthetics engineering since

geomembranes were first used in hydraulic structures. A good example is the current confidence on the extended service life of geomembranes. Additional information on the use of geosynthetics in dams is provided by and can be found in Christopher and Dahlstrand (1989), Zornberg and Weber (2003), Zornberg (2005), and Scuero et al. (2005).

37.2.7 Protection Function

Geosynthetics (mainly geotextiles) can be used to provide stress relief and protect other materials such as geosynthetics (mainly geomembranes) against damage. A common example is the use of geotextiles to provide protection against puncture of geomembranes in waste and liquid containment systems. Adequate mechanical protection must be provided to resist both short-term equipment loads and long-term loads imparted by the waste. Experience has shown that geotextiles can play an important role in the successful installation and long-term performance of geomembranes by acting as a cushion to prevent puncture damage of the geomembrane. In the case of landfill base liners, geotextiles can be placed (1) below the geomembrane to resist puncture and wear due to abrasion caused by sharp-edged rocks in the subgrade, and (2) above the geomembrane to resist puncture caused either by the drainage aggregate or direct contact with waste materials. In the case of landfill cover liners, geotextiles can be placed below the geomembrane to reduce risk of damage by sharp objects in the landfill and above the geomembrane to prevent damage during placement of drainage aggregate or cover soil. Key characteristics for the geotextile cushions are polymer type, mass density, method of manufacture, and construction survivability. The selection process of a geotextile that fulfills a protective function of a geomembrane involves the following three steps: (1) selection of polymer type and method of manufacture; (2) evaluation of the geotextile's capacity to provide puncture protection for the geomembrane; and (3) evaluation of construction survivability. Detailed procedures and methods for conducting these evaluations are described by Holtz et al. (1997, 1998), Koerner (2005), Narejo et al. (1996), and Wilson-Fahmy et al. (1996).

Another protection application associated with groundwater is erosion control blankets and mats. In this case, the geosynthetic protects the ground surface from the prevailing atmospheric conditions (i.e., wind, rain, snow, etc.). Specialty geocomposites have been developed for the specific purpose of erosion control. The general goal of these products is to protect soil slopes from both sheet and gully erosion, either permanently or until vegetation is established. Information on the design of geosynthetics for separation applications is provided by Holtz et al. (1997, 1998) and Koerner (2005).

37.3 Geosynthetic Types

As indicated in the introduction Section 37.1, there are a number of different geosynthetics. The characteristics of these materials vary considerably, primarily due to the method of manufacturing and the types and amount of polymers used for their production. This section provides a brief description of these materials and their primary characteristics. Additional information on the manufacturing process and characteristics of geosynthetics is provided by Koerner (2005) and Holtz et al. (1997, 1998) as well as by manufacturer's organizations, such as the Geosynthetic Manufacturer's Association (www.gmanow.com) and the PVC Geomembrane Institute (pgi-tp.ce.uiuc.edu).

37.3.1 Geotextiles

Among the different geosynthetic products, geotextiles are the ones that present the widest range of properties. They can be used to fulfill all the different functions listed in Table 2.2 for many different geotechnical, environmental, and hydraulic applications. For example, Figure 37.6 shows the construction of a reinforced slope in which geotextiles were selected as multipurpose inclusions within the fill, as they can provide not only the required tensile strength (reinforcement function), but also the required transmissivity (drainage function), needed for that particular project (Zornberg et al., 1995).

FIGURE 37.6 Placement of a high-strength nonwoven geotextile to perform a dual function of reinforcement and in-plane drainage in a reinforced slope.

Geotextiles are manufactured from polymer fibers or filaments that are later formed to develop the final product. Approximately 85% of the geotextiles used today are based on polypropylene resin. An additional 10% are polyester and the remaining 5% is a range of polymers including polyethylene, nylon, and other resins used for specialty purposes. As with all geosynthetics, however, the base resin has various additives, such as for ultraviolet light protection and long-term oxidative stability.

The most common types of fibers or filaments used in the manufacture of geotextiles are monofilament, multifilament, staple filament, and slit-film. If fibers are twisted or spun together, they are known as a yarn. Monofilaments are created by extruding the molten polymer through an apparatus containing small-diameter holes. The extruded polymer strings are then cooled and stretched to give the filament increased strength. Staple filaments are also manufactured by extruding the molten polymer; however, the extruded filaments are cut into 25- to 100- mm portions. The staple filaments or fibers may then be spun into longer yarns. Slit-film filaments are manufactured by either extruding or blowing a film of a continuous sheet of polymer and cutting it into filaments by knives or lanced air jets. Slit-film filaments have a flat, rectangular cross-section instead of the circular cross-section shown by the monofilament and staple filaments.

The filaments, fibers, or yarns are formed into geotextiles using either woven or nonwoven methods. Figure 37.7 shows a number of typical woven and nonwoven geotextiles. Woven geotextiles are manufactured using traditional weaving methods and a variety of weave types. Nonwoven geotextiles are manufactured by placing and orienting the filaments or fibers onto a conveyor belt, which are subsequently bonded by needle punching or by melt bonding. The needle-punching process consists of pushing numerous barbed needles through the fiber web. The fibers are thus mechanically interlocked into a stable configuration. As the name implies, the heat (or melt) bonding process consists of melting and pressurizing the fibers together.

Common terminology associated with geotextiles includes machine direction, cross machine direction, and selvage. Machine direction refers to the direction in the plane of fabric in line with the direction of

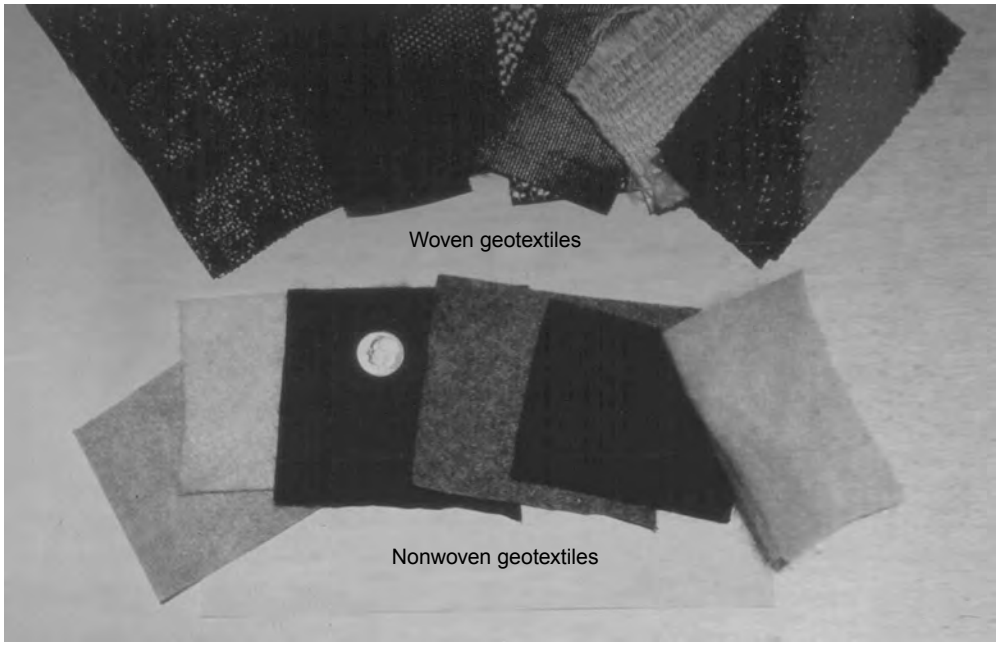

FIGURE 37.7 Typical woven and nonwoven geotextiles.

manufacture. Conversely, cross machine direction refers to the direction in the plane of fabric perpendicular to the direction of manufacture. The selvage is the finished area on the sides of the geotextile width that prevents the yarns from unraveling. Adjacent rolls of geotextiles are seamed in the field by either overlapping or sewing. Sewing is generally the case for geotextiles used as filters in landfill applications, but may be waived for geotextiles used in separation. Heat bonding may also be used for joining geotextiles used in filtration and separation applications.

Numerous tests have been developed to evaluate the properties of geotextiles. In developing geotextile specifications, it is important that the designer understands the material tests and that material properties important for the geotextile's intended use are specified. Table 37.3 describes the tests commonly performed in geotextile products (ASTM, 1995). Geotextiles can generally be specified with index and performance properties. As previously discussed, critical filtration applications are exceptions and the use of pre-qualified specific products from performance flow tests are strongly recommended.

37.3.2 Geomembranes

Geomembranes are flexible, polymeric sheets that have very low hydraulic conductivity (typically less than 10^{-11} cm/sec) and, consequently, are used as liquid or vapor barriers. The most common types of geomembranes are high density polyethylene (HDPE), very flexible polyethylene (VFPE), polyvinyl chloride (PVC), flexible polypropylene (fPP) and reinforced chlorosulfonated polyethylene (CSPE). Figure 37.8 shows a number of geomembranes currently available in the geosynthetics market.

Polyethylene is the type of geomembrane most commonly used in landfill applications for base and cover liner systems. This is primarily because of its high chemical resistance and durability. Specifically, high-density polyethylene (HDPE) is typically used in base liner systems. This material is somewhat rigid but generally has good physical properties and can withstand large stresses often imposed on the geomembrane during construction.

VFPE and PVC are the most commonly used geomembrane materials besides HDPE. The term VFPE encompasses various polyethylene grades such as very low density polyethylene (VLDPE) and certain types of linear low density polyethylene (LLDPE). The linear structure and lack of long-chain branching

TABLE 37.3 Standard Tests for Geotextiles

Property	Test standard	Test name
Thickness	ASTM D 5199	Standard Test Method for Measuring Nominal Thickness of Geotextiles and Geomembranes
Mass per Unit Area	ASTM D 5261	Standard Test Method for Measuring Mass per Unit area of Geotextiles
Grab rupture	ASTM D 4632	Standard Test Method for Breaking Load and Elongation of Geotextiles (Grab Method)
Uniaxial tensile strength geotextiles	ASTM D 4595	Standard Test Method for Tensile Properties of Geotextiles by the Wide-Width Strip Method
Geogrids	ASTM D 6637	Standard Test Method for Determining Tensile Properties of Geogrids by the Single or Multi-Rib Tensile Method
Multiaxial tensile, puncture or burst tests	ASTM D 6241	Standard Test Method for the Static Puncture Strength of Geotextiles and Geotextile Related Products Using a 50-Mm Probe
Trapezoid tear strength	ASTM D 4533	Standard Test Method for Trapezoid Tearing Strength of Geotextiles
Apparent opening size	ASTM D 4751	Standard Test Method for Determining Apparent Opening Size of a Geotextile
Permittivity	ASTM D 4491	Standard Test Methods for Water Permeability of Geotextiles by Permittivity
Gradient ratio	ASTM D 5101	Standard Test Method for Measuring the Soil-Geotextile System Clogging Potential by the Gradient Ratio
Transmissivity	ASTM D 4716	Standard Test Method for Constant Head Hydraulic Transmissivity (In-Plane Flow) of Geotextiles and Geotextile Related Products
Ultraviolet resistance	ASTM D 4355	Standard Test Method for Deterioration of Geotextiles from Exposure to Ultraviolet Light and Water (Xenon-Arc Type Apparatus)
Seam strength	ASTM D 1683	Failure in Sewn Seams of Woven Fabrics
Seam strength	ASTM D 4884	Standard Test Method for Seam Strength of Sewn Geotextiles

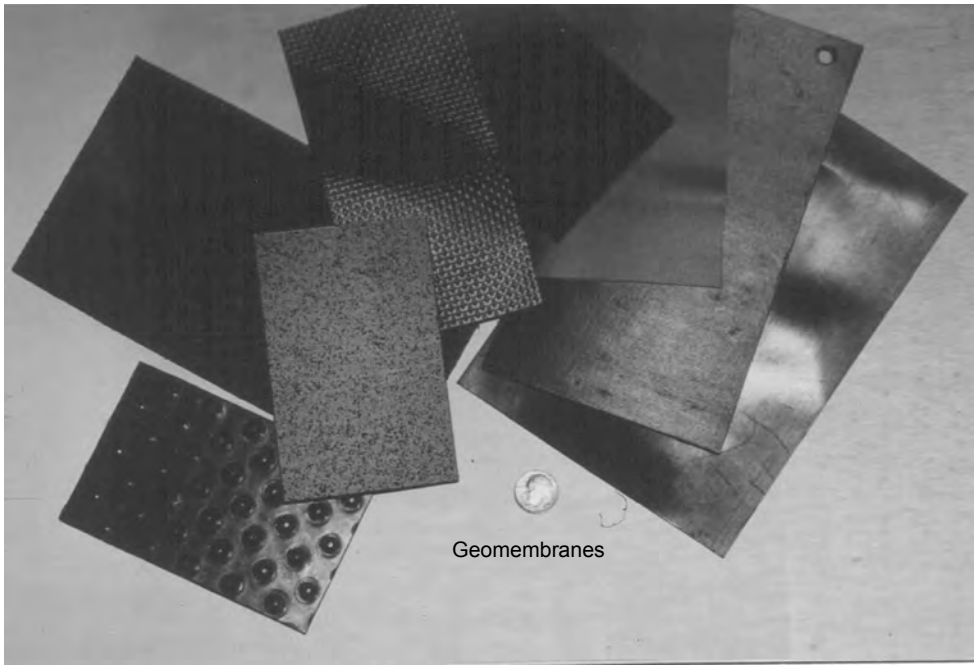

FIGURE 37.8 Typical geomembranes.

TABLE 37.4 Criteria for Selection of HDPE, PVC, or CSPE Geomembranes

Criteria	Considerations for selection
Liquid barrier	All three polymers have acceptable characteristics as liquid barriers, although HDPE geomembranes have the best characteristics in terms of chemical resistance and long-term durability. All three have extremely low hydraulic conductivity and are impermeable for practical purposes.
Mechanical properties	Although the mechanical properties vary somewhat with geomembrane thickness, HDPE is relatively stiff and has relatively small yield strain. PVC, in contrast, is relatively extensible and does not exhibit yield. The tensile properties of CSPE often fall between those of HDPE and PVC but are difficult to generalize because CSPE is usually made with embedded reinforcing fabrics which affect tensile response.
Construction survivability	All three polymers have an acceptable ability to maintain integrity when subjected to concentrated stresses. However, the best performance is obtained with more extensible geomembranes. Therefore, based on the relative extensibility, PVC generally offers the most favorable performance.
Installation	Key considerations include ease of placement and seaming. PVC and CSPE are easier to place than HDPE because their greater flexibility makes them conform more easily to the foundation and makes them less prone to thermal expansion wrinkles. Acceptable placement and wrinkle control, however, can be achieved with all three polymers if appropriate installation procedures are used. All three polymers are easily seamed, with HDPE usually achieving the highest seam strength and quality.
Chemical resistance	HDPE has the highest degree of compatibility with a wide variety of chemicals encountered in wastes. CSPE has good resistance to many chemicals, but is attacked by some that are relatively common, namely chlorinated solvents and hydrocarbons. PVC typically is the least chemically resistant of these polymers.
Long-term durability	HDPE offers the best performance. HDPE is a highly inert and durable material that is not susceptible to chemical degradation under conditions generally encountered in landfills. In addition, HDPE is not susceptible to physical degradation (extraction). The durability of PVC geomembranes is less favorable than that of HDPE. This is because PVC geomembranes are composed of approximately two-thirds PVC resin and one-third plasticizers. Over time, physical degradation (extraction) may cause plasticizer loss which results in reduced geomembrane flexibility. The durability of CSPE geomembranes is typically between that of HDPE and PVC.

in both LLDPE and VLDPE arise from their similar polymerization mechanisms. Due to the large settlements that may occur, cover liner systems commonly require a flexible geomembrane. VFPE is often used in this application as it provides similar chemical resistance as HDPE but is more flexible and can more readily conform to underlying refuse settlements without puncturing. Flexible polypropylene (fPP) geomembranes have recently (1990) been developed by combining the polypropylene (PP) and the ethylene propylene elastomer (EPE). This product was developed to obtain physical characteristics similar to the low density polyethylene while offering the flexibility similar to the polyvinyl chloride geomembranes.

PVC geomembranes are used in liners for many waste containment applications, such as contaminated soils containment and liquid storage ponds. While PVC may not be as durable as polyethylene geomembranes, the merits of PVC geomembranes are that they are generally less expensive than polyethylene geomembrane and can be factory manufactured in relatively large panels. The large panel sizes allow easier installation as there are fewer field fabricated seams.

In landfill applications, geomembranes are typically used as a base or a cover liner in place of or in addition to low-hydraulic conductivity soils. The key performance factors related to the selection of geomembrane polymer types for landfill applications are summarized in Table 37.4. Geomembrane thickness ranges from 0.75 to 2.5 mm (30 to 100 mils). Table 37.5 summarizes the key performance factors related to

TABLE 37.5 Criteria for Minimum Thickness of HDPE Geomembrane

Criteria	Considerations for selection of thickness
Abrasion resistance	The abrasion resistance of HDPE geomembranes increases with geomembrane thickness. Experience indicates that geomembranes with thickness < 1 mm may not have acceptable abrasion resistance.
Response to differential settlements	The thicker the HDPE geomembrane, the higher its stiffness. This issue is more significant for geomembrane cover systems than for geomembrane base liner systems because the cover system must be flexible enough to accommodate differential settlements. From this viewpoint, a thickness of not more than 2 mm is desirable.
Effective welding	The thinner the HDPE geomembrane, the more difficult is the welding of adjacent panels. For most effective welding, a desirable thickness is of at least 1 mm (40 mils), and preferably 1.5 to 2 mm.

the selection of the thickness of HDPE geomembranes for landfill applications. Geomembranes are placed after subgrade preparation, and placement is followed by seaming, inspection, and backfilling. A properly designed geomembrane has the potential of hundreds of years of service lifetime, but installation must follow high quality management principles. In the early uses of geomembranes for waste containment applications, the main concerns were related to the chemical compatibility between geomembranes and waste, and to the service life of geomembranes. Now, construction quality issues are viewed as the principal limitations to the performance of geomembranes.

For continuity of the impermeable barrier, geomembranes should be seamed in the field. The fundamental mechanism of seaming polymeric geomembrane sheets together is to temporarily reorganize (melt) the polymer structure of the two surfaces to be joined in a controlled manner. This reorganization can be done either through thermal or chemical processes. These processes may involve the addition of extra polymer in the bonded area. There are four general categories of seaming methods: extrusion welding, thermal fusion or melt bonding, chemical fusion, and adhesive seaming. Thermal fusion and extrusion welding are the methods most commonly used, and are described next.

In thermal fusion or melt bonding (the most common seaming method), portions of the opposing surfaces are truly melted. Temperature, pressure, and seaming rate play important roles as excessive melting weakens the geomembrane and inadequate melting results in low seam strength. The hot wedge, or hot shoe, method consists of an electrically heated resistance element in the shape of a wedge that travels between the two sheets to be seamed. A standard hot wedge creates a single uniform width seam, while a dual hot wedge (or "split" wedge) forms two parallel seams with a uniform unbonded space between them. This space can then be conveniently used to evaluate seam quality and continuity by pressurizing the unbonded space with air and monitoring any drop in pressure that may signify a leak in the seam (Figure 37.9).

Extrusion welding is at present used exclusively on geomembranes made from polyethylene. A ribbon of molten polymer is extruded over the edge of, or in between, the two surfaces to be joined. The molten extrudate causes the surface of the sheets to become hot and melt, after which the entire mass cools and bonds together. The technique is called extrusion fillet seaming when the extrudate is placed over the leading edge of the seam, and is called extrusion flat seaming when the extrudate is placed between the two sheets to be joined. Fillet extrusion seaming is essentially the only practical method for seaming polyethylene geomembrane patches, for seaming in poorly accessible areas such as sump bottoms and around pipes, and for seaming of extremely short seam lengths.

The material properties of geomembranes are divided into the properties of the raw polymer or resin used in the manufacture of the geomembrane sheet and the manufactured geomembrane properties. Table 37.6 lists the tests commonly performed for evaluation of the raw polymer properties. Table 37.7 summarizes the tests commonly performed to evaluate the manufactured geomembrane sheet properties (ASTM, 1995). As with the geotextiles, many of these tests provide index or quality control properties.

FIGURE 37.9 Monitoring seaming of a geomembrane liner.

TABLE 37.6 Tests for Raw Geomembrane Polymers

Property	Test standard	Test name
Density	ASTM D 792	Standard Test Method for Specific Gravity and Density of Plastics by the Density-Gradient Technique
Density	ASTM D 1505	Standard Test Method for Density of Plastics by the Density-Gradient Technique
Melt index	ASTM D 1238	Standard Test Method for Flow Rates of Thermoplastics by Extrusion Plastometer
Chemical identification methods (fingerprinting)		Thermogravimetric Analysis (TGA) Differential Scanning Calorimetry (DSC) Thermomechanical Analysis (TMA) Infrared Spectroscopy (IR) Chromatography (GC) Gel Permeation Chromatography (GPC)

37.3.3 Geogrids

Geogrids constitute a category of geosynthetics designed preliminary to fulfill a reinforcement function. Geogrids have a uniformly distributed array of apertures between their longitudinal and transverse elements. The apertures allow direct contact between soil particles on either side of the installed sheet, thereby increasing the interaction between the geogrid and the backfill soil.

Geogrids are composed of polypropylene, polyethylene, polyester, or coated polyester. They are formed by several different methods. The coated polyester geogrids are typically woven or knitted. Coating is generally performed using PVC or acrylics to protect the filaments from construction damage and to maintain the grid structure. The polypropylene geogrids are either extruded or punched sheet drawn, and polyethylene geogrids are exclusively punched sheet drawn. Figure 37.10 shows a number of typical geogrid products. In the past several years, geogrids have also been manufactured by interlacing polypropylene or polyester strips together and welding them at their cross-over points (i.e., junctions).

TABLE 37.7 Standard Tests for Geomembranes

Property	Test standard	Test name
Thickness	ASTM D 5199	Standard Test Method for Measuring Nominal Thickness of Geotextiles and Geomembranes
Tensile behavior	ASTM D 6693	Test Method for Determining Tensile Properties of Nonreinforced Polyethylene and Nonreinforced Flexible Polypropylene Geomembranes
Tensile behavior	ASTM D 7003	Test Method for Strip Tensile Properties of Reinforced Geomembranes
Tensile behavior	ASTM D 882	Test Methods for Tensile Properties of Thin Plastic Sheeting (Method A Used for PVC)
Tensile behavior	ASTM D 4885	Standard Test Method for Determining Performance Strength of Geomembranes by the Wide Strip Tensile Method
Tear resistance	ASTM D 1004	Test Method for Initial Tear Resistance of Plastic Film and Sheeting
Puncture resistance	ASTM D 2065	Puncture Resistance and Elongation Test
Puncture resistance	ASTM D 5494	Test Method for the Determination of Pyramid Puncture Resistance of Unprotected and Protected Geomembranes
Puncture resistance	ASTM D 5514	Test Method for Large-Scale Hydrostatic Puncture Testing of Geosynthetics
Environmental stress crack	ASTM D 1693	Standard Test Method for Environmental Stress-Cracking of Ethylene Plastics
Environmental stress crack	ASTM D 5397	Test Method for Evaluation of Stress Crack Resistance of Polyolefin Geomembranes Using Notched Constant Tensile Load Test
Carbon black	ASTM D 1603	Standard Test Method for Carbon Black in Olefin Plastics
Carbon black	ASTM D 5596	Standard Practice for Microscopic Evaluation of the Dispersion of Carbon Black in Polyolefin Geosynthetics
Durability	ASTM D 5721	Practice for Air-Oven Aging of Polyolefin Geomembranes
chemical resistance	ASTM D 5747	Practice for Tests to Evaluate the Chemical Resistance of Geomembranes to Liquids
Seam strength	ASTM D 4437	Standard Practice for Determining the Integrity of Field Seams Used in Joining Flexible Polymeric Sheet Geomembranes
Leak detection	ASTM D 7007	Practices for Electrical Methods for Locating Leaks in Geomembranes Covered with Water or Earth Materials

Although geogrids are used primarily for reinforcement, some products are used for asphalt overlay and some are combined with other geosynthetics to be used in water proofing or in separation and stabilization applications. In waste containment systems, geogrids may be used to support a lining system over a weak subgrade or to support final landfill cover soils on steep refuse slopes. Geogrids are also used for support of liners in the design of "piggyback" landfills, which are landfills built vertically over older, usually unlined landfills. Regulatory agencies often require that a liner system be installed between the old and new landfill. As the old refuse is highly compressible, it provides a poor base for the new lining system. A geogrid may be used to support the lining system and bridge over voids that may occur beneath the liner as the underlying refuse components decompose.

As with other geosynthetics, geogrids have several physical, mechanical, and durability properties. Many of the test methods used for geotextiles and geomembranes also apply to geogrids. In particular, a key design parameter for reinforcement is the tensile strength, which is performed with the specimen width incorporating typically a few ribs of the geogrid. The allowable tensile strength of geogrids (and of other geosynthetics used for soil reinforcement applications) is typically significantly less than its ultimate tensile strength. The allowable tensile strength is determined by dividing the ultimate tensile strength by partial factors to account for installation damage, creep deformation, chemical degradation, and biological degradation. The partial factors for installation damage, chemical degradation, and biological degradation range from 1.0 to 1.6, with the partial factor of safety for creep ranging from 1.5 to 3.5 (Koerner, 2005). The design engineer should review all recommendations, available codes, national evaluations, and the like and determine appropriate partial factors for the specific projects (i.e., manufacturers' recommendations should be carefully evaluated based on project-specific requirements and not blindly accepted).

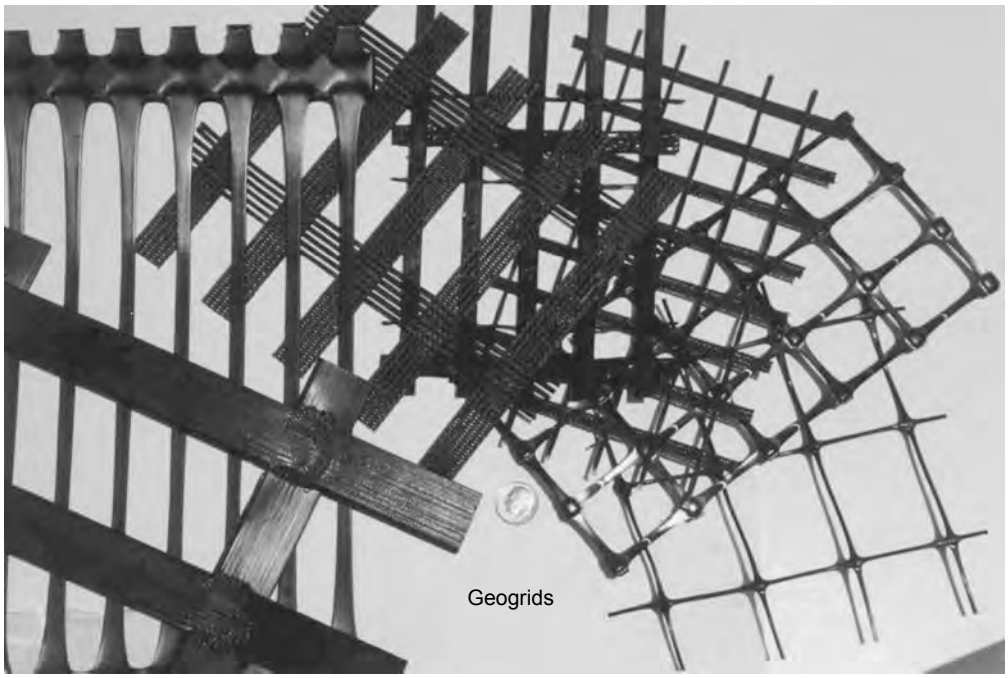

FIGURE 37.10 Typical geogrids.

37.3.4 Geosynthetic Clay Liners

Geosynthetic clay liners (GCLs) are rapidly expanding products in the geosynthetics market. GCLs are infiltration barriers consisting of a layer of unhydrated, loose granular or powdered bentonite placed between two or on top of one geosynthetic layer (geotextile or geomembrane). GCLs are produced in panels that are joined in the field by overlapping. They are generally used as an alternative to compacted clay liners (Bouazza, 2002).

Due to the inherent low shear strength of hydrated bentonite, GCL usage had initially been limited to applications where stability of the overlying materials was not a concern. In the late 1980s, however, methods were developed to reinforce the GCLs, producing a composite material with higher shear strength properties. This allowed the use of GCLs in landfill applications (Figure 37.11).

Some advantages of GCLs over compacted clay liner are that they occupy significantly less space to achieve equivalent performance, plus they are flexible, self-healing, and easy to install. In locations where low hydraulic conductivity clays are not readily available, they may offer significant construction cost savings. In addition, as they are factory manufactured with good quality control, field construction quality assurance costs are typically less than with compacted clay liners.

Bentonite is a clay formed primarily from the mineral montmorillonite. While several types of montmorillonite exist, including calcium and sodium montmorillonite, the term bentonite typically refers to a sodium montmorillonite. Water is strongly attracted to the surface of the negatively charged montmorillonite crystal and is readily absorbed by it. In its unhydrated state, the montmorillonite crystals are densely packed. Once hydrated, the structure becomes very open and swells. The high water absorption and swell characteristics of bentonite lead to its low hydraulic conductivity and low hydrated shear strength.

Geosynthetic clay liners are manufactured by laying down a layer of dry bentonite, approximately 5 mm thick, on a geosynthetic material and attaching the bentonite to the geosynthetic. Two general configurations are currently employed in commercial processes (Figure 37.12): bentonite sandwiched between two geotextiles or bentonite glued to a geomembrane. The primary purpose of the geosynthetic component

FIGURE 37.11 Installation of a GCL during construction of a landfill base liner.

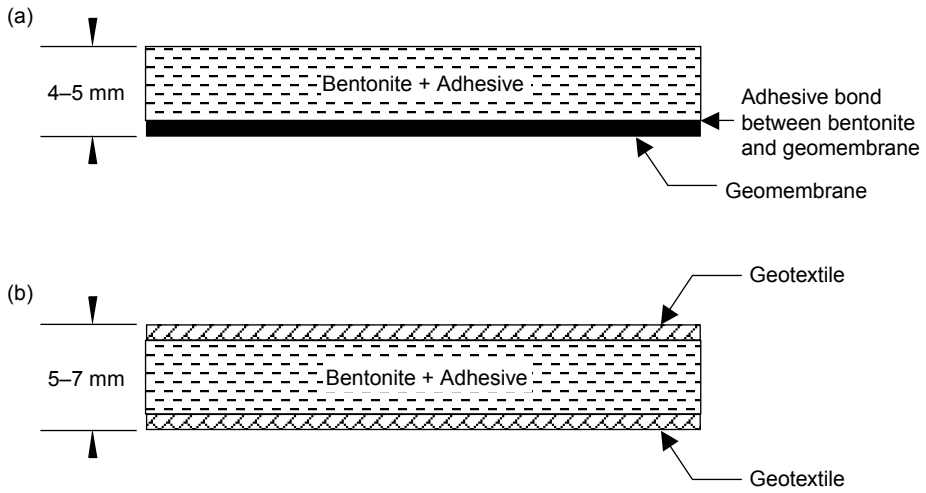

FIGURE 37.12 GCL configurations: (a) bentonite glued to a geomembrane; (b) bentonite sandwiched between two geotextiles.

is to hold the bentonite together in a uniform layer and to permit transportation and installation of the GCL without loss of bentonite.

The outer geosynthetic layer of GCLs can be mechanically bonded using stitching or needle punching (resulting in reinforced GCLs). A different process consists in using an adhesive bond to glue the bentonite to the geosynthetic (resulting in unreinforced GCLs). The mechanical bonding of reinforced GCLs increases their internal shear strength. Geosynthetic clay liners contain approximately 5 kg/m^2 of bentonite that has a hydraulic conductivity of approximately 1×10^{-9} cm/sec. Infiltration under unit

hydraulic gradient through a material with hydraulic conductivity of 1×10^{-9} cm/sec would result in an infiltration rate of 0.3 mm per year.

As a GCL is a composite material, its relevant properties are those of the geotextile alone, of the bentonite alone, and of the composite. Geotextile properties were discussed in Section 37.3.1. The geotextile properties relevant to GCLs include mass per unit area, grab tensile, wide-width tensile, and puncture resistance. Relevant properties of the bentonite are obtained from free swell tests, which measure the absorption of water into a bentonite based on its volume change, and plate water absorption tests, which measure the ability of powdered bentonite to absorb water. The relevant properties of the composite GCL material include bentonite content, which is simply a measure of the mass of bentonite per unit area of GCL, permeameter testing (ASTM D 5084) used to estimate the GCL hydraulic conductivity, tensile strength characterized either by grab tensile or wide-width tensile tests, and puncture resistance tests performed to assess the relative puncture resistance between GCLs and geomembranes or other geosynthetics. The internal and interface shear strength of GCLs should also be determined as stability is a major concern for side slopes in bottom liner or cover systems that include GCLs. This is because of the very low shear strength of hydrated sodium bentonite. Proper shear strength characterization is needed for the different materials and interfaces in hydraulic barriers (Koerner, 2005). The analysis of a large database of test results on the internal shear strength of GCLs is presented by Zornberg et al. (2005).

37.3.5 Geocomposite Sheet Drains

A geocomposite consists of a combination of different types of geosynthetics. In particular, the geosynthetics industry has developed a number of geocomposite drains, which are polymeric drainage cores with continuously open flow channels sandwiched between geotextile filters. Geocomposite sheet drains are discussed in this section while geocomposite strip (wick) drains are discussed in Section 37.3.6.

Geocomposite sheet drainage systems have been engineered to replace costly aggregate and perforated pipe subsurface drainage systems. They have reached rapid acceptance because they provide adequate drainage and reduce the material cost, installation time, and design complexity of conventional aggregate systems.

The core of geocomposite sheet drains are extruded sheets of plastic formed into a configuration that promotes drainage. The core of the geocomposite sheet drains are most commonly composed of polyethylene but may also be composed of polypropylene, polystyrene, high-impact polystyrene, or other materials. The structure of the core drainage products ranges from a dimpled core to a geonet. Geonets, a commonly used drainage product, generally consist of two or three sets of parallel solid or foamed extruded ribs that intersect at a constant angle to form an open net configuration. Channels are formed between the ribs to convey either liquid or gases. Figure 37.13 shows a number of geonets currently available in the market. Dimpled cores type products tend to have a greater flow capacity than geonets; however, they generally have a much lower crush resistance and tend to be more compressible than geonets. As indicated in Section 37.2.5, the transmissivity of the geocomposite drain must be evaluated under anticipated site-specific normal pressures and a factor of safety included to account for creep of the product over the life of the system (Koerner, 2005).

The geotextile serves as both a separator and a filter, and the geonet or built-up core serves as a drain. There may be geotextiles on both the top and bottom of the drainage core and they may be different from one another. For example, the lower geotextile may be a thick needlepunched nonwoven geotextile used as a protection material for the underlying geomembrane, while the top geotextile may be a thinner nonwoven or woven product. Composite drainage nets are typically formed by thermally bonding the geotextile and geonet. Gluing and solvent welding can also be used to bond the geosynthetic core to the geotextile. In producing geocomposite drainage nets, the melt temperatures of the geotextile and geonet must be compatible so that the properties of each material are retained. Figure 37.14 shows a number of available geocomposite sheet drainage materials.

As the purpose of the core is drainage, the most important properties to include in specifications are thickness, crush strength, and long-term transmissivity under load. Table 37.8 summarizes the tests

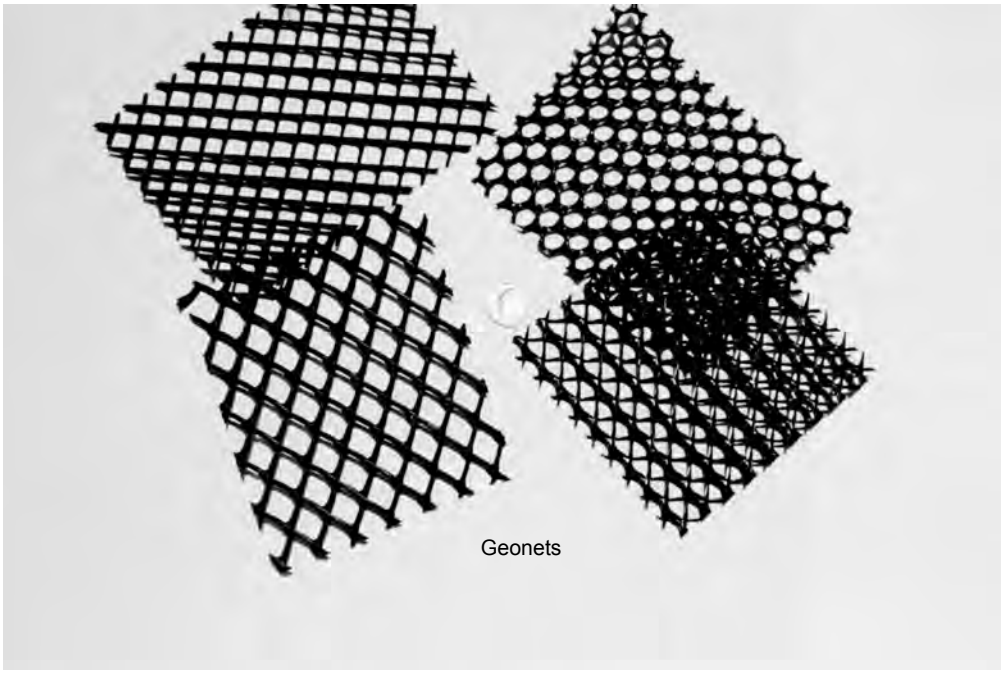

FIGURE 37.13 Typical geonets used as the core of geocomposite sheet drains.

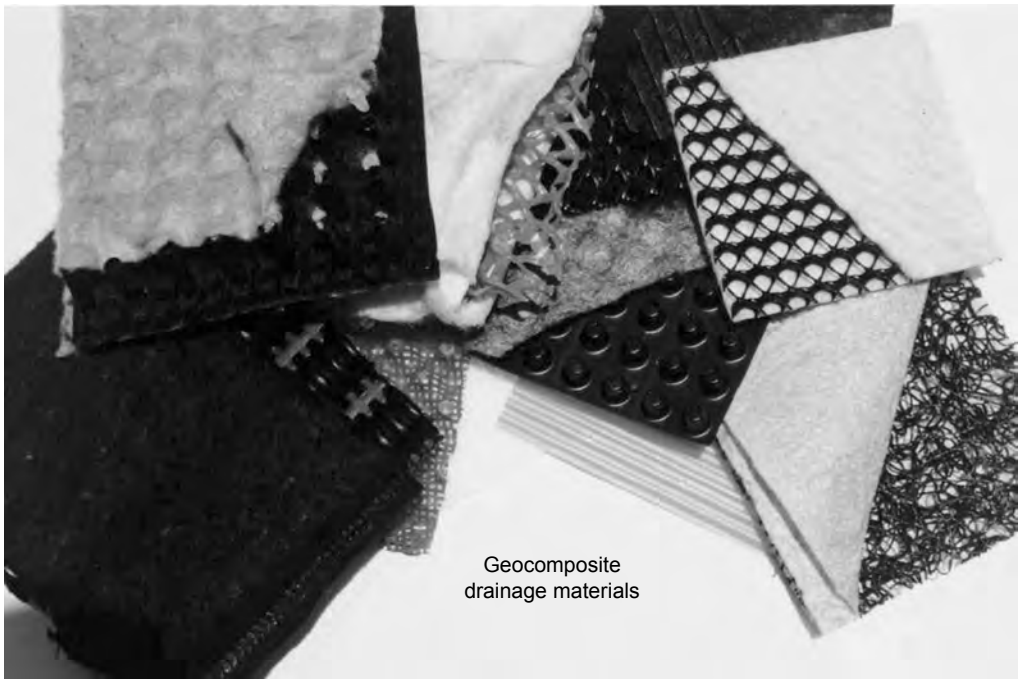

FIGURE 37.14 Typical geocomposite sheet drains.

TABLE 37.8 Standard Tests for Geocomposite Drainage Nets

Property	Test standard	Test name
Composite and core thickness	ASTM D 5199	Standard Test Method for Measuring Nominal Thickness of Geotextiles and Geomembranes
Core crush strength	ASTM D 1621	Standard Test Method for Compressive Properties of Rigid Cellular Plastics
Composite compression	ASTM D 6244	Test Method for Vertical Compression of Geocomposite Pavement Panel Drains
Composite compression	ASTM D 6364	Test Method for Determining Short-Term Compression Behavior of Geosynthetics
Composite transmissivity	ASTM D 4716	Standard Test Method for Determining the (In-plane) Flow Rate per Unit Width and Hydraulic Transmissivity of a Geosynthetic Using a Constant Head
Core carbon black	ASTM D 4218	Standard Test Method for Determination of Carbon Black Content in Polyethylene Compounds by the Muffle Furnace Technique
Geotextile filter	See Table 37.3	Grab Tensile Tear Strength CBR Puncture Strength AOS Permittivity

commonly performed to evaluate the properties of geocomposite sheet drains. It is also important to evaluate filtration requirements for the geotextile. Design and specification of composite drains is covered by Giroud et al. (2000), Koerner (2005), and Holtz et al. (1997, 1998).

37.3.6 Geocomposite Strip (Wick) Drains

Geocomposite strip drains, also called "wick drains," have been developed to replace the use of sand drains in applications involving the increase in consolidation rate of soft, saturated fine-grained soils. Geocomposite strip drains actually do not wick moisture, but simply provide a conduit for excess pore water pressure induced flow. They are placed vertically through high water content silts and clays to produce shortened drainage paths and thus increase the rate of consolidation. Other names commonly used for these products are "band shaped drains" and "prefabricated vertical drains."

Sand drains were originally introduced in the 1930s as a method for improvement of soft soil foundations. The method of rapid consolidation of saturated fine-grained soils using sand drains involves placement of vertical columns of sand (usually 200 to 450 mm in diameter) at spacings of 1.5 to 6.0 m centers throughout the subsurface to be dewatered. Due to the low installed product cost and speed of installation, the use of geocomposite strip drains dominates over the use of sand drains in projects involving dewatering of saturated fine-grained soils. Their lengths are site-specific and extend to the bottom of the soft layer, and, thus, lengths generally will vary along a project. Once installed, a surcharge load is placed on the ground surface to mobilize excess pore water pressures. This surcharge load is placed in incremental lifts, which induce pore water pressure in the underlying soil. The pore water pressure is then dissipated through the vertical drains. Water takes the shortest drainage path (i.e., horizontally radial) to the vertical drain, at which point it flows vertically as the drain has a much higher hydraulic conductivity than the fine-grained soil being consolidated. The rate at which surcharge fill is added is critical in this process.

Most commercially available geocomposite strip drains have adequate capacity to drain the water expelled during consolidation of the fine-grained soils. As their flow capacity is usually adequate, selection of the vertical drains is governed by the consolidation rate required in the project. Hansbo's equation (Hansbo, 1979) is generally used to estimate the time required to achieve a desired percentage of consolidation as a function of the horizontal coefficient of consolidation of the foundation soil, the equivalent diameter of the geocomposite strip drain, and the spacing of the drains. As with geocomposite sheet drains,

FIGURE 37.15 View of expanded geocell (photo courtesy of Presto Product Company).

the primary function of the geotextile covering is filtration. Determining the filtration requirements for the geotextile is an essential element of the design.

Installation of geocomposite strip drains is very rapid and uses lightweight construction equipment fitted with hollow leads (called a "lance" or mandrel) for insertion to the desired depth. The bottom of the lance should be covered by an expendable shoe that keeps soil out of the lance so as not to bind the strip drain within it. The allowable flow rate of geocomposite strip drains is determined by the ASTM D4716 test method. Typical values of ultimate flow rate at a hydraulic gradient of 1.0 under 207 kPa normal stress vary from 1.5 to 3.0 m^3/sec.-m. This value must then be reduced on the basis of site-specific partial factors of safety. Specifications for geocomposite strip drains are provided by Holtz et al. (1997).

37.3.7 Geocells

Geocells (or cellular confinement systems) are three-dimensional, expandable panels made from strips, typically 50 to 100 mm wide. When expanded during installation, the interconnected strips form the walls of a flexible, three-dimensional cellular structure into which specified infill materials are placed and compacted (Figure 37.15). This creates a system that holds the infill material in place and prevents mass movements by providing tensile reinforcement. Cellular confinement systems improve the structural and functional behavior of soil infill materials.

Geocells were developed in the late 1970s and early 1980s for support of military vehicles on weak subgrade soils. The original type of geocell consists of HDPE strips 200 mm wide and approximately 1.2 mm thick. They are ultrasonically welded along their 200 mm width at approximately 330 mm intervals and are shipped to the job site in a collapsed configuration. At the job site they are placed directly onto the subgrade surface and propped open in an accordion-like fashion with an external stretcher assembly. They are then filled generally with gravel or sand (although other infill materials such as concrete, can be used) and compacted using a vibratory hand-operated plate compactor. Geocell applications include protection and stabilization of steep slope surfaces, protective linings of channels and hydraulic structures, static

and dynamic load support on weak subgrade soils, and multilayered earth-retaining and water-retaining gravity structures.

Geocells have proven very effective in providing a stable foundation over soft soils. The cellular confinement system improves the load-deformation performance of infill materials because cohesionless materials gain considerable shear strength and stiffness under confined conditions. Confining stresses are effectively induced in a geocell by means of the hoop strength developed by the HDPE cell walls. The overall increase in the load carrying performance of the system is provided through a combination of the cell wall strength, the passive resistance of the infill material in adjacent cells, and the frictional interaction between the infill soil and the cell walls. The cellular structure distributes concentrated loads to surrounding cells thus reducing the stress on the subgrade directly beneath the geocell.

Infill selection is primarily governed by the nature and intensity of anticipated working stresses, availability and cost of candidate materials, and aesthetic requirements for a fully vegetated appearance. Aggregates, vegetated topsoil, and concrete constitute typical geocell infill types. A complete cellular confinement system may also include geotextiles, geomembranes, geonets, geogrids, integral polymeric tendons, erosion-control blankets, and a variety of earth anchors.

37.3.8 Erosion Control Products

Erosion-control products represent one of the fastest growing application areas in the geosynthetics industry. Erosion-control products provide protection against sheet and gully erosion on soil slopes either until vegetation is established or for long-term applications. These products can be classified as temporary degradable erosion control blankets, long-term nondegradable erosion control mats, and permanent hard armored systems.

Temporary degradable erosion control blankets are used to enhance the establishment of vegetation. These products are used where vegetation alone would provide sufficient site protection once established after the erosion control product has degraded. Some of these products are completely biodegradable (e.g., straw, hay, jute, and hydraulic mulches), while others are only partially biodegradable (e.g., erosion control meshes and nets).

Long-term nondegradable erosion control mats provide permanent reinforcement of vegetation root structure. They are used in critical erosion-control applications where immediate high-performance erosion protection, followed by the permanent reinforcement of established vegetation is required. These soft armor related products provide erosion control, aid in vegetative growth, and eventually become entangled with the vegetation to provide reinforcement to the root system.

Finally, the permanent hard armored systems include riprap on geotextile filters, modular concrete block over geotextile filter systems, gabions over geotextile filters, geocell products with gravel or concrete infill, vegetated concrete block systems, and fabric-formed revetments.

Figure 37.16 shows an erosion control mat installed to help vegetation establishment on a steep reinforced soil slope. Installation of flexible erosion control products is straightforward. The products are usually placed on a prepared soil surface (e.g., facing of the reinforced embankment in Figure 37.16) by stapling or pinning them to the soil surface. Intimate contact between the blanket or mat and the soil is very important as water flow beneath the material has usually been the cause of poor functioning.

37.3.9 HDPE Vertical Barrier Systems

The use of geomembranes (Section 37.3.2) as horizontal barrier layers has been extended for the case of seepage control in remediation projects, in which vertically deployed geomembranes are used in vertical cutoff trenches. The construction process involves excavation of a trench and placement of a seamed geomembrane in the open trench. This procedure is usually not possible for deep trenches due to the potential collapse of the sidewalls, so the use of slurry to stabilize the trench becomes necessary. The mixture of water and bentonite clay balances the pressures exerted by the *in situ* soils. The geomembrane

FIGURE 37.16 Erosion control mat placed to help establish the vegetation on the face of a 1H:1V reinforced soil slope.

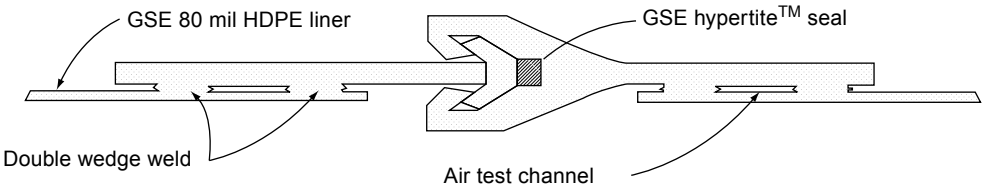

FIGURE 37.17 Interlocking system for HDPE vertical barriers (figure courtesy of GSE Lining Technology, Inc.).

is placed in the slurry after trench excavation to the intended depth. Once the geomembrane is in place the backfill can be introduced, displacing the slurry and forcing the geomembrane to the side of the trench.

As installation of vertically deployed conventional geomembranes is difficult, other systems have become available. These systems involve the use of thick HDPE or nonplasticized PVC geomembranes in the form of tongue-and-groove sheeting. Sealing of the interlocks is often achieved by using chloroprene-based, hydrophilic seals. Figure 37.17 shows one type of interlocking system with a hydrophilic seal. The seal is an extruded profile, typically 8 mm in diameter, which can expand up to eight times its original volume when exposed to water. These interlocking HDPE vertical barrier systems are being increasingly used as an alternative to soil-bentonite slurry walls, especially in projects involving areas of limited access, high disposal costs, depths where performance of a slurry wall is questionable and high concentrations of saline and chemicals.

An additional advantage of the HDPE vertical barrier system is that it can work both as containment and a collection system (e.g., a composite sheet drain) and can be constructed in one trench. A recently developed method utilizes a biopolymer, or biodegradable, slurry. These slurries allow the HDPE panels and collection system (e.g., geocomposite sheet drains) to be installed in the same trench. Unlike bentonite, these slurries will either biodegrade or can be reversed to allow the collection system to drain clear and free of fines.

Another method of achieving construction of a containment and collection system in the same trench has been developed which utilizes a trenchless, vibratory method for installation of the HDPE panels and geocomposite sheet drains. First, a collection trench is constructed to the required depth. This is followed with the installation of the geomembrane panel using modified pile-driving techniques. Panel widths ranging typically between 0.91 to 1.83 m are driven to depths up to 12 m. This construction method is most often reserved for sites on which excavation and disposal costs are high, access is limited, or the barrier is too close to a body of water. A case history in which this installation method was used for placement of an HDPE vertical barrier system is described in Section 37.5.1 .

A recent development in the installation of these systems is the use of a "one-pass" deep trencher. Installation of HDPE vertical barrier systems using this technology has proven to be fast and safe. A special trencher equipment can install a vertical geomembrane wall with a collection system consisting of a HDPE pipe and gravel fill in one trench, in one pass. Figure 37.18 shows the placement of an HDPE panel using this one-pass deep trencher.

FIGURE 37.18 One pass trencher for installation of an HDPE vertical barrier system. (Photo courtesy of Groundwater Control, Inc.)

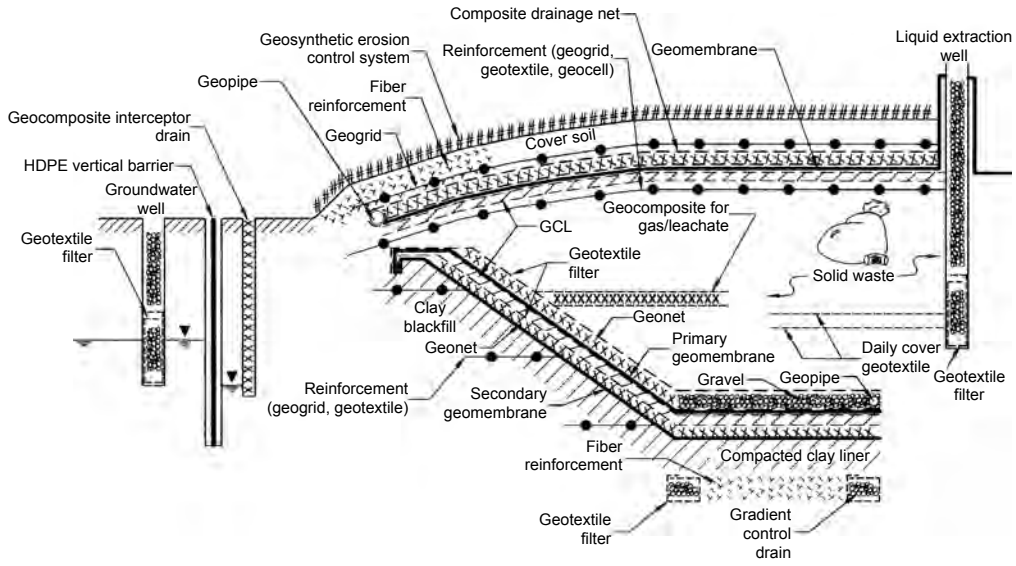

FIGURE 37.19 Multiple use of geosynthetics in landfill design.

37.4 Geosynthetic Applications in Landfill Design

The multiple uses of geosynthetics in the design of modern municipal solid waste landfills is a good illustration of an application in which different geosynthetics are used to perform all the functions discussed in Section 37.2. Virtually all the different types of geosynthetics discussed in Section 37.3 have been used in the design of both base and cover liner systems of landfill facilities. The extensive use of geosynthetics in modern landfills has been triggered by the economical and technical advantages that geosynthetics offer in relation to traditional liner systems. A geomembrane infiltration barrier and geocomposite sheet drain collection layers of a few millimeters in thickness can provide equivalent performance as a soil infiltration barrier with a gravel collection layer and graded granular filter layer of up to several meters in thickness.

Landfill base liners are placed below the waste to minimize the release of liquids from the waste (i.e., leachate). Leachate is the main source of contamination of the soil underlying the landfill and, most importantly, the groundwater. Landfill cover liners are placed above the final waste configuration to prevent water, usually from rain or snow, from percolating into the waste and producing leachate. Waste containment systems employ geosynthetics to varying degrees. Figure 37.19 illustrates the extensive multiple uses of geosynthetics in both the cover and the base liner systems of a modern landfill facility.

The base liner system illustrated in Figure 37.19 is a double composite liner system. Double composite liner systems are used in some instances for containment of municipal solid waste and are frequently used for landfills designed to contain hazardous waste. The base liner system shown in this figure includes a geomembrane/GCL composite as the primary liner system and a geomembrane/compacted clay liner composite as the secondary system. The leak detection system, located between the primary and secondary liners, is a geotextile/geonet composite. The leachate collection system overlying the primary liner on the bottom of the liner system consists of gravel with a network of perforated pipes. A geotextile protection layer beneath the gravel provides a cushion to protect the primary geomembrane from puncture by stones in the overlying gravel. The leachate collection system overlying the primary liner on the side slopes of the liner system is a geocomposite sheet drain (geotextile/geonet composite) merging into the gravel on the base. A geotextile filter covers the entire footprint of the landfill and prevents clogging of the leachate collection and removal system. The groundwater level may be controlled at the bottom of the landfill

by gradient control drains built using geotextile filters. Different types of geosynthetics (e.g., geogrids, geotextiles, fibers) can be selected for stabilization of the foundation soils.

The cover system of the landfill illustrated in Figure 37.19 contains a composite geomembrane/GCL barrier layer. The drainage layer overlying the geomembrane is a geocomposite sheet drain (composite geotextile/geonet). In addition, the soil cover system may include geogrid, geotextile, or geocell reinforcements below the infiltration barrier system. This layer of reinforcements may be used to minimize the strains that could be induced in the barrier layers by differential settlements of the refuse or by a future vertical expansion of the landfill. In addition, the cover system could include a geogrid or geotextile reinforcement above the infiltration barrier to provide stability to the vegetative cover soil. Fiber reinforcement may also be used for stabilization of the steep portion of the vegetative cover soil. A geocomposite erosion control system above the vegetative cover soil is indicated in the figure and provides protection against sheet and gully erosion.

Figure 37.19 also illustrates the use of geosynthetics within the waste mass, which are used to facilitate waste placement during landfilling. Specifically, the figure illustrates the use of geotextiles as daily cover layers and of geocomposites within the waste mass for collection of gas and leachate. Geotextile filters are also extensively used for leachate collection and detection blanket drains and around the gravel in leachate collection trenches at the base of the landfill. Geosynthetics can also be used as part of the groundwater and leachate collection well system. The use of geotextiles as filters in groundwater and leachate extraction wells is also illustrated in the figure. Finally, the figure shows the use of a HDPE vertical barrier system and a geocomposite interceptor drain along the perimeter of the landfill facility. Although not all of the components shown in Figure 37.19 would normally be needed at any one landfill facility, the figure illustrates the many geosynthetic applications that can be considered in landfill design.

Bouazza et al. (2002) provide an update on the use of geosynthetics in the design of waste containment facilities. A case history involving the design of a liner system with multiple uses of geosynthetics is described in Section 37.5.2.

37.5 Case Histories

37.5.1 Case History of Vertical Barrier System

Although the use of geosynthetics in many geotechnical and environmental projects is related to groundwater applications (e.g., landfill liners, which prevent groundwater contamination), a geosynthetic application directly related to groundwater remediation and control is the use of HDPE panels as vertical barrier systems. A case history is presented herein to illustrate the use of HDPE panels as part of a remediation plan for a site contaminated with coal tar (Burson et al., 1997).

The site was a defunct manufactured gas plant located in York, Pennsylvania. The site is surrounded by commercial and residential areas and a creek (Codorus Creek) borders the site for a distance of approximately 305 m. During years of operation and the subsequent closure of the manufactured gas plant, some process residuals migrated to the subsurface soils and groundwater. Over time, the presence of a coal tar-like material in the form of a dense non-aqueous phase liquid (DNAPL), was observed seeping from the bank of the Codorus Creek. DNAPL was also noted in some on-site monitoring wells.

Several remediation scenarios were evaluated with the purpose of intercepting the tar-like material migrating through the soil and into groundwater, encountered approximately 5.0 m below ground surface. A system consisting of a combination of soil improvement by jet grouting, a vertical barrier using HDPE panels, and a network of recovery wells was finally selected.

The use of vertical HDPE panels and trenchless technology allowed placement of the barrier as close as 3 m from the bank of the Codorus Creek, which was difficult to achieve with conventional slurry wall technology. The HDPE barrier system selected for this project was a 2 mm thick geomembrane, which allowed for the vibratory, trenchless installation. Sealing of the interlocks was achieved with a chloroprene-based, hydrophilic seal (see Figure 37.17). HDPE panels were keyed into the soil improved by jet grouting,

FIGURE 37.20 Installation of HDPE barrier wall utilizing conventional pile driving equipment. (Photo courtesy of Groundwater Control Inc.)

as discussed below. The panels were installed using conventional vibratory pile driving equipment, without a trench, thus reducing the amount of contaminated spoils to be disposed (Figure 37.20).

To complete closure of the contaminated material, jet grouting was used to provide a seal to control DNAPL migration between the bottom of the HDPE panels and the irregular bedrock contact. Jet grouting consists of high pressure injection of cement and bentonite slurry, horizontally into the soil strata to improve its mechanical and hydraulic properties. The containment wall was approximately 290 m in length. The soil along the alignment of the barrier system consisted of granular fills, with large amounts of cinder material. Also mixed into the fill were varying amounts of rubble and debris. These highly permeable soils were underlain by the competent bedrock. Holes were pre-drilled down to bedrock, and the jet grouting improvement was done by injecting the grout horizontally from the competent rock up to an elevation approximately 6 m below the ground surface.

A groundwater recovery system was implemented once the barrier was completed. Since its installation in the fall of 1995, the HDPE panel jet grout barrier system has performed as intended.

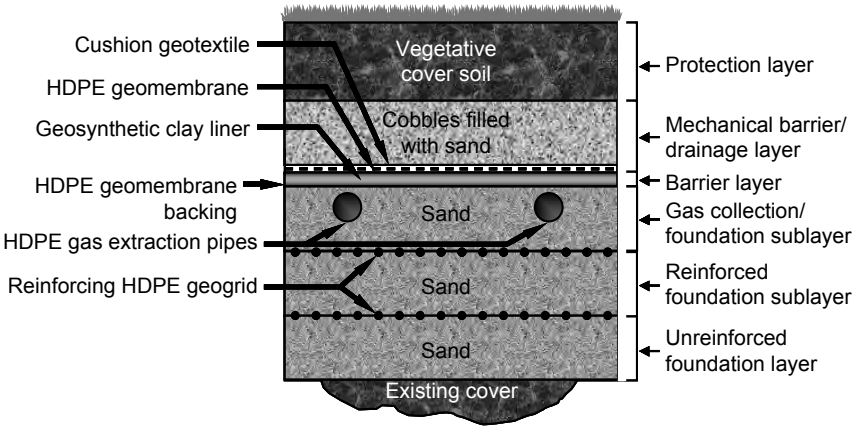

FIGURE 37.21 Cover system reinforced using geogrids.

37.5.2 Case History of Multiple Use of Geosynthetics in Landfill Cover Design

The cover system at the McColl Superfund Site, Fullerton, California is a good example of a site where multiple systems of soil reinforcement were used for stabilization of the final cover system. One of these uses involves placement of geogrids along the cover system. The project also included the construction of conventional reinforced structures (Collins et al., 1998; Hendricker et al., 1998).

The site has 12 pits containing petroleum sludge and oil-based drilling muds. The sludge was generated by the production of high-octane aviation fuel and was placed into the pits between 1942 and 1946. Between 1952 and 1964, the site was used for disposal of oil-based drilling muds. These wastes and their reaction products and byproducts were found as liquid, gas, and solid phases within the pits. At the time of deposition, essentially all of the waste materials were mobile. Over time, much of the waste had hardened. The drilling mud is a thixotropic semi-solid sludge, which can behave as a very viscous fluid.

Key considerations for the selection of the final remedy were to: (1) provide a cover system that includes a barrier layer and a gas collection and treatment system over the pits to minimize infiltration of water and release of hazardous or malodorous gas emissions; (2) provide a subsurface vertical barrier around the pits to minimize outward lateral migration of mobile waste or waste byproducts and inward lateral migration of subsurface liquid; and (3) provide slope stability improvements for unstable slopes at the site.

The geogrid reinforcement for the cover system over the more stable pits was constructed with two layers of uniaxial reinforcement placed orthogonally to one another. Connections at the end of each geogrid roll were provided by Bodkin joints. Adjacent geogrid panels did not have any permanent mechanical connections. This proved to be somewhat problematic, as additional care was required during placement of the overlying gas collection sand to minimize geogrid separation. Details of the cover system involving geogrid reinforcement are shown in Figure 37.21.

A geocell reinforcement layer was constructed over the pits containing high percentages of drilling mud. While the construction of this reinforcement layer proceeded at a slower pace than the geogrid reinforcement, it did provide an immediate platform to support the load. As the bearing capacity of the underlying drilling mud was quite low, the geocell provided load distribution, increasing the overall bearing capacity of the cover system. Details of the cover system involving geogrid reinforcement are shown in Figure 37.22.

In addition to reinforced covers, three conventional reinforced soil structures were constructed at the site. One of the structures was necessary to provide a working pad for construction of the subsurface vertical barrier. This reinforced earth structure had to support the excavator with a gross operating weight of 1100 kN that was used to dig the soil-bentonite cutoff wall. Another reinforced earth structure at the site

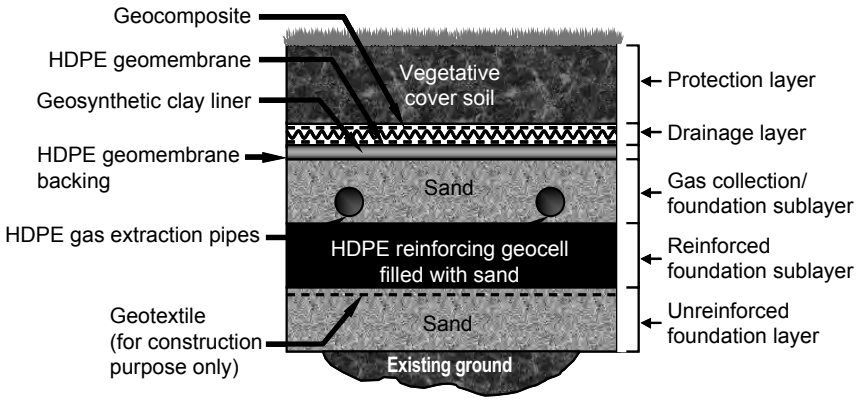

FIGURE 37.22 Cover system reinforced using geocells.

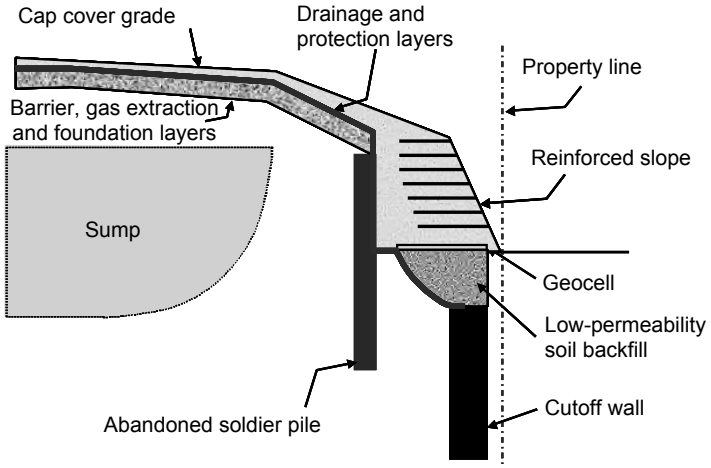

FIGURE 37.23 Buttressing reinforced slope at McColl Superfund site.

had to span a portion of the completed cutoff wall. Due to concerns that the stress of the reinforced earth structure on the underlying soil-bentonite cutoff wall would lead to excessive deformation of the wall due to consolidation of the cutoff wall backfill, a flexible wall fascia was selected. As shown in Figure 37.23, a soldier pile wall was constructed to provide stability of the system during construction. The use of geosynthetic alternatives in this project was more suitable and cost effective than their conventional counterparts.

Glossary

Alloys, polymeric a blend of two or more polymers (e.g., a rubber and plastic) to improve a given property (e.g., impact strength).

Apparent opening size (AOS), O_{95} for geotextile, a property which indicates the diameter of the approximate largest particle that would effectively pass through the geotextile. At least 95% of the openings apparently have that diameter or are smaller as measured by the dry sieve test.

Chemical stability stability of a geosynthetic; ability to resist degradation from chemicals, such as acids, bases, solvents, oils and oxidation agents; and chemical reactions, including those catalyzed by light.

Chlorosulfonated polyethylene (CSPE) family of polymers that is produced by polyethylene reacting with chlorine and sulfur dioxide. Present CSPEs contain 25 to 43% chlorine and 1.0 to 1.4% sulfur.

Clogging movement by mechanical action or hydraulic flow of soil particles into the voids of fabric and retention therein, thereby reducing the hydraulic conductivity of the geotextile.

Cross-machine direction the axis within the plane of a fabric perpendicular to the predominant axis of the direction of production.

Cross-plane The direction of a geosynthetic that is perpendicular to the plane of its manufactured direction. Referred to in hydraulic situations.

Fiber basic element of fabrics and other textile structures, characterized by having a length at least 100 times its diameter or width that can be spun into a yarn or otherwise made into a fabric.

Filament yarn the yarn made from continuous filament fibers.

Filtration in geotextiles; the process of retaining soil in place while allowing water to pass from soil. In chemistry, removal of particles from a fluid stream.

Geocell a three-dimensional structure filled with soil, thereby forming a mattress for increased stability when used with loose or compressible subsoils.

Geocomposite a manufactured material using geotextiles, geogrids, and geomembranes in laminated or composite form. May or may not include natural materials.

Geogrid open grid structure of orthogonal filaments and strands of polymeric material used primarily for tensile reinforcement.

Geomembrane very low hydraulic conductivity synthetic membrane liners or barriers used with any geotechnical engineering related material so as to control fluid migration in a man-made project, structure, or system.

Geonet a geosynthetic consisting of integrally connected parallel sets of ribs overlying similar sets at various angles for planar drainage of liquids or gases.

Geopipe any plastic pipe used with foundation, soil, rock, earth, or any other subsurface related material as an integral part of a human-made project, structure, or system.

Geosynthetic a planar product manufactured from polymeric material used with soil, rock, earth, or other geotechnical engineering related material as an integral part of a constructed project, structure, or system.

Geosynthetic clay liner (GCL) factory-manufactured hydraulic barriers consisting of a layer of bentonite clay or other very low permeability material supported by geotextiles and geomembranes, and mechanically held together by needling, stitching, or chemical adhesives.

Geotextile any permeable textile used with foundation, soil, rock, earth, or any other geotechnical engineering-related material as an integral part of a constructed project, structure, or system.

Grab test in fabric testing, a tension test in which only a part of the width of the specimen is gripped in the clamps.

Gradient ratio the ratio of the average hydraulic gradient across the fabric and the 25 mm of soil immediately next to the fabric to the average hydraulic gradient across the 50 mm of soil between 25 and 75 mm above the fabric, as measured in a constant head permeability test.

Heat bonded thermally bonded by melting the fibers to form weld points.

Hot wedge common method of heat seaming thermoplastic geomembranes by a fusing process wherein heat is delivered by a hot wedge passing between the opposing surfaces to be bonded.

Hydraulic transmissivity for a geotextile or related product, the volumetric flow rate of water per unit width of specimen per unit gradient in a direction parallel to the plane of the specimen.

Index test a test procedure that may contain a known bias but which may be used to establish an order for a set of specimens with respect to the property of interest.

In-plane the direction of a geosynthetic that is parallel to its longitudinal, manufactured, or machine direction. Referred to in hydraulic situations.

Leachate liquid that has percolated through or drained from solid waste or other human-emplaced materials and contains soluble, partially soluble, or miscible components removed from such waste.

Liner a layer of emplaced materials beneath a surface impoundment or landfill that serves to restrict the escape of waste or its constituents from the impoundment or landfill.

Machine direction the direction in the plane of the fabric parallel to the direction of manufacture.

Mass per unit area the proper term to represent and compare the amount of material per unit area (units are or g/m^2) of a geosynthetic.

Monofilament a single filament of a fiber (normally synthetic).

Mullen burst hydraulic bursting strength of textiles.

Multifilament a yarn consisting of many continuous filaments or strands.

Needlepunched in geotextiles, mechanical bonding of staple or filament fibers with barbed needles to form a compact fabric.

Nonwoven fabric a textile structure produced by bonding or interlocking of fibers, or both, accomplished by mechanical, thermal, or chemical means.

Permittivity of geotextiles and related products, the volumetric flow rate of water per unit cross sectional area per unit head under laminar flow conditions, in the normal direction through a geotextile.

Plasticizer a plasticizer is a material, frequently solvent-like, incorporated in a plastic or a rubber to increase its ease of workability, its flexibility, or distensibility.

Polyester fiber generic name for a manufactured fiber in which the fiber-forming substance is any long-chain synthetic polymer composed of an ester of a dihydric alcohol and terepthalic acid.

Polyethylene a polyolefin formed by bulk polymerization (for low density) or solution polymerization (for high density) where the ethylene monomer is placed in a reactor under high pressure and temperature.

Polymer a macromolecular material formed by the chemical combination of monomers having either the same or different chemical composition. Plastics, rubbers, and textile fibers are all high-molecular-weight polymers.

Polyolefin a family of polymeric materials that includes polypropylene and polyethylene, the former being very common in geotextiles and the latter in geomembranes.

Polyvinyl chloride (PVC) a synthetic thermoplastic polymer prepared from vinyl chloride.

Quality assurance (QA) a planned system of activities whose purpose is to provide a continuing evaluation of the quality control program, initiating corrective action where necessary. It is applicable to both the manufactured product and its field installation.

Quality control (QC) actions that provide a means of controlling and measuring the characteristics of (both) the manufactured and the field installed product.

Separation the function of geosynthetics as a partition between two adjacent materials (usually dissimilar) to prevent mixing of the two materials.

Specification a precise statement of a set of requirements to be satisfied by a material, product, system, or service that indicates the procedures for determining whether each of the requirements is satisfied.

Spun-bonded fabrics fabric formed by continuous filaments that have been spun (extruded), drawn, laid into a web and bonded (chemical, mechanical, or thermal bonding) together in one continuous process.

Staple fibers fibers of short lengths; frequently used to make needlepunched nonwoven fabrics.

Subgrade intrusion localized aggregate penetration of a soft cohesive subgrade and resulting displacement of the subgrade into the cohesionless material.

Subgrade pumping the displacement of cohesive or low-cohesion fines from a saturated subgrade into overlying aggregate as the result of hydraulic forces created by transmittal of wheel-load stresses to the subgrade.

Survivability the ability of a geosynthetic to be placed and to perform its intended function without undergoing degradation.

Tensile strength the maximum resistance to deformation developed for a specific material when subjected to tension by an external force.

Trapezoid Tear Test test method used to measure the tearing strength of geotextiles.

Transmissivity for a geosynthetic, the volumetric flow rate per unit thickness under laminar flow conditions, in the in-plane direction of the fabric or geocomposite.

Ultraviolet degradation the breakdown of polymeric structure when exposed to natural light.

Woven geotextilea planar geotextile structure produced by interlacing two or more sets of elements such as yarns, fibers, rovings of filaments where the elements pass each other usually at right angles and one set of elements are parallel to the fabric axis.

Wide-width strip tensile test a uniaxial tensile test in which the entire width of a 200 mm wide specimen is gripped in the clamps and the gauge length is 100 mm.

Yarn a generic term for continuous strand strands (1 or more) of textile filaments, monofilaments, or slit form suitable for knitting, weaving, or otherwise intertwining or bonding to form a textile fabric.

Sources for these and other definitions of terms can be found in ASTM (1997) and Koerner (2005).

References

ASTM. 1995. *ASTM Standards on Geosynthetics*. Sponsored by ASTM Committee D-35 on Geosynthetics, Fourth Edition, 178p.

Bhatia, S.K. and Smith, J.L. 1996a. "Geotextile Characterization and Pore-Size Distribution: Part I. A Review of Manufacturing Processes," *Geosynthetics International*, 3, 85–105.

Bhatia, S.K. and Smith, J.L. 1996b. "Geotextile Characterization and Pore-Size Distribution: Part II. A Review of Test Methods and Results," *Geosynthetics International*, 3, 155–180.

Bhatia, S.K., Smith, J.L., and Christopher, B.R. 1996. "Geotextile Characterization and Pore-Size Distribution: Part III. Comparison of methods and Application to Design," *Geosynthetics International*, 3, 301–328.

Bouazza, A. 2002. Geosynthetic clay liners. *Geotextiles and Geomembranes*, 20, 1–17.

Bouazza, A., Zornberg, J.G., and Adam, D. 2002. "Geosynthetics in Waste Containment Facilities: Recent Advances." State-of-the-Art keynote paper, *Proceedings of the Seventh International Conference on Geosynthetics*, Nice, France, September 22–27, A.A. Balkema, Vol. 2, pp. 445–510.

Burson, B., Baker, A.C., Jones, B., and Shailer, J. 1997. "Development and Installation of an Innovative Vertical Containment System," *Proceedings of the Geosynthetics '97* Conference, Long Beach, California, March, Vol. 1, pp. 467–480.

Christopher, B.R. and Dahlstrand, T.K. 1989. *Geosynthetics in Dams — Design and Use*, Association of State Dam Safety Officials, Lexington, KY, 311 p.

Christopher, B.R. and Fisher, G.R. 1992. "Geotextile Filtration Principles, Practices and Problems," *Journal of Geotextile and Geomembranes*, Elsevier, 11, 4–6, 337–354.

Collins, P., Ng, A.S., and Ramanujam, R. 1998. Superfund Success, Superfast. *Civil Engineering, December*, 42–45.

Elias, V., Christopher, B.R., and Berg, R.R. 2001. *Mechanically Stabilized Earth Walls and Reinforced Soil Slopes*. Publication Number FHWA-NH-00-043, NHI-FHWA.

Giroud, J.P. 1996. "Granular Filters and Geotextile Filters," *Proceedings of Geofilters '96*, Montreal, pp. 565–680.

Giroud, J.P. with cooperation of Beech, J.F. and Khatami, A. 1993. *Geosynthetics Bibliography. Volume 1*. IGS, Industrial Fabrics Association International (IFAI) Publishers, St. Paul, MN, 781 p.

Giroud, J.P. with cooperation of Beech, J.F., Khatami, A., and Badu-Tweneboah, K. 1994. *Geosynthetics Bibliography. Volume 2*. IGS, IFAI Publishers, St. Paul, MN, 940 p.

Giroud, J.P., Zornberg, J.G., and Zhao, A. 2000. "Hydraulic Design of Geosynthetic and Granular Liquid Collection Layers." *Geosynthetics International*, Special Issue on Liquid Collection Systems, 7, 285–380.

Halse, Y., Koerner, R.M., and Lord, A.E., Jr. 1987. "Filtration Properties of Geotextiles Under Long Term Testing," *Proceedings of ASCE/Penn DOT Conference on Advances in Geotechnical Engineering*, Hershey, PA, pp. 1–13.

Hansbo, S. 1979. "Consolidation of Clay by Band Shaped Perforated Drains," *Ground Engineering*, July, 16–25.

Hendricker, A.T., Fredianelli, K.H., Kavazanjian, E., and McKelvey, J.A. 1998. Reinforcement Requirements at a Hazardous Waste Site. *Proceedings of the 6th International Conference on Geosynthetics*. IFAI, Atlanta, Vol. 1, 465–468.

Holtz, R.D., Christopher, B.R., and Berg, R.R. 1997. *Geosynthetic Engineering*. Bitech Publishers Ltd., Richmond, British Columbia, Canada, 452 p.

Holtz, R.D., Christopher, B.R., and Berg, R.R. 1998. *Geosynthetic Design and Construction Guidelines*, U.S. Department of Transportation, Federal Highway Administration, Washington DC, Report No. HI-95-038, 396 p.

Industrial Fabrics Association International. 1996. North American Market for Geosynthetics. 97 p.

Koerner, R.M. 2005. *Designing with geosynthetics*, 5th ed. Prentice Hall, 783 p.

Narejo, D., Koerner, R.M., and Wilson-Fahmy, R.F. 1996. "Puncture Protection of Geomembranes Part II: Experimental," *Geosynthetics International*, 3, 629–653.

Palmeira, E. and Fannin, J. 2002. "Soil-Geotextile Compatibility in Filtration." State-of-the-Art keynote paper, *Proceedings of the Seventh International Conference on Geosynthetics*, Nice, France, September 22–27, A.A. Balkema, Vol. 3, pp. 853–872.

Scuero, A. M., Vaschetti, G., Sembenelli, P., Aguiar Gonzalez, E., Bartek, P., Blanco Fernandez, M., Brezina, P., Brunold, H., Cazzuffi, D., Girard, H., Lefranc, M., do Vale, M., Massaro, C., Millmore, J., and Schewe, L. (2005). Geomembrane Sealing Systems for Dams. International Commission on Large Dams.

Vidal, H. 1969. "La Terre Armée." Annales de l'Institut Technique du Bâtiment et des Travaux Publics, Series: Materials (38), No. 259–260, pp.1–59.

Wilson-Fahmy, R.F., Narejo, D., and Koerner, R.M. 1996. "Puncture Protection of Geomembranes Part I: Theory," *Geosynthetics International*, 3, 605–628.

Zornberg, J.G. 2002. "Discrete Framework for Limit Equilibrium Analysis of Fibre-Reinforced Soil." *Géotechnique*, 52, 593–604.

Zornberg, J.G. (2005). "Advances on the Use of Geosynthetics in Hydraulic Systems." *Proceedings of the Nineteenth Geosynthetic Research Institute Conference* (GRI-19), Geosynthetics Institute, Las Vegas, NV, December 14–16, pp. 1–17 (CD-ROM).

Zornberg, J.G. and Weber, C.T. 2003. "Geosynthetics Research Needs for Hydraulic Structures" *Proceedings of the Seventeenth Geosynthetic Research Institute Conference*, Hot Topics in Geosynthetics IV, December 15–16, Las Vegas, Nevada, pp. 183–197.

Zornberg, J.G., Barrows, R.J., Christopher, B.R., and Wayne, M.H. 1995. "Construction and Instrumentation of a Highway Slope Reinforced with High Strength Geotextiles." *Proceedings of the Geosynthetics '95* Conference, Nashville, TN, February, Vol. 1, pp.13–27.

Zornberg, J.G., Sitar, N., and Mitchell, J.K. 1998. "Performance of Geosynthetic Reinforced Slopes at Failure." *Journal of Geotechnical and Geoenvironmental Engineering, ASCE*, 124, 670–683.

Zornberg, J.G., McCartney, J.S., and Swan, R.H. 2005. "Analysis of a Large Database of GCL Internal Shear Strength Results," *Journal of Geotechnical and Geotechnical Engineering, ASCE*, 131, 367–380.

Further Information

Koerner (2005) provides an excellent, well-illustrated overview of the different types of geosynthetics and their applications.

Holtz, Christopher and Berg (1997, 1998) provide well-documented practical design and construction information on the different uses of geosynthetic products.

Giroud et al. (1993, 1994) provide a two-volume comprehensive database on technical literature relative to geosynthetics, including technical papers from conferences, technical papers from journals, books, theses, and research reports.

Technical advances on geosynthetics are also published in the two official journals of the IGS: Geosynthetics International, and Geotextiles and Geomembranes. Similarly, the Geotechnical Fabrics Report (GFR), published by the Industrial Fabrics Association International (IFAI) provides updated information, including the annual Specifier's Guide, which offers a summary of the properties of products available in the geosynthetics market.

The ASTM Standards on Geosynthetics, sponsored by ASTM Committee D-35 on Geosynthetics (ASTM, 1995), provides information on the standard test procedures for the different types of geosynthetics.

The proceedings of the International Conferences on Geosynthetics, organized by the International Geosynthetic Society (IGS), offer a relevant source of information on the different topics related to geosynthetics. These international conferences are organized every four years. Equally relevant are the proceedings of conferences organized by the regional chapters of IGS. Finally, the proceedings of the series of conferences organized by the Geosynthetics Research Institute (GRI) provide information on specific topics relevant to geosynthetic design.

Geosynthetic manufacturers' literature is also a valuable source of information, which provides product-specific properties, suggested design methods, and recommended factors of safety.

34

Evapotranspirative Cover Systems for Waste Containment

Jorge G. Zornberg and
John S. McCartney
University of Texas at Austin

34.1 Introduction

The management of hazardous and municipal wastes may have important implications on groundwater quality. The current trend in waste management in the United States involves its disposal and isolation within containment facilities to minimize human and environmental contact. One of the key engineered components in municipal and hazardous waste containment systems is the cover system. The cover system is the surface culmination of a landfill, so it interacts closely with the atmosphere. Cover design and analysis involves concepts from various disciplines such as geotechnical engineering, environmental

engineering, soil science, agriculture engineering, climatology, biology, and hydrology. Integration of concepts from these various disciplines presents important challenges to researchers, designers, regulators, and stakeholders. This is particularly the case in evapotranspirative covers, the understanding of which relies heavily on the quantification of atmospheric processes at the land surface and of water flow though unsaturated soil.

The water balance components used to quantify the conservation of water mass in an engineered cover may include evaporation and plant transpiration (together referred to as evapotranspiration), precipitation, overland runoff, soil moisture storage, lateral drainage, and basal percolation. Basal percolation, an important variable to quantify the overall performance of landfill covers, is the volume of water that exits the lower boundary of the engineered cover with time. The water that cannot be removed from the cover by evapotranspiration or lateral drainage reaches the underlying waste mass, possibly mobilizing contaminants that may eventually reach the groundwater. Accordingly, one of the primary objectives of a landfill cover system is to control basal percolation. Additional objectives of landfill covers include accommodating differential settlements without compromising its performance, and controlling landfill gas release. In addition, the cover should remain stable under static and seismic conditions, minimize long-term maintenance, allow land re-use, and provide an aesthetic appearance.

The design of final cover systems for new municipal and hazardous waste containment systems in the United States is prescribed by the US Resource Conservation and Recovery Act (RCRA) Subtitles D and C, respectively. Federal- and state-mandated cover systems for municipal and hazardous waste landfills have endorsed the use of resistive barriers. Resistive cover systems involve a liner (e.g., a compacted clay layer) constructed with a low saturated hydraulic conductivity soil (typically 10^{-9} m/sec or less) to reduce basal percolation. Figure 34.1(a) shows the water balance components in a resistive system, in which basal percolation control is achieved by maximizing overland runoff. To enhance cover performance and lower construction costs, RCRA regulations allow the use of alternative cover systems if comparative analyses and field demonstrations can satisfactorily show their equivalence with prescriptive systems. Evapotranspirative covers are alternative systems that have been recently proposed and successfully implemented in several high-profile sites. Evapotranspirative covers are vegetated with native plants that survive on the natural precipitation and have been shown to be stable over long periods of time. Figure 34.1(b) shows the water balance components in an evapotranspirative cover system. Evapotranspiration and moisture storage are components that influence significantly the performance of this system. Internal lateral drainage may also be a relevant component in some cover types (capillary barriers on steep slopes). The novelty of this approach is the mechanism by which basal percolation control is achieved: an evapotranspirative cover acts not as a barrier, but as a sponge or a reservoir that stores moisture during precipitation events, and then releases it back to the atmosphere as evapotranspiration or lateral drainage. Silts and clays of low plasticity are the soils most commonly used in evapotranspirative covers, as they can store water while minimizing the potential for cracking upon desiccation.

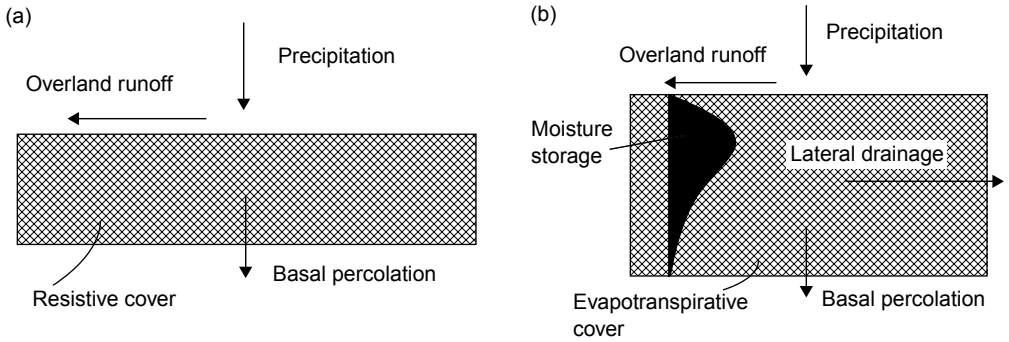

FIGURE 34.1 Water balance components: (a) in a resistive barrier and (b) in an evapotranspirative cover

Additional advantages of evapotranspirative covers over typical clay barrier systems include minimizing desiccation cracking, ease of construction, and low maintenance. Also, effective evapotranspirative covers can be constructed with a reasonably broad range of soils, which can lead to significant cost savings. The adequacy of evapotranspirative cover systems has been verified by field experimental assessments (Anderson et al., 1993; Dwyer, 1998), and procedures have been developed for quantitative evaluation of the variables governing their performance (Khire et al., 1999; Zornberg et al., 2003). The scope of this chapter includes: (i) basic hydraulic concepts for unsaturated soils relevant to evapotranspirative covers, (ii) types of evapotranspirative covers, (iii) design and modeling issues, (iv) field monitoring approaches, and (v) case studies.

34.2 Unsaturated Soil Hydraulic Concepts Relevant to Evapotranspirative Cover Performance

34.2.1 Water Flow through Unsaturated Porous Media

Designing a truly impermeable barrier (i.e., one leading to zero basal percolation) should not be within an engineer's expectations. Instead, the objective of the cover should be to minimize the basal percolation of water to acceptable levels. Quantification of the basal percolation is challenging as it involves analysis of water flow through unsaturated soils subject to complex atmospheric boundary conditions. Both air and water are present in the voids of unsaturated soils. The relative amounts of water and air in the soil, typically quantified on a volumetric basis, highly influence the soil hydraulic behavior. Figure 34.2 illustrates some of the common phase relationships used for the analysis of water flow processes in unsaturated soils. The volumetric moisture content θ, is defined as the ratio between the volume of water and the total control volume. The porosity n, which is the ratio between the volume of voids and the total control volume, corresponds to the volumetric moisture content at saturation (i.e., $n = \theta_s$). The degree of saturation S, commonly used to normalize the moisture content of a soil is the ratio between the volumetric moisture content and the porosity. Finally, the volumetric air content is the difference between the porosity and the volumetric moisture content.

In an unsaturated soil, water is held within the pores against the pull of gravity by a combination of adsorptive and capillary pressures (Olson and Langfelder, 1965). Adsorptive pressures are present in soils due to electrical fields and short-range attractive forces (van Der Waal forces) that tend to draw water toward the soil particles in highly plastic clays, where the net negative charges on water dipoles and surface of clay particles interact with the cations in the pore water. The capillary pressure is quantified as the difference between the pore air pressure and the pore water pressure. Water is a wetting fluid for most soil particles, which implies that the air-water menisci between individual soil particles are convex, tensioned membranes. Accordingly, the air pressure is greater than the water pressure, which has a negative magnitude. The adsorptive and capillary pressures are typically considered together as a single

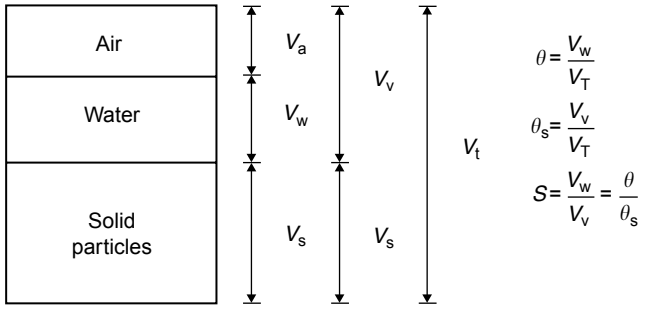

FIGURE 34.2 Volumetric phase diagram for unsaturated soils.

variable, referred to as the matric suction, ψ, which has units of pressure (kPa). The capillary rise in a pipette provides an analogy useful to assess the influence of pore sizes on the matric suction, given by the following expression

$$\psi = P_a - P_w = h_c \rho_w g = \frac{2\sigma_{aw} \cos\gamma}{R} \tag{34.1}$$

where P_a is the pore air pressure, P_w is the pore water pressure, h_c is the height of capillary rise in a pipette of radius R, ρ_w is the density of water, g is the acceleration of gravity, σ_{aw} is the surface tension between water and air, and γ is the wetting contact angle (typically 10° for quartz minerals). Equation 34.1 assumes that air is under atmospheric pressure ($P_a = 0$) and indicates that the suction is inversely proportional to the pore radius. Accordingly, for the same volumetric moisture content, a fine-grained soil (with comparatively small pore radii) will have a higher suction than a coarse-grained soil. The relationship between moisture content and suction is thus related to the pore size distribution of the soil as discussed in Section 34.2.2.

Flow of water through soils is driven by a gradient in the hydraulic energy, which is quantified by the fluid potential (energy per unit mass of water). The fluid potential is given by an expanded form of Bernoulli's equation:

$$\Phi = gz + \frac{1}{2}\left(\frac{v}{n}\right)^2 + \frac{-\psi}{\rho_w} + \frac{P_o}{\rho_w} \tag{34.2}$$

where Φ is the fluid potential, z is the vertical distance from the datum, v is the water discharge velocity, n is the porosity, and P_o is the osmotic suction. In Equation 34.2, the four terms on the right-hand side correspond to the potential energy, the kinetic energy, the energy due to the water pressure ($\psi = -P_w$ if $P_a = 0$), and the energy due to osmosis. The discharge velocity (v/n) is comparatively small, leading to a negligible kinetic energy component. The osmotic suction is typically considered constant throughout an evapotranspirative cover, and consequently does not lead to a contribution to the hydraulic gradient. As in the case of water-saturated soils, Darcy's law for unsaturated soils indicates that flow is driven by the gradient in total hydraulic potential. However, the available pathways for water flow in unsaturated soil decrease as the moisture content decreases (or as suction increases). This is quantified by the hydraulic conductivity function $K(\psi)$, which accounts for the decrease in conductivity with increasing suction (or decreasing moisture content). The K-function is discussed in Section 34.2.2.2. The discharge velocity through a soil in the vertical direction z can be estimated using Darcy's law and Equation 34.2, as follows:

$$v = \frac{Q}{A} = -\frac{K(\psi)}{g}\frac{\partial\Phi}{\partial z} = -K(\psi)\frac{\partial}{\partial z}\left(1 - \frac{1}{\rho_w g}\frac{\partial\psi}{\partial z}\right) \tag{34.3}$$

where Q is the volumetric flow rate, and A is the area of soil perpendicular to the flow direction. Figure 34.3 shows a control volume of thickness dz for one-dimensional (1-D) water flow through a soil layer with thickness L using the base of the soil layer as datum. The continuity principle in this control volume can be expressed by:

$$\frac{\partial\theta}{\partial t} = -\frac{\partial v}{\partial z} \tag{34.4}$$

where the left-hand side represents the change in moisture storage in the control volume, and the right-hand side represents the change in flow rate across the control volume. Substitution of Equation 34.3 into Equation 34.4 leads to the governing equation for 1-D flow through unsaturated porous materials, referred to as Richards' equation:

$$\frac{\partial\theta}{\partial\psi}\frac{\partial\psi}{\partial t} = \frac{\partial}{\partial z}\left[K(\psi)\left(1 - \frac{1}{\rho_w g}\frac{\partial\psi}{\partial z}\right)\right] \tag{34.5}$$

Richards' equation is a coupled, nonlinear parabolic equation, which can be solved using finite differences or finite elements. Numerical solutions to Richards' equation can be challenging because the constitutive function [$K(\psi)$ and $\theta(\psi)$] are highly nonlinear and may have undefined or zero derivatives. Further,

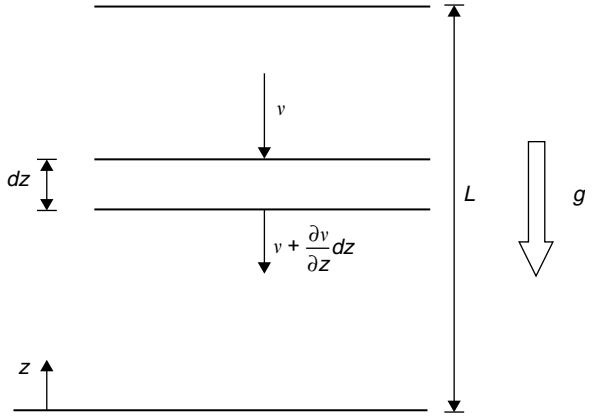

FIGURE 34.3 Control volume for vertical flow through an evapotranspirative cover

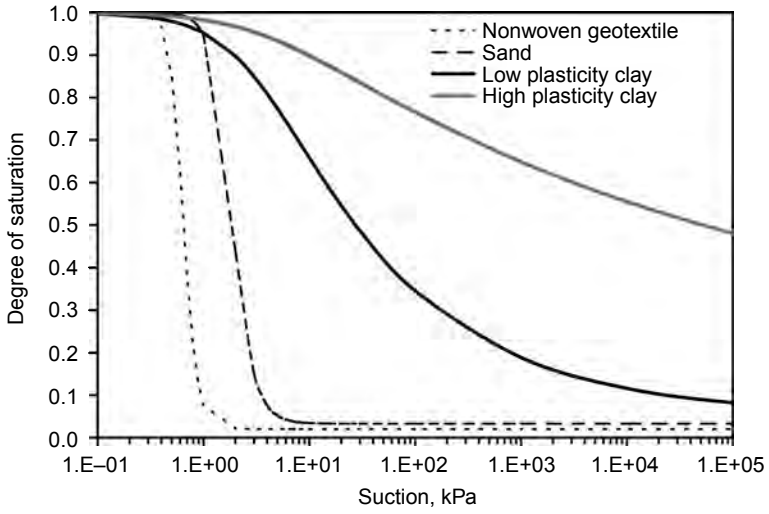

FIGURE 34.4 Typical SWRCs for different geotechnical materials

selection of boundary conditions may not be straightforward for several practical problems. Boundary conditions typically used for evapotranspirative covers include atmospheric flux boundary conditions at the surface (infiltration or evaporation), and unit hydraulic gradient (i.e., zero change in suction with depth) at the base. A discussion on the boundary conditions for evapotranspirative covers may be found in Fayer and Jones (1990). Additional difficulties for solving water flow problems for unsaturated soils arise when considering moisture removal from plant roots, desiccation cracking, animal intrusion, and volumetric changes.

34.2.2 Unsaturated Soil Hydraulic Properties

34.2.2.1 Soil Water Retention Curve

The moisture storage of the soil is an important performance variable of evapotranspirative covers. The moisture storage is typically quantified using the relationship between volumetric moisture content and soil suction, referred to as the Soil Water Retention Curve (SWRC). Figure 34.4 shows the SWRCs for different geotechnical materials. The coarser materials (sand and geotextile) show a highly nonlinear

response, with a significant decrease in moisture content (or degree of saturation) in a narrow range in suction. The fine-grained materials (silt and clay) show a more gradual decrease in moisture content with increasing suction. The nonlinearity observed in these relationships is partly caused by the range of pore size distributions for these materials. An important characteristic in a SWRC is the air entry value. During initial drying of a fully saturated soil specimen water does not flow from the soil until the suction corresponding to the air entry value is reached. When this suction is reached, air enters the specimen and the moisture content decreases. Once the air entry value is reached, the moisture content drops from saturation to a value that remains approximately constant with increasing suction. This low moisture content value is often referred to as the residual moisture content. The residual condition occurs because the water becomes occluded (or disconnected) within the soil pores, with no available pathways for water flow to occur.

The SWRC for a given material is not only sensitive to the pore size distribution, but also the soil mineralogy, density, and pore structure (Hillel, 1988). The SWRC can show significantly different wetting and drying paths, a phenomenon referred to as hysteresis (Topp and Miller, 1966; Kool and Parker, 1987). During drying, the largest pores drain first, followed by the smaller pores. During wetting, the smaller pores fill first, but the presence of large pores may prevent some from filling. Also, wetting of a dry media often leads to entrapment of air in the larger pores, which prevents saturation of the media unless positive pressure is applied to the water. Air entrapment causes the wetting path to be relatively flat for high suctions (e.g., over 100 kPa), with a steep increase in volumetric moisture content at lower suctions.

Several techniques are available to determine the SWRC experimentally (Klute et al., 1986; Wang and Benson, 2004). Two main groups of techniques have been used to define the SWRC. The first group of techniques ("physical" techniques) involves an initially water-saturated material from which water is slowly expelled by imposing a suction to a specimen boundary. Flow continues until it reaches a condition at which the moisture content and suction are in equilibrium. The most commonly used physical technique is the axis translation technique. A common test that is based on this technique is the pressure plate test (Figure 34.5(a)), which involves placing a soil specimen on a high air-entry ceramic plate and applying air pressure to the specimen. The air pressure causes the pore water to pass through the ceramic plate since the water pressure on the effluent side of the plate is kept at atmospheric pressure (zero). At equilibrium, the air pressure corresponds to the suction. The outflow volume is measured using a constant head Mariotte bottle. This approach is repeated for successively higher pressures that gradually dry the specimen, after which the pressure may be decreased to measure the wetting behavior. At the end of the testing, the gravimetric moisture content may be measured destructively, and the moisture content at each pressure increment can be back-calculated from the outflow measurements. Additional details can be found in the ASTM standard for SWRC determination (ASTM D6836 2002). Another technique, the hanging column, is shown in Figure 34.5(b). This test also involves a ceramic plate, but connects the bottom of the plate to a manometer tube. A negative water pressure is imposed on the water level in the ceramic plate by holding the manometer tube beneath the plate.

The second group of techniques ("thermodynamic" techniques) involves allowing water to evaporate from a specimen in a closed chamber under controlled relative humidity. The relative humidity is controlled by allowing water to evaporate from a saturated salt solution placed within the chamber, as shown in Figure 34.5(c). Another commonly used thermodynamic technique is the chilled mirror

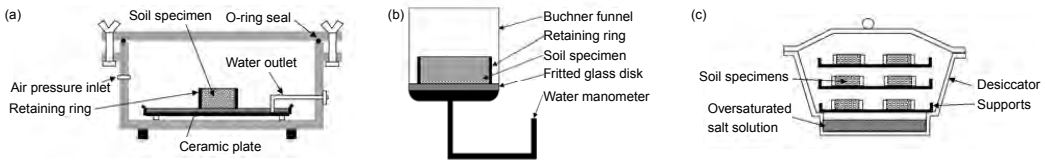

FIGURE 34.5 Conventional methods to determine the SWRC: (a) pressure plate; (b) hanging column; and (c) saturated salt solutions.

hygrometer (Wang and Benson, 2001). This device infers the total soil suction (matric and osmotic) by measuring the vapor pressure in the soil, which is related to the temperature at which moisture condenses on a mirror. When condensation occurs, a change in the optical properties of the mirror is detected. In general, physical techniques are used for relatively low suctions (e.g., under 1500 kPa), while thermodynamic techniques are used for higher suctions.

Conventional techniques to define the SWRC require significant time to obtain limited data. For example, determination of the SWRC for a high-plasticity clay specimen may take several months. Also, conventional determination methods require the use of several specimens and destructive measurement of moisture content. Problems specific to SWRC testing involve diffusion of air across porous ceramics, lack of control of volume change during drying and wetting (e.g., Cabral et al., 2004), and inability to impose a stress state representative of field conditions.

Centrifugation can be used to alleviate shortcomings of conventional characterization of the SWRC. Centrifugation increases the body forces on a porous media, accelerating fluid flow as time increases quadratically with g-level. Centrifuges were first used in the early 1930s to define the SWRC by soil scientists and petroleum engineers (Gardner, 1937; Hassler and Bruner, 1945). Saturated specimens can be placed upon a saturated ceramic plate that conducts only liquid. During centrifugation, the increased body force causes water to exit the specimen through the ceramic while air enters the surface of the specimen. The suction profile within the specimen can be defined if the bottom boundary is maintained saturated (zero suction). The suction distribution obtained at equilibrium (i.e., when flow ceases) is:

$$\psi(r) = \frac{\rho_w \omega^2}{2}[r_0^2 - r^2] + \psi(0) \tag{34.6}$$

where r_0 is the outer radius of the centrifuge specimen, r is the distance toward the center of rotation with a datum at the outer radius, ω is the angular velocity, and $\psi(0)$ is the suction at the bottom boundary of the specimen (zero if a saturated ceramic plate is used as the bottom boundary condition). Analytical techniques can be used to associate the average moisture content (measured destructively) with the suction at the soil surface (Forbes, 1994).

A SWRC is typically quantified by fitting experimental data to power law, hyperbolic, or polynomial functions (Brooks and Corey, 1946; van Genuchten, 1980; Fredlund and Xing, 1994). Although the Brooks and Corey (1946) model is able to represent a sharp air entry suction, the van Genuchten (1980) model is most commonly used in numerical analyses because it is differentiable for the full range of suctions. The van Genuchten model is given by:

$$\theta = \theta_r + (\theta_s - \theta_r)[1 + (\alpha\psi)^N]^{-(1-(1/N))} \tag{34.7}$$

where θ_r is the residual moisture content, θ_s is the saturated moisture content (porosity), and α (units of kPa^{-1}) and N (dimensionless) are fitting parameters. Preliminary estimates of the SWRC could be obtained using databases that rely on the granulametric distribution of soils (Fredlund and Xing, 1994).

34.2.2.2 Hydraulic Conductivity Function

The relationship between hydraulic conductivity and suction, also referred to as the K-function, provides a measure of the increased impedance to moisture flow with decreasing moisture content. The saturated hydraulic conductivity K_s provides a measure of the minimum impedance to moisture flow through soil. Figure 34.6 shows K-functions for different geotechnical materials. Near saturation, the coarser materials (sand and geotextile) have high hydraulic conductivity, while the fine-grained materials (silt and clay) have lower hydraulic conductivity. However, as the soil dries, the coarse materials end up being less conductive than the fine-grained materials. That is, as the fine-grained materials can retain more water in the pores as suction increases, they still have available pathways for water flow, and are thus more conductive than coarser materials. The superior performance in arid climates of evapotranspirative covers relative to conventional resistive covers can be attributed to the lower unsaturated hydraulic conductivity of the selected cover soils.

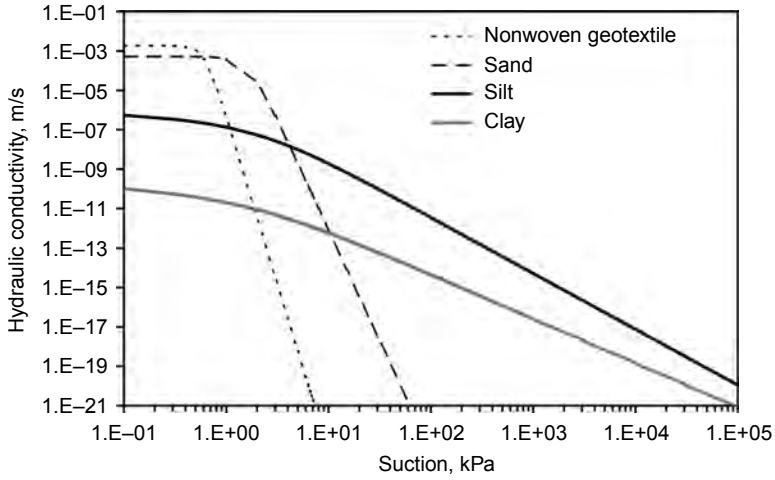

FIGURE 34.6 Typical K-functions for different geotechnical materials.

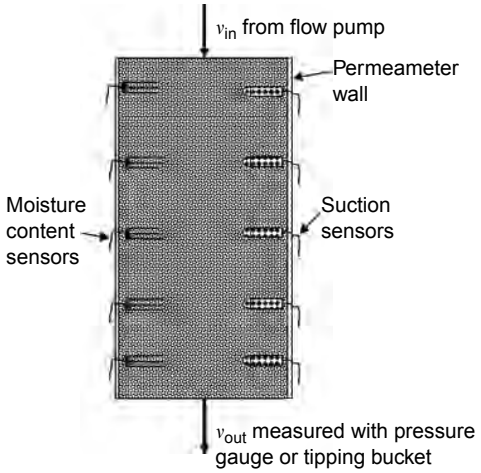

FIGURE 34.7 Parameter set up for measurement of K-function.

Conventional methods used to define the K-function are costly, time consuming, and prone to experimental error. Accordingly, the K-functions (e.g., such as those in Figure 34.6) are often predicted based on pore size distributions such as van Genuchten–Mualem model (1980), as follows:

$$K(\theta) = K_{sat}\sqrt{\frac{\theta-\theta_r}{\theta_s-\theta_r}}\left[1-\left(1-\left(\frac{\theta-\theta_r}{\theta_s-\theta_r}\right)^{1-N}\right)^{1/(1-N)}\right]^2 \tag{34.8}$$

$K(\psi)$ can be defined by substituting Equation 34.7 for θ into Equation 34.8. Other predictive relationships for the K-function are given by Burdine (1953) and Campbell (1974).

Several techniques have been proposed for direct determination of the K-function in the laboratory (Benson and Gribb, 1997). Conventional techniques to measure the K-function involve flow of liquid through a specimen confined within a permeameter. Flow is applied using either ceramic plates or flow pumps. Figure 34.7 shows a typical permeameter setup used to measure the hydraulic conductivity (Meerdink et al., 1996; Lu and Likos, 2005; McCartney et al., 2005b). Permeameters have differed in

specimen confinement and size, control of boundary conditions, and availability of instrumentation. The K-function can be estimated using steady or transient flow processes. During steady moisture infiltration with a deep water table, a unit hydraulic gradient (e.g., $i = 1$) is typically observed in the soil profile, sufficiently far from a water table boundary. Accordingly, suction does not change with depth and water flow is driven only by gravity. In this case, the hydraulic conductivity equals the imposed steady-state discharge velocity. Additional points are obtained by changing the imposed flow. During transient flow processes, the suction and moisture content profiles are measured as a function of depth and time, and the K-function can be estimated using the instantaneous profile method (Watson, 1966; Olson and Daniel, 1979; Meerdink et al., 1996). While techniques based on transient processes yield more information about the K-function, steady state techniques provide more reliable information. As for the SWRC, conventional techniques used to define the K-function require significant time to obtain limited data. Problems specific to K-function testing include boundary effects on the flow process, difficulties in uniformly distributing water from flow pumps to the specimen, and tedious testing procedures.

To alleviate these shortcomings, centrifuge testing has been used to define the K-function in geotechnical projects involving the design of ET covers (Zornberg et al., 2003; Dell'Avanzi et al., 2004). Nimmo et al. (1987) developed the Internal Flow Control Steady-State Centrifuge (IFC-SSC) method, which uses a system of reservoirs to control the fluid flow rate and suction at the upper and lower surfaces of a specimen. Conca and Wright (1994) developed the Unsaturated Flow Apparatus (UFA), which uses a sophisticated rotary joint to a low fluid flow rate into the specimen. The UFA uses open-flow centrifugation, which does not impose a suction value on the specimen. For steady state conditions, the SSC and UFA use Darcy's law to determine the K-function:

$$K(\psi) = \frac{-v}{[-(1/(\rho_w g))(d\psi/dz) - ((\omega^2 r)/g)]} \tag{34.9}$$

where v is the imposed discharge velocity. Points on the K-function curve are defined using Equation 34.9 after reaching steady state flow conditions. The SSC and UFA do not allow the direct monitoring of the relevant variables (suction, moisture, discharge velocity) in-flight during testing. If the suction gradient in Equation 34.9 is assumed to be negligible, the hydraulic conductivity becomes inversely proportional to ω^2. The SSC and UFA centrifuges must be periodically stopped to measure the specimen mass to ensure steady state flow, and the moisture content must be measured destructively at the end of the test.

Although the SSC and UFA allow a faster testing time than conventional K-function testing methods, their shortcomings led to the development of an improved centrifuge device, referred to as the Centrifuge Permeameter for Unsaturated Soils (CPUS) (McCartney and Zornberg, 2005a). This device incorporates the use of a low-flow hydraulic permeameter and a high-g centrifuge capable of continuously, non-destructively, and non-intrusively measuring suction, moisture content, and fluid flow rate in a single specimen during centrifugation. Accordingly, CPUS allows an expedited determination of both the SWRC and K-function from a single specimen in a single test. Measuring the SWRC and K-function during a flow process is consistent with actual flow problems, unlike conventional techniques such as the axis-translation technique. Figure 34.8(a) shows a view of the CPUS centrifuge and Figure 34.8(b) shows a schematic view of the CPUS permeameter and its instrumentation layout. A special low-flow fluid union is used to supply fluid from the stationary environment to the rotating specimen within the centrifuge. CPUS facilitates the use of experimentally obtained, rather than theoretically derived hydraulic properties in the design of evapotranspirative cover systems.

34.3 Types of Evapotranspirative Covers

34.3.1 Monolithic Covers

Monolithic covers are evapotranspirative covers that consist of a single soil layer placed directly over the waste (Zornberg et al., 2003). Figure 34.9a shows a schematic view of a monolithic soil cover. The soil layer

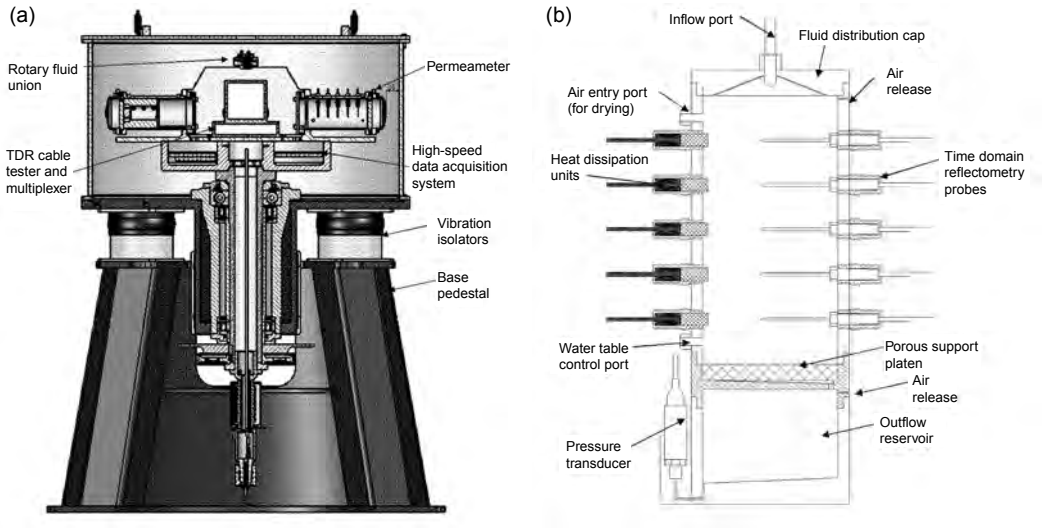

FIGURE 34.8 Centrifuge parameter for unsaturated soils: (a) centrifuge layout and (b) Permeameter.

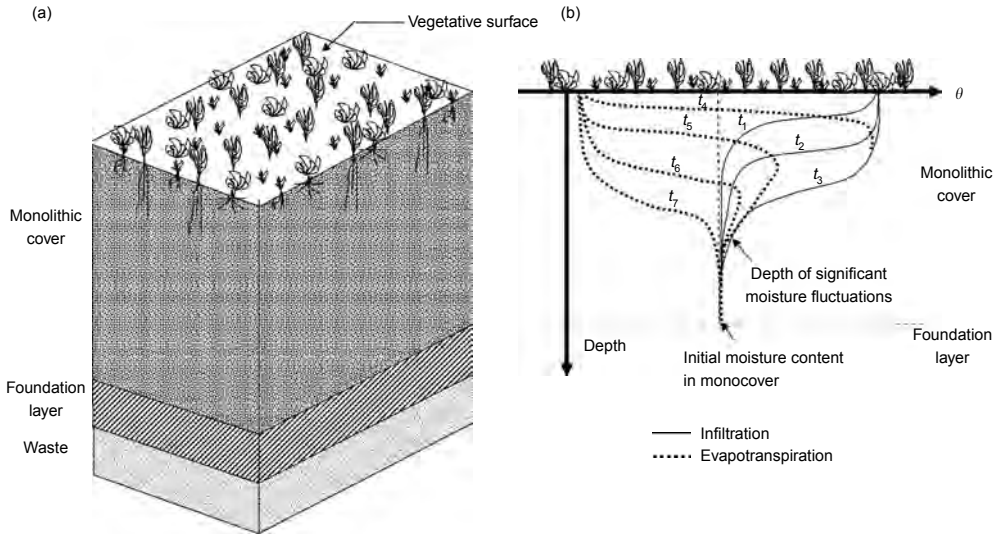

FIGURE 34.9 Monolithic cover: (a) soil profile and (b) typical seasonal moisture content fluctuations.

acts both as a substrate for vegetation and a hydraulic barrier. A foundation layer consisting of the same soil type is typically used to provide a level surface above the waste. Early research focused on investigation of the long-term behavior of natural soil layers in arid regions, assuming that the behavior is analogous to that of an engineered monolithic cover (Waugh et al., 1994). These studies found that moisture content fluctuations in natural analogues in recent geologic history are typically confined to the upper few feet of soil, indicating the adequacy of monolithic covers as an acceptable long-term solution to waste disposal.

The major aspects in monolithic covers are the proper characterization of the hydraulic properties (K-function and SWRC) of the soils as well as the determination of the appropriate thickness of the engineered soil cover. Figure 34.9b shows schematic moisture profiles, illustrating typical seasonal fluctuations in a properly performing monolithic cover. The moisture profiles illustrate wetting during infiltration events and subsequent drying due to evapotranspiration. Although some moisture fluctuations

are expected to reach the base of the cover in extreme events, most of the moisture fluctuations are expected to take place only within the upper portion of the cover. Monolithic cover design requires selection of the cover thickness and soil moisture storage necessary to keep the basal percolation below a minimum allowable (design) value, given the expected weather conditions for a site.

The soil moisture storage of a cover can be calculated as the integral of the volumetric moisture content profile with depth. The upper bound on soil moisture storage depend on the shape of the SWRC. The greater the moisture retained in a soil for the suction values expected in the field, the greater the moisture storage. A parameter that has been used to quantify the moisture storage is the field capacity, which is defined as the threshold moisture content value above which the soil no longer retains water by capillarity under the effects of gravity (Zornberg et al., 1999). When water is added to a soil that is at field capacity, drainage occurs. The field capacity may be obtained from infiltration tests, although a generally accepted value for silt and low plasticity clay soils is the moisture content corresponding to a suction of 33 kPa (Nachabe, 1998; Meyer and Gee, 1999). The storage capacity of a monolithic cover can be preliminarily estimated by multiplying the volumetric moisture content at field capacity (obtained using the SWRC) by the cover thickness.

34.3.2 Capillary Barriers

Capillary barriers are evapotranspirative covers that consist of a layered soil system typically involving a fine-grained soil (silt, clay) placed over a coarse-grained material (sand, gravel, nonwoven geotextile). Capillary barriers use the contrast in hydraulic properties between the fine- and coarse-grained soils to enhance the ability of the fine-grained material to store moisture (Shackelford et al., 1994; Stormont and Anderson, 1999; Khire et al., 1999; 2000). Figure 34.10a and Figure 34.10b show SWRCs and K-functions for sand (coarse-grained component), and low plasticity clay (fine-grained component). The capillary break concept relies on the continuity of suction, even at the interface between two different materials. Figure 34.10a shows that when a clay–sand system is at an initially high suction (e.g., 1000 kPa), the clay has a degree of saturation of 0.2 while the underlying sand is at residual moisture content. Figure 34.10b indicates that at this high suction, the clay has a hydraulic conductivity of approximately 1×10^{-13} m/sec while the sand has an even higher impedance to flow. Consequently, if moisture infiltrates into the fine-grained material after a precipitation event and reaches the interface with the coarse-grained material it can only progress into the coarse-grained material at a very slow rate. Consequently, water will accumulate at the interface until the suction at the interface reaches a value at which the hydraulic conductivity of the coarse grained material is no longer below that of the fine-grained material (3.0 kPa in Figure 34.10b). This suction value is referred to as the breakthrough suction. A breakthrough suction of 3.0 kPa is significantly below the suction corresponding to field capacity (typically considered at 33 kPa for clay), which indicates that the degree of saturation in the clay will be relatively high (95%) when breakthrough occurs. For suction values less than that corresponding to field capacity, water would have drained downwards by gravity had the capillary break not been present. When the breakthrough suction is reached, leakage is observed in the coarse-grained layer at a rate approaching that corresponding to the saturated hydraulic conductivity of the barrier layer.

Figure 34.10c shows a schematic view of a capillary break cover. Similar to the monolithic cover, the soil layer acts both as a substrate for vegetation and a hydraulic CRL (or capillary retention layer, CRL). However, a coarse-grained material (capillary break layer, CBL) is placed over the foundation material to create a capillary break at the interface between the CRL and the CBL). Figure 34.10d shows schematic moisture profiles illustrating the expected seasonal fluctuations in a properly performing capillary break cover. Unlike the monolithic cover, the moisture front can reach the bottom of the barrier layer without resulting in basal percolation, provided that the moisture at the interface does not exceed the breakthrough value. An important benefit of capillary breaks is that the moisture storage within the fine-grained soil can exceed its freely draining state (field capacity). Consequently, more water can be stored in a capillary break cover than in a monolithic cover of equivalent thickness. Alternatively, a thinner fine-grained layer can be used in a capillary break cover to obtain the same moisture storage as in a monolithic cover. The magnitude

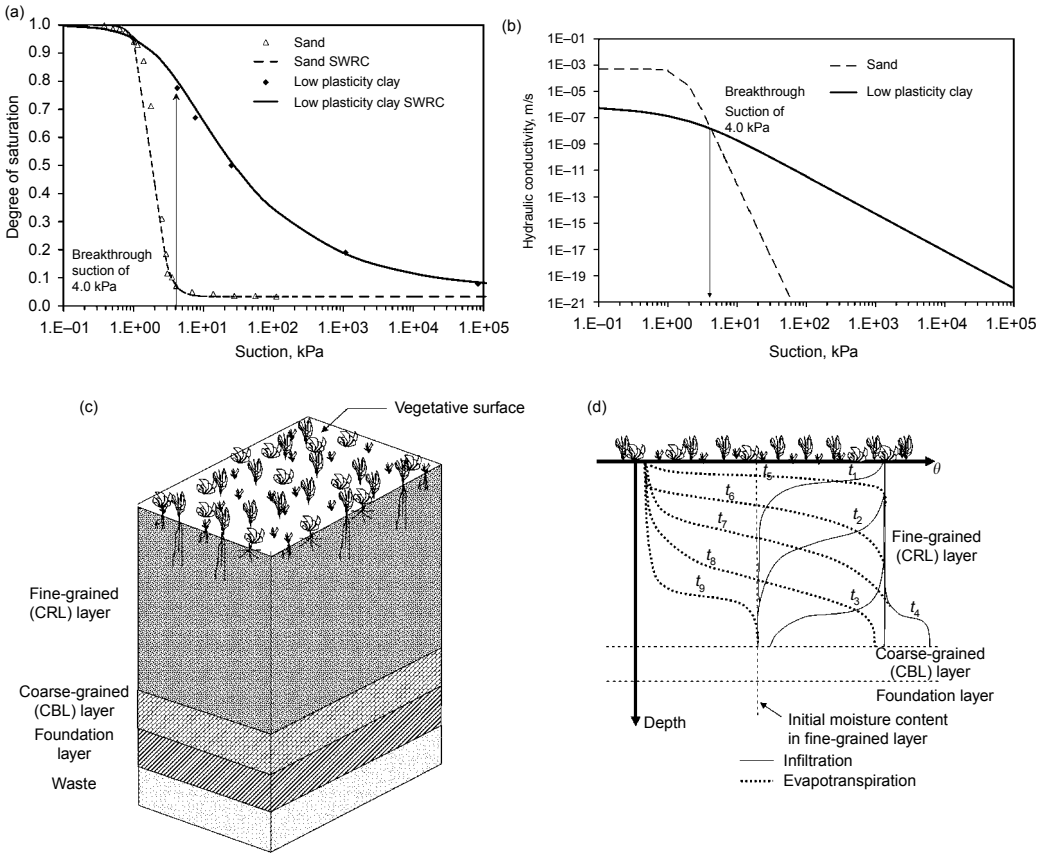

FIGURE 34.10 Capillary barrier details: (a) conceptual SWRC illustration of the capillary break effect; (b) conceptual K-function illustration of capillary break effect; (c) capillary break soil profile; and (d) typical seasonal moisture content fluctuations.

and long-term changes in the conditions leading to breakthrough are aspects under current investigation, especially in inclined covers (Parent and Cabral, 2004). Inclined covers may experience lateral diversion, which leads to greater moisture contents in the lower portion of a slope, resulting in a greater likelihood for breakthrough. Conservatism should be used in capillary barrier design, as these barriers have typically been reported to experience breakthrough during spring snowmelt when plant evapotranspiration is at a minimum (Khire et al., 1999; 2000). In addition, preferential flow through larger pores may lead to significant variability in the breakthrough suction (Kampf and Holfelder, 1999).

34.3.3 Anisotropic Barriers

Anisotropic barriers are similar to capillary barriers, but their design accounts for the internal lateral drainage through one or more drainage layers resulting from the inclination of the cover (Stormont, 1995; Bussiere et al., 2003; Parent and Cabral 2005). Figure 34.11a shows a schematic view of an anisotropic barrier. Anisotropic layers typically involve a soil vegetation substrate overlying a coarse-grained drainage layer, which are in turn underlain by a primary barrier layer and a second coarse-grained layer to provide a capillary break. The coarse-grained drainage layer functions both as a capillary break to the vegetation substrate and as a drainage layer for breakthrough water. The water collected by the drainage layer, along with moisture migrating laterally within the vegetation substrate is typically diverted to a ditch before a significant amount of water can infiltrate into the primary barrier. Figure 34.11b shows moisture profiles

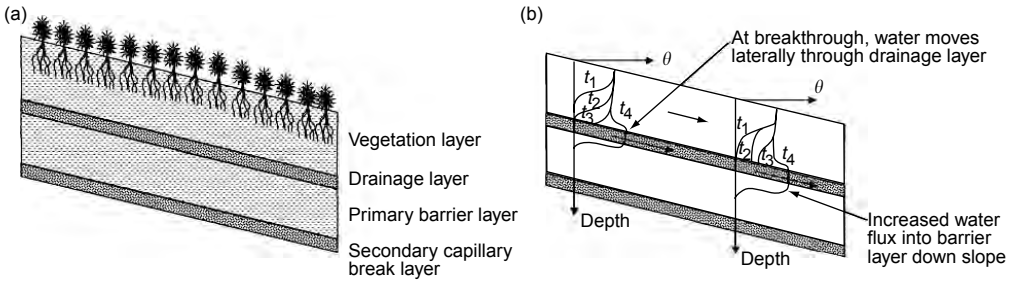

FIGURE 34.11 Anisotropic barrier: (a) soil profile and (b) typical moisture content fluctuations during infiltration.

illustrating the expected trends along the length of an anisotropic barrier during a wet season. The capillary break at the drainage layer increases the moisture storage capacity of the vegetative substrate. Infiltration of water into the barrier layer generally occurs toward the toe of the slope due to water accumulation from infiltration and lateral drainage. Design of anisotropic covers is more complex than that of monolithic or capillary break covers due to the need to quantify the required hydraulic properties for the layered profile as well as the volume of laterally diverted water. Field comparisons between the performance of test-scale capillary break, anisotropic, and monolithic covers performed by Dwyer (1998) indicate that the anisotropic cover performed well compared to the other covers for the same weather conditions over a five-year monitoring program. However, its construction was the most difficult of the three covers.

34.4 Relevant Issues for Design of Evapotranspirative Covers

34.4.1 Design Strategies

Despite the conceptual simplicity of evapotranspirative covers, their design is not trivial and typically involves numerical and field demonstration components. The design of an evapotranspirative cover involves the identification of performance criteria that are used to evaluate the suitability of different design alternatives. This phase typically requires close interaction between the designer, site stakeholders, and local regulators. The goal is to identify the criteria that will provide for human safety, constructability, and cost effectiveness. The design process typically involves identification of different cover design alternatives. This includes: (i) identification of suitable local borrow soil sources, (ii) characterization of the hydraulic properties of pre-selected soils under different placement conditions, (iii) determination of the cover geometry, (iv) identification of site-specific critical meteorological conditions, and (v) identification of suitable plant communities and vegetative cover properties. Design typically involves use of numerical models to predict the cover performance and field demonstrations aimed at evaluating the different design alternatives. Performance monitoring programs have been typically implemented after construction to verify the adequacy of the selected design alternative. Recent developments in evapotranspirative cover design have employed decision analysis, statistical characterization of design variables, and cost estimations to identify the optimal combination of performance variables. Such design approaches may help optimize the collection of laboratory data, identify if a site-specific field testing program is necessary, and quantify the risk of failure associated with design alternatives.

34.4.2 Performance Criteria and Regulatory Issues

Evapotranspirative covers are considered alternative covers and, as such, their design involves comparison of their performance with that of prescriptive cover systems (i.e., equivalency demonstration). Development of suitable performance criteria for ET cover systems generally involves equivalence demonstration with prescriptive covers (Morris and Stormont, 1997; McCartney and Zornberg, 2002; Albright et al., 2004). Because of the site-specific interactions between an evapotranspirative cover and the

local climate and environment, performance criteria for evapotranspirative covers must account for site-specific conditions. This section outlines different types of performance criteria that have been put forth for evapotranspirative covers. The type of performance criteria will impact both the design procedures and the methods of post-closure monitoring.

Determination of a percolation criterion has been approached from two different perspectives, at least in recent evapotranspirative cover projects in the United States. The first involves defining a *quantitative* maximum value of basal percolation (e.g., expressed in mm/year) that should not be exceeded. The second involves a *comparative* approach aiming at achieving a basal percolation value in the evapotranspirative cover that is smaller than that through a prescriptive cover under the same weather conditions.

The maximum basal percolation value (quantitative percolation criterion) is typically defined in agreement with regulatory agencies, yet it should be based on actual performance data from prescriptive type covers or on the results of verified numerical models. A quantitative criterion establishes that the basal percolation through the evapotranspirative cover, P_e (mm/year), should be less than the Maximum Quantitative Percolation Value, MQPV (e.g., mm/year), deemed to satisfy equivalence, as follows:

$$P_e < \text{MQPV} \tag{34.10}$$

where MQPV is a predefined criterion and P_e is determined from field monitoring and from numerical simulations. The choice of a quantitative percolation criterion implies that the cover must be designed for a wide range of possible meteorological conditions to ensure fulfillment of the criterion for worst case scenarios. On the other hand, if the MQRV is selected conservatively, the cover design may lead to unrealistically high material and construction costs.

A comparative percolation criterion for evapotranspirative covers involves defining the maximum ratio between the basal percolation through an evapotranspirative cover and that through a prescriptive cover. This percolation criterion recognizes that the performance of the evapotranspirative cover should be compared to that of a resistive cover under the same meteorological conditions. Specifically, the basal percolation through the evapotranspirative cover (P_e) should be less than that through the prescriptive cover (P_p), affected by the Maximum Comparative Percolation Ratio (MCPR) established for the project. That is, equivalence is deemed satisfied when the following condition is fulfilled:

$$P_e < \text{MCPR} \cdot P_p \tag{34.11}$$

where MCPR is dimensionless and P_e and P_p are basal percolation values (e.g., in mm/year). Adopting an MCPR of 1.0 implies that the evapotranspirative cover should perform better than a prescriptive cover under the same weather conditions. The methods used to define basal percolation values P_e and P_p may involve the use of a numerical model or of monitored field test plots. The first approach may not account for factors that are not adequately modeled using unsaturated flow models such as desiccation, surface settlement, animal burrowing, and fingering. The second approach may result in additional costs and may not account for critical weather conditions and long-term factors.

Performance criteria may also involve interpretation of the moisture profiles in the cover rather than quantification of percolation values. Specifically, quantitative criteria can involve comparison of the moisture storage within the cover with a certain threshold value. Similarly, criteria may involve comparison of the moisture at the base of the cover with a certain threshold moisture value (that can in turn correspond to a maximum value of $K(\theta)$ calculated from Equation 34.8). Ideally, performance criteria would involve interpretation of both basal percolation and moisture profile information (McCartney and Zornberg, 2002).

34.4.3 Important Design Variables

34.4.3.1 Soil Hydraulic Properties

The soil hydraulic properties relevant to the performance of evapotranspirative covers include the saturated hydraulic conductivity (K_s), the soil-water retention curve (SWRC), and the K-function.

Determining the required soil hydraulic properties is a challenging aspect of evapotranspirative cover design. Target values of the hydraulic properties are typically selected based on the required cover performance and on the expected weather conditions at the site. An important difficulty in the methods used to evaluate hydraulic properties in the laboratory is their high sensitivity to sample preparation and testing procedures. For example, the relative compaction of the soil and its compaction moisture content will typically affect the soil hydraulic properties. Finally, the differences between hydraulic properties determined in the laboratory and those in the field add to the difficulty in soil characterization. In addition to specimen preparation variability, the hydraulic properties in the field may change with time due to hysteresis (different behavior during wetting and drying), soil cracking, settlement, plant or animal intrusion, and erosion.

34.4.3.2 Cover Geometry

Cover geometry variables include the thickness of the cover, as well as the cover inclination. As the performance of the soil cover depends on its capacity to store liquid, a thicker cover will have a higher moisture storage capacity. The slope of the cover will impact its stability, the amount of water drained laterally, as well as the amount of overland runoff during precipitation events. Some evapotranspirative covers have been constructed with significantly high slope inclinations (as high as 1.5H:1V). This is the case of the OII landfill in Pomona, California (see Section 34.6.2). Steep slopes may require stabilization to account for seismic and static stability.

34.4.3.3 Critical Meteorological Variables

Critical meteorological conditions are site specific and play a significant role in the selection of the required soil properties, cover thickness, and slope inclination. A general guideline is that evapotranspirative covers are suitable for regions in which the potential evapotranspiration is greater than the precipitation. An important aspect of the design process involves identification of a worst-case precipitation record. Multi-year records must be obtained to consider the patterns in cover performance over both wet and dry years. In addition to the precipitation, the solar radiation, minimum and maximum air temperatures, wind speed, relative humidity, and percentage cloud cover are often used in numerical models to calculate the potential evapotranspiration. These variables are generally available from local or national weather station databases.

34.4.3.4 Vegetation Parameters

Vegetative cover properties determine the amount of water that can be removed from the cover by transpiration. Water uptake by plants has been quantified empirically as a function of variables such as the wilting point suction, leaf area index, evapotranspiration partitioning model parameters, and root density distribution. Although researchers have been incorporating plant behavior in numerical models since the 1950s, the quantification of these variables is still unclear. The wilting point suction is the suction above which the plants are unable to draw water from the soil. Plants will typically stop transpiring and grow dormant under such conditions. The leaf area index is the leaf area coverage per unit ground area, and is typically correlated with the moisture demand of plants. A plant with more foliage will be able to photosynthesize faster, leading to more transpiration. Evapotranspiration can be estimated using the Penman-Monteith model (Monteith, 1965), which requires knowledge of the daily maximum and minimum temperatures, dew point temperature, solar radiation, percent cloud cover, wind speed, and precipitation (Zornberg and McCartney, 2003). However, once the evapotranspiration has been estimated, it must be partitioned into evaporation and transpiration components for use in numerical models (Fayer et al., 1992). The Ritchie model can be used to correlate the relative contribution of the plant transpiration with the leaf area index. The root density distribution depends on the particular plant, although it is typically measured to avoid plants with roots deeper than the cover thickness. A diverse group of native shrubs and grasses is recommended. Selection

of plants with different heights also prevents intrusion of burrowing animals while providing erosion control.

34.4.4 Numerical Modeling Issues

Analysis of the performance of alternative covers has been performed using: (i) unsaturated flow analyses, and (ii) simplified water balance analyses (Albright et al., 2002). Unsaturated flow analysis entails solving Richards' equation for certain surface boundary conditions (e.g., water infiltration, overland runoff, evaporation, transpiration) and bottom boundary conditions (e.g., unit hydraulic gradient, seepage face). The governing equations are solved using numerical techniques such as the finite element method or the finite difference method. Relevant outputs from these analyses include the transient moisture redistribution and basal percolation. Four commonly used Richards' equation-based codes that have been used in the analysis of evapotranspirative covers are UNSAT-H (Fayer and Jones, 1990), HYDRUS-1D (Simunek et al., 1998), LEACHM (Hutson and Wagenet, 1992), and Vadose/W (GeoSlope, 2004). The current version of UNSAT-H allows modeling of hysteresis in the SWRC, and was observed to have a close fit to observed data (Khire et al., 1999). HYDRUS-1D is more user-friendly and has built-in libraries for soil hydraulic properties and initial estimates for most performance variables. LEACHM has the distinct advantage of being an open-source code, while being particularly useful for conducting sensitivity analyses that allow identification of relevant variables (Zornberg et al., 2003). VADOSE/W is a commercial code that considers fully coupled heat and mass transfer with vapor flow, vegetation, gas diffusion and ground freezing in a finite element formulation in one or two dimensions. It solves a modified form of the Richards' equation with pressure as the dependent variable, not water content, which improves solution stability. Despite their ability to solve Equation 34.5 subject to complex boundary conditions, it is still challenging to use Richards' equation-based codes for predicting small basal percolation values with a high level of accuracy. It should be noted that the mass balance errors for numerical models may be of the same order of magnitude as basal percolation values of relevance for the analysis of evapotranspirative covers.

Analyses involving water balance use the conservation of mass at the soil surface to estimate the basal percolation through the cover. This approach treats the soil layer as a sponge, able to hold a certain maximum amount of water (at the field capacity suction) against the pull of gravity. Basal percolation is calculated as the volume of moisture in the cover that exceeds the field capacity moisture storage after accounting for moisture removed by evapotranspiration and lateral drainage. Water balance codes that have been used for evapotranspirative cover include the Hydrologic Evaluation of Landfill Performance (HELP) (Schroeder et al., 1994), which is distributed by the US Environmental Protection Agency (EPA), and the Erosion Productivity Impact Calculator (EPIC) (Williams et al., 1984). A significant limitation of the water balance approach is that it does not consider transient moisture redistribution, which plays an important role in moisture removal from the cover by evapotranspiration. Also, as the water balance approach considers that the only driving mechanism for water flow is gravity, it implicitly considers that the hydraulic gradient is always equal to 1.0.

34.5 Performance Monitoring of Evapotranspirative Covers

34.5.1 Monitoring Strategies

In the past decade, there has been a significant effort to expand the evapotranspirative cover knowledge base by constructing full-scale field test plots involving the monitoring of basal percolation and moisture profiles (Benson et al., 1999, 2001; Dwyer, 1998; O'Kane et al., 1998; Zornberg and McCartney, 2003). Monitoring schemes allow direct quantification of the response of evapotranspirative covers to atmospheric conditions. The field monitoring program should be consistent with the performance criteria used for the cover design. Different technologies have been considered to evaluate the basal percolation, moisture profiles, suction profiles, and meteorological variables, as discussed further in the following sections.

34.5.2 Regulatory Issues Specific to Compliance Demonstration

The selection of a quantitative or comparative percolation criterion for an evapotranspirative cover project (Section 34.4.2) may have significant implications on the compliance demonstration for the cover. As mentioned, the threshold basal percolation (MQPV) to be used in a quantitative percolation criterion is difficult to define. However, once the MQPV has been defined the monitoring program used for compliance demonstration phase using a quantitative percolation criterion is reasonably straightforward, as it involves monitoring the basal percolation to verify that it remains below the MQPV. Yet, limitations in field monitoring and numerical modeling must be understood to correctly interpret the data collected for compliance demonstration. On the other hand, the monitoring program used for compliance demonstration when using a comparative percolation criterion for the design may not be straightforward. For example, an approach could involve continued comparison monitored in the basal percolation values of two covers (prescriptive and alternative) over the lifetime of the evapotranspirative cover. Accordingly, the time period used for compliance demonstration is a key factor. For instance, compliance could be based on either the average basal percolation value during a time period or on the maximum basal percolation amounts associated with specific precipitation events.

34.5.3 Lysimetry

Gravity lysimeters are the most common tools for directly monitoring basal percolation. They typically consist of a drainage layer underlain by a hydraulic barrier (Benson et al., 1999, 2001), such as a geocomposite or gravel drainage layer placed on top of a geomembrane. The geocomposites used in gravity lysimeters consist of a geonet sandwiched between two nonwoven geotextiles. A geonet is a thin polymeric sheet with slotted grooves that provide high lateral transmissivity. Geotextiles are polymeric fabrics used as filters, protection layers, and drainage layers. Geomembranes are polymeric sheets that have equivalent hydraulic conductivity values on the order of 10^{-15} m/sec. When a soil cover is placed above the lysimeter, it is intended that percolation through the cover soil will reach the geocomposite, and be transmitted down-slope to a collection bin. For effective performance, it is important to avoid that the presence of the lysimeter interferes with water flow (i.e., by introducing a capillary break).

The main advantage of lysimeters is that they can be constructed to cover large areas (10 to 100 ft on side), which allows a spatial averaging of the water flow through a potential system of saturated preferential pathways in the cover (areas with lower density, cracks, animal burrows, or decayed plant roots). However, lysimeters have several shortcomings, the most significant being that they provide little insight into reasons for poor or adequate cover performance. Another shortcoming is that, despite their high transmissivity and permittivity when saturated, the geotextile component of a lysimeter may cause a capillary break when in contact with unsaturated soils (Stormont and Morris, 2000; Zornberg and McCartney, 2003; McCartney et al., 2005b). A capillary break at the lysimeter–soil interface distorts the suction and moisture content profiles in an evapotranspirative cover and may lead to significant underestimation of basal percolation. In addition, lysimeters create barriers to upward flow from lower depths (Scanlon and Milly, 1994). This is typically caused by water vapor flow in response to thermal gradients, and may lead to overestimation of the basal percolation at the site.

34.5.4 Monitoring of Moisture and Suction Profiles

As the overall performance of an evapotranspirative cover system relies on its ability to store moisture until it is removed by evapotranspiration, moisture content or suction profiles can be monitored to assess why the evapotranspirative cover performs adequately (or not). Continued monitoring of *in situ* soil volumetric moisture content profiles is important in many geoenvironmental engineering and hydrological projects. In particular, monitoring of soil volumetric moisture content can provide relevant feedback on the migration of moisture through evapotranspirative covers.

Time Domain Reflectometry (TDR) technology has been used to measure the volumetric moisture content in evapotranspirative covers (Dwyer, 1998; O'Kane et al., 1998; Siddiqui et al., 2000; Albright and

Benson, 2002; Zornberg and McCartney, 2003). TDR involves measuring the velocity of an electromagnetic pulse applied to a transmission line that terminates in a shielded probe placed within the soil mass (Topp et al., 1980; Siddiqui et al., 2000; Suwansuwat and Benson, 1999). The pulse is reflected due to changes in impedance along the transmission line-probe system (e.g., the beginning of the probe and the end of the probe). The velocity of the reflected pulse is affected by the dielectric constant of the water within the soil mass, which is an order of magnitude greater than that of air and soil particles. The bulk dielectric constant of the soil mass, calculated from the velocity of the reflected pulse, can then be correlated with the soil volumetric moisture content. Conventional TDR systems use a cable tester to generate high frequency electromagnetic pulses (∼10 to 100 GHz) and measure the reflected waveform (with a resolution on the order of nanoseconds). Although conventional TDR systems are generally adequate for a wide range of soil types, their accuracy decreases for high moisture contents, saline soils, and highly conductive clays. Their shortcomings include the relatively high cost of probes and cable tester systems and comparatively complicated installation procedures to prevent probe damage.

Water content reflectometer (WCR) probes have often been used as an alternative to conventional TDR probes (Dwyer, 1998; Albright and Benson, 2002; Chandler et al., 2004). WCR probes infer the moisture content by measuring the dielectric content of the soil, similar to TDRs. However, WCRs use smaller electronic circuitry placed within the probe itself that generate a lower frequency electromagnetic pulse (∼40 MHz) (Chandler et al., 2004). WCR probes have lower power requirements and allow longer cable lengths than conventional TDRs. In addition, WCR probes can use conventional field dataloggers instead of cable testers, which makes them attractive for field applications. Despite these advantages, the use of comparatively low frequencies may lead to decreased resolution in volumetric moisture content measurements and to correlations that are more sensitive to the soil electrical conductivity and temperature than TDRs (Kim and Benson, 2002).

Suction measurements can also be made to complement moisture content evaluations. Concurrent suction and moisture content monitoring can provide data suitable to interpret evapotranspirative cover performance. Specifically, the suction and moisture content measurements can provide information for *in situ* determination of the SWRC. This can be used to interpret the SWRC during wetting and drying, interface phenomena like capillary breaks, and optimization of the SWRC to be used in numerical models. Suction measurements have been conducted in the field using several types of techniques, such as tensiometers (Ridley and Burland, 1995; Sisson et al., 2002; Tarantino and Mongiovì, 2003) and heat dissipation units (HDUs) (Flint et al., 2002; Nichol et al., 2003). Tensiometers consist of a pressure transducer with a porous ceramic stone filter. Due to continuity of suction, the suction within the ceramic stone will come into equilibrium with that of the surrounding soil. As water is drawn from the ceramic stone, the pressure transducer will measure a negative pressure value. HDUs consist of a heating unit and a thermocouple placed within a ceramic stone. The HDU infer the soil suction by applying a heat pulse to the heating unit in the ceramic stone, and measuring the transient changes in temperature of the ceramic stone using the thermocouple. The thermal properties of the ceramic are related to its moisture content, with a wet ceramic having higher thermal conductivity than a dry ceramic. Accordingly, the thermal response of the ceramic to the applied heat pulse can be calibrated against the suction in the ceramic, which is the same as the suction in the soil.

34.5.5 Monitoring of Meteorological Variables and Overland Runoff

Site-specific monitoring of meteorological variables is important to proper interpretation of evapotranspirative cover performance, as these variables vary on a regional and local scale. Precipitation is generally measured using tipping bucket rain gauges. These gauges collect water in a two-sided bucket with a capacity of approximately 4 ml. The bucket is placed on a pivot so that water flowing into the gauge is funneled into one side of the bucket. After the capacity of the bucket is reached, the weight of the water causes the bucket to tip on the pivot, spilling the water and allowing water to be funneled into the other side of the bucket. The gauge records the time of each tip. Overland runoff has been typically measured using geomembrane swales anchored on the soil surface on the perimeter of the cover. Difficulties have

been encountered in the use of such swales due to thermal expansion of the exposed geomembranes. Other variables typically measured on the site include wind speed and direction using an anemometer, temperature, and solar radiation.

34.6 Case Studies

34.6.1 Site Survey

Table 34.1 shows a survey of evapotranspirative covers in the United States that have implemented field monitoring programs. A total of 53 evapotranspirative covers were identified at 48 sites in the United States. Among these, 19 of the sites have undergone or are undergoing construction or closure of an evapotranspirative cover, while the rest involve compliance demonstration using test covers. The number of sites with performance monitoring shown in this table reflects the growing number of alternative cover construction projects because of their technical and economic benefits. The table also provides the water balance variables monitored at each site and the study period. Although information is limited for some of the private covers, it appears that most covers have used lysimetry and moisture profile monitoring as part of compliance demonstration programs. Two of the sites, the OII landfill in Monterey Park, California, and the Rocky Mountain Arsenal, near Denver, Colorado, are discussed next.

34.6.2 OII Landfill

The first evapotranspirative cover system approved by the US EPA for a hazardous waste Superfund site was in 1997 (Zornberg et al., 2003). The cover was constructed at the OII Superfund site in Monterey Park, California, approximately 16 km east of downtown Los Angeles. The design of this cover involved five phases that were undertaken to define the cover layout configuration. The design phases included: (i) evaluation of a baseline evapotranspirative cover, (ii) equivalence demonstration of the baseline cover by comparison with the basal percolation through a prescriptive cover, (iii) evaluation of the sensitivity of different design parameters (e.g., cover thickness, soil characteristics, rooting depth, and potential use of irrigation schemes) on the basal percolation through the cover, (iv) use of compilation of the results of this analysis as basis for the design of the final evapotranspirative cover, and (v) equivalence demonstration using soil-specific hydraulic properties of each cover soil.

The criterion used for the design of the cover system at the OII Superfund site was comparative, and required that the basal percolation through the proposed evapotranspirative cover be less than the basal percolation through a prescriptive, resistive cover. That is, the Maximum Comparative Percolation Ratio (MCPR) at this project was 1.0. The prescriptive cover, defined by a consent decree, consisted of a 1200-mm thick system, which included a 300-mm thick vegetative layer, a 300-mm thick clay layer, and a 600-mm thick foundation layer. The vegetative and foundation layers both were considered to have a saturated hydraulic conductivity of 1×10^{-6} m/sec, and the clay layer to have a saturated hydraulic conductivity of 1×10^{-8} m/sec.

A laboratory testing program was implemented to characterize the candidate borrow soils using soil specimens remolded under different compaction and moisture conditions. The experimental program included determination of hydraulic, shear strength, desiccation potential, and edaphic properties. Table 34.2 summarizes the laboratory test results for one of the candidate borrow soils measured in the laboratory for use in the equivalence demonstration. Following identification of the candidate soil borrow sources and determination of their hydraulic properties, soil-specific equivalence demonstrations were performed for the proposed evapotranspirative cover. Soil-specific parameters used in the unsaturated flow analyses included the SWRC, saturated hydraulic conductivity and K-function (obtained by centrifugation). In addition, soil-specific information from compaction tests was used in the analyses to define the soil placement conditions (unit weight and moisture content) that would optimize the performance of the cover.

TABLE 34.1 Survey of ET Cover Case Studies

	Cover details		Water balance variables measured					Study period		
Site name	Cover type	Cover location	Meterological variables	Percolation	Water content	Suction	Runoff	Start date	End date	Full scale or test section
Greater Wenatchee Regional Landfill[a]	Capillary break	Wentachee, WA	X	X	X		X	1992	1995	0 test sections
Greater Wenatchee Regional Landfill[a]	Monolithic	Wentachee, WA	X	X	X		X	1992	1995	1 test section
Live Oak Landfill[a]	Monolithic	Atlanta, GA	X	X	X		X	1993	1996	1 test section
Sacramento site[a]	Monolithic	Sacramento, CA		X				1999	2002	2 test sections
Beltsville facility[a]	Monolithic	MD	X	X	X		X	?	?	Test section
Phelan landfill[a]	Monolithic	Sacramento, CA	X	X	X		X	?	?	Test section
National Council for Air and Stream Improvement[a]	Monolithic	NM	X	X	X		X	?	?	Test section
Grede Foundries[a]	Monolithic	Reedsburg, WI	X	X	X		X	1995	1996	Test section
Texas Low-Level Radioactive Waste Disposal Authority Facility[a]	Monolithic	Sierra Blanca, TX	X	X	X		X	1995	1997	Test section
US Marine Corps Air and Ground Combat Center[a]	Monolithic	Twentynine Palms, CA	X	X	X		X	1998	1999	Test section
Marine Corps Base[a]	Monolithic	HI	X	X	X		X	?	?	Test section
US Ecology Co. Landfill[a]	Monolithic	Sheffield, IL	X	X	X		X	?	?	
Hamburg Test Site	Capillary break	Hamburg, Germany	X	X		X	X	1988	1992	1 test section
Omega Hills Landfill[a]	Capillary break	Milwaukee, WI		X			X	?	?	1 test section
Los Alamos National Laboratory[a]	Capillary break	Los Alamos, NM	X	X				1991	1995	1 test section
Los Alamos National Laboratory[a]	Capillary break	Los Alamos, NM	X	X	X		X	1991	1995	2 test sections
Arid Lands Ecology Reserve, Hanford[a]	Monolithic	Richland, WA	X	X	X			1985	1990	4 test sections
Hanford Field Lysimeter Test Facility[a]	Capillary break	Richland, WA	X	X	X		X	1987	1996	8 test sections
Hanford[a]	Capillary break	Richland, WA	X	X				?	?	2 test sections
Hanford[a]	Monolithic	Richland, WA	X		X			1987	1989	6 test sections
NMSU Las Cruces Site[a]	Monolithic	Las Cruces, NM	X	X	X	X		?	?	1 test section
Beatty Site[a]	Monolithic	Mojave Desert, NV	X	X	X	X		?	?	1 test section
Hanford Site[a]	Monolithic	Richland, WA	X	X	X	X		?	?	1 test section
Hill AFB[a]	Capillary break	UT	X	X	X	X	X	1990	1993	2 test sections

Sandia National Laboratories	Capillary break	Albuquerque, NM	X	X	X		X	1997	2002	1 test section
Sandia National Laboratories	Monolithic	Albuquerque, NM	X	X	X		X	1997	2002	1 test section
Sandia National Laboratories	Anisotropic	Albuquerque, NM	X	X	X		X	1997	2002	1 test section
Rocky Mountain Arsenal[a]	Monolithic	Denver, CO	X	X	X		X	1992	2003	4 test sections
Nevada test site	Monolithic	NV	X	[a]	X			1996	2002	2 test sections
Idaho National Engineering and Environmental Laboratory[a]	Monolithic	ID	X	X	X		X	1984	1995	1 test section
El Paso Site	Capillary break	El Paso, TX	X	X		X		2000	2001	1 test section
Questa Mine	Monolithic/ Oxygen cover	NM	X	X	X	X		2000	2001	1 test section
Equity Silver Mine	Monolithic/ Oxygen cover	BC, Canada	X	X	X	X	X	1992	1995	1 test section
Vereenigning Ash Dump	Ash Dump cover	South Africa	X		X	X	X	1995	1995	1 test section
F. R. Bowerman Landfill	Monolithic	CA			X			?	?	Full scale
Operating Industries, Inc. (OII)	Monolithic	Monterey Park, CA			X			?	?	Full scale
Puente Hills	Monolithic	CA			X			?	?	Full scale
Yucaipa	Monolithic	Orange Country, CA			X			?	?	Full scale
Lopez Canyon	Monolithic	Los Angeles, CA			X			?	?	Full scale
Yeermo	Monolithic	Los Angeles, CA			X			?	?	Full scale
Riverside Co.	Monolithic	Riverside Country, CA			X			?	?	Full scale
29 Palms Marine Base	Monolithic	CA			X			?	?	Full scale
Potrero Hills	Monolithic	CA	X		X		X	1997	1999	Full scale
Chiquita Canyon	Monolithic	CA			X			?	?	Full scale
Needles Landfill	Monolithic	CA			X			?	?	Full scale
Fairmead Landfill	Monolithic	CA			X			?	?	Full scale
Rocketdyne Site	Monolithic	Chattsworth, CA			X			?	?	Full scale
China Grade Landfill	Monolithic	Kern Country, CA		X	X			?	?	Full scale
McPherson Area Solid Waste Utility	Monolithic	McPherson, KS		X				?	?	Full scale
Ft. Carson	Monolithic	CO		X	X			?	?	Full scale
Lakeside Reclamation Landfill	Monolithic	Beaverton, OR			X			?	?	Full scale
MSW Landfill	Monolithic	NE			X			?	?	Full scale
Duvall Custodial Landfill	Monolithic	WA			X			?	?	Full scale

[a] ACAP Sites.

TABLE 34.2 Hydraulic and Geotechnical Properties for OII Landfill Cover Soils

Series	USCS classification (ASTM D2487)	Average % passing #200 sieve (% fines)	Atterberg limits		Saturated hydraulic conductivity (m/s)	Campbell model parameters		Relative compaction[a] (%)
			Average PL (%)	Average LL (%)		a	b	
T1	CL	66	43	18	2.80E-06	−4.89	7.028	93.9
T2	CL	66	43	18	1.10E-05	−4.89	6.328	87.2
T3	CL	66	43	18	3.70E-05	−4.89	5.495	83.1
T4	CL	66	43	18	3.30E-06	−4.89	7.278	88.5
T5	CL	66	43	18	1.70E-05	−4.89	6.463	87.8
T6	CL	66	43	18	1.90E-04	−4.86	6.678	77.7

[a] In relation to standard Proctor test (ASTM 698).

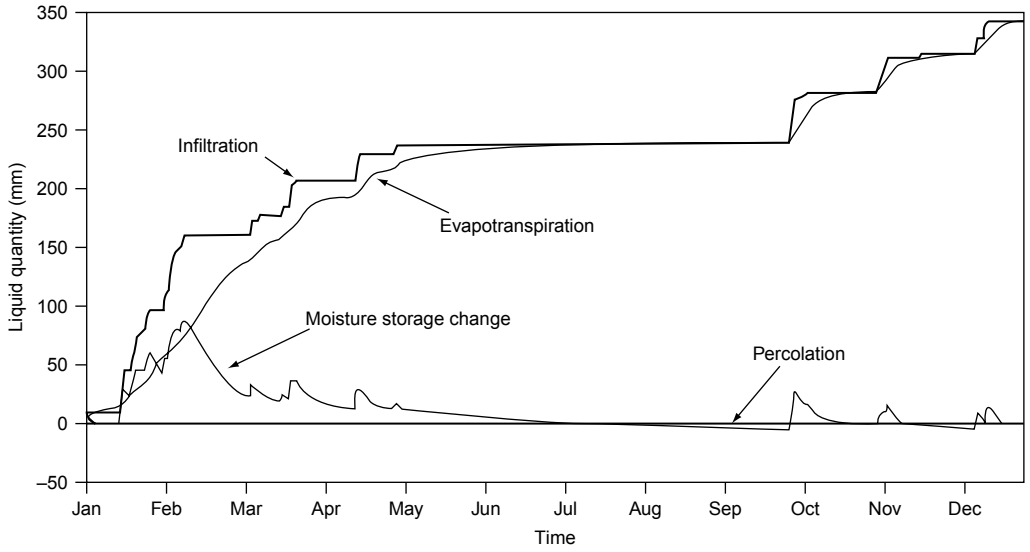

FIGURE 34.12 Seasonal variation in the water balance variables (Zornberg et al. 2003).

The code LEACHM (Hutson and Wagenet, 1992) was used to predict the basal percolation through both the prescriptive and the evapotranspirative covers to compare their performance using site-specific soil and meteorological conditions. LEACHM uses Campbell's (1974) equation to describe the relationship between suction and volumetric moisture content for soil:

$$\psi = a(\theta/\theta_s)^b \tag{34.12}$$

where a and b are constants obtained from curve fitting. The a and b values as well as the saturated hydraulic conductivity for one of the candidate evapotranspirative cover soils are listed in Table 34.2. The simulated water balance variables for the OII site are shown in Figure 34.12. This figure indicates that the moisture storage of the cover increases during periods of infiltration and subsequently decreases during period of evapotranspiration. The infiltration is typically higher in the early party of the year, while the evapotranspiration is higher in the late spring and summer months. Figure 34.13a shows equivalence results, as quantified by the percolation ratio (basal percolation through the ET cover divided by the basal percolation through the prescriptive cover) with time. This equivalence demonstration shown in the figure corresponds to an evapotranspirative cover system constructed using soils placed under compaction conditions defined by series T1 (Table 34.2). The percolation ratio is below 0.1 (and well below the MCPR

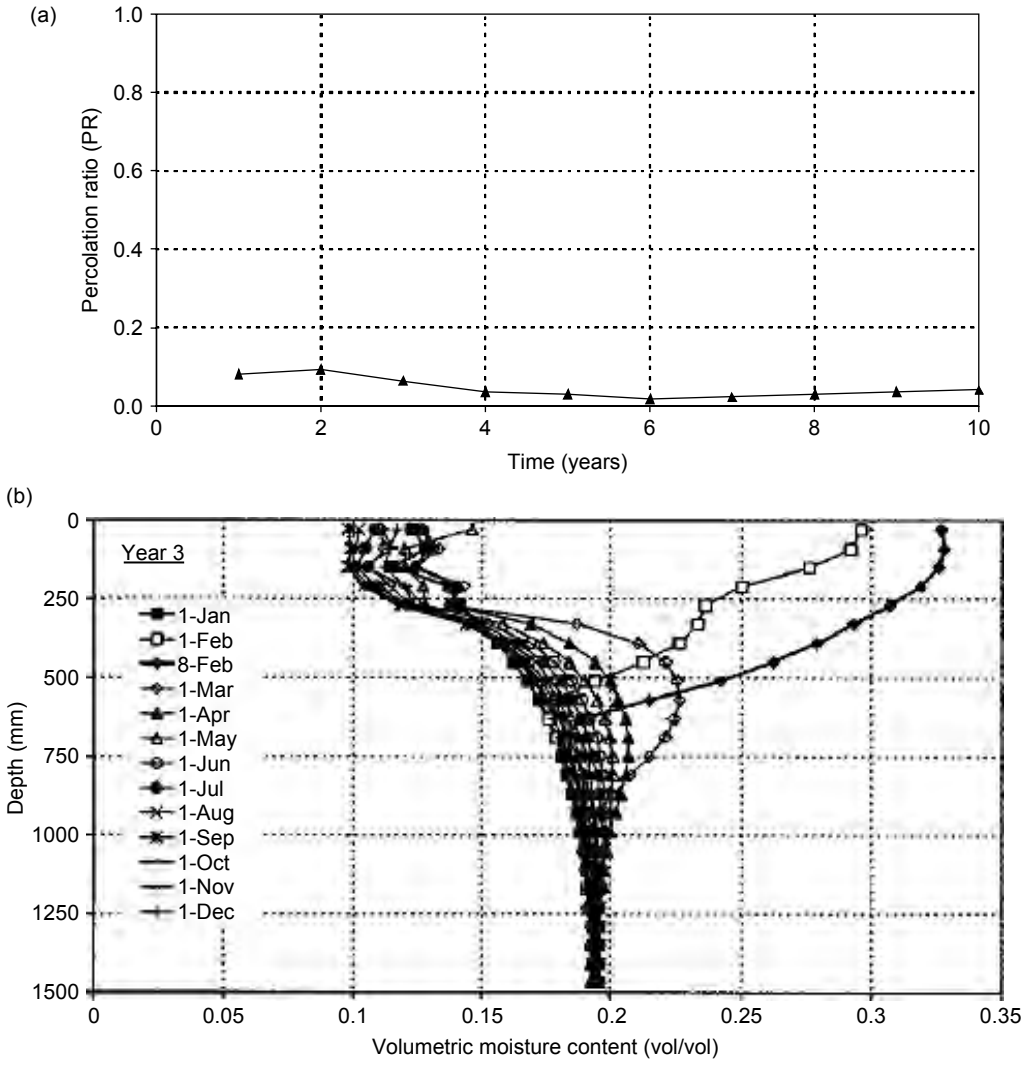

FIGURE 34.13 Performance variables for the O11 landfill evapotranspirative cover estimated using LEACHM: (a) comparative percolation ratio and (b) volumetric moisture content profiles during wettest simulation year (Zornberg et al. 2003).

of 1.0) for each year of the soil-specific, 10-year simulation. The engineered evapotranspirative cover constructed using the local soils, and placed under conditions defined by the T1 series, was then deemed to satisfy compliance with the prescriptive cover according to this demonstration. Figure 34.13b shows a prediction of the typical moisture content profiles expected for the cover. This figure indicates that the moisture fluctuations take place within the top meter of the soil cover, which reflects proper monolithic cover performance as discussed in Section 34.3.1.

34.6.3 Rocky Mountain Arsenal

Almost 200 acres of RCRA-Equivalent evapotranspirative covers have been recently designed to contain contaminated materials at the Rocky Mountain Arsenal (RMA), located near Denver, Colorado, USA. The climate in Denver is semiarid, with an average annual precipitation of 396 mm and an average pan evaporation of 1394 mm (as quantified for the 1948 to 1998 period). The wettest months of the year

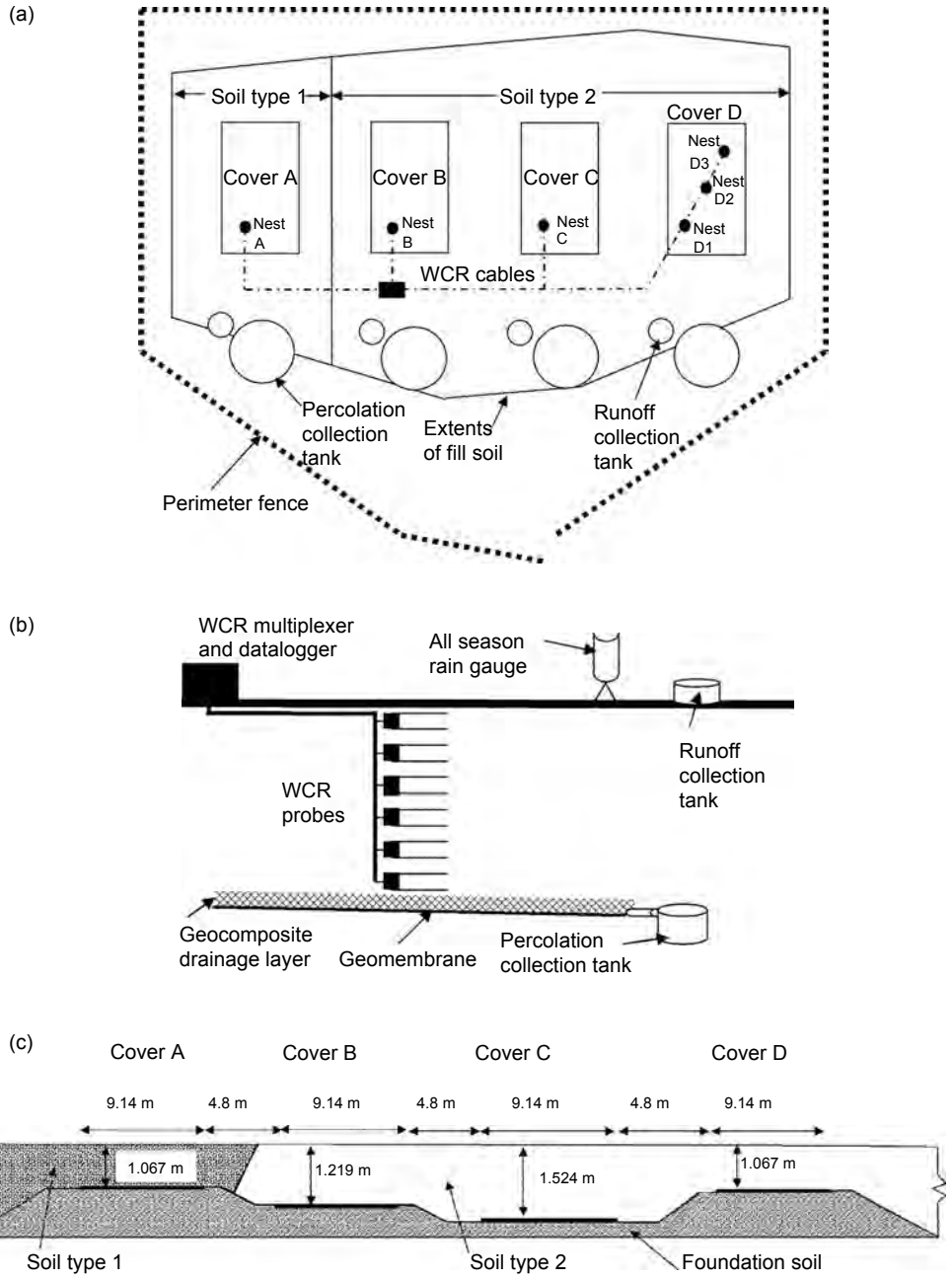

FIGURE 34.14 Layout for the monitoring program at the Rocky Mountain Arsenal: (a) plan view; (b) schematic view of instrumentation; and (c) elevation view.

(April to October) are also the months with the highest pan evaporation, which is appropriate for an evapotranspirative cover.

The Record of Decision (ROD) for the site requires a compliance demonstration to show equivalence of the alternative design with a prescriptive cover before construction of the final evapotranspirative covers. The design and compliance of the covers at the RMA site is governed by a quantitative percolation criterion. A MQPV threshold of 1.3 mm/year was selected at this site, which was based on eight years of leachate data collected from two landfill covers built to RCRA Subtitle C standards in Hamburg, Germany, according

TABLE 34.3 Hydraulic and Geotechnical Properties for Rocky Mountain Arsenal Cover Soils

Cover	Soil cover thickness (mm)	USCS classification (ASTM D2487)	Average % passing #200 sieve (% fines)	Atterberg limits		Saturated hydraulic conductivity (m/s)	van Genuchten model parameters				Relative compaction[a] (%)
				Average PL (%)	Average LL (%)		α (kPa^{-1})	N	θ_r	θ_s	
A	1143	SC	43.4	9	24.4	1.60E-05	0.6118	1.39	0.03	0.482	72.9
B	1270	CL	60.2	12.8	27.6	4.70E-06	0.3386	1.335	0.025	0.470	72.8
C	1676	CL	59.2	11.7	26.7	4.70E-06	0.3386	1.335	0.025	0.470	72.8
D	1168	CL	61.5	12	26.8	4.70E-06	0.3386	1.335	0.025	0.470	72.8

[a] In relation to standard Proctor test (ASTM 698).

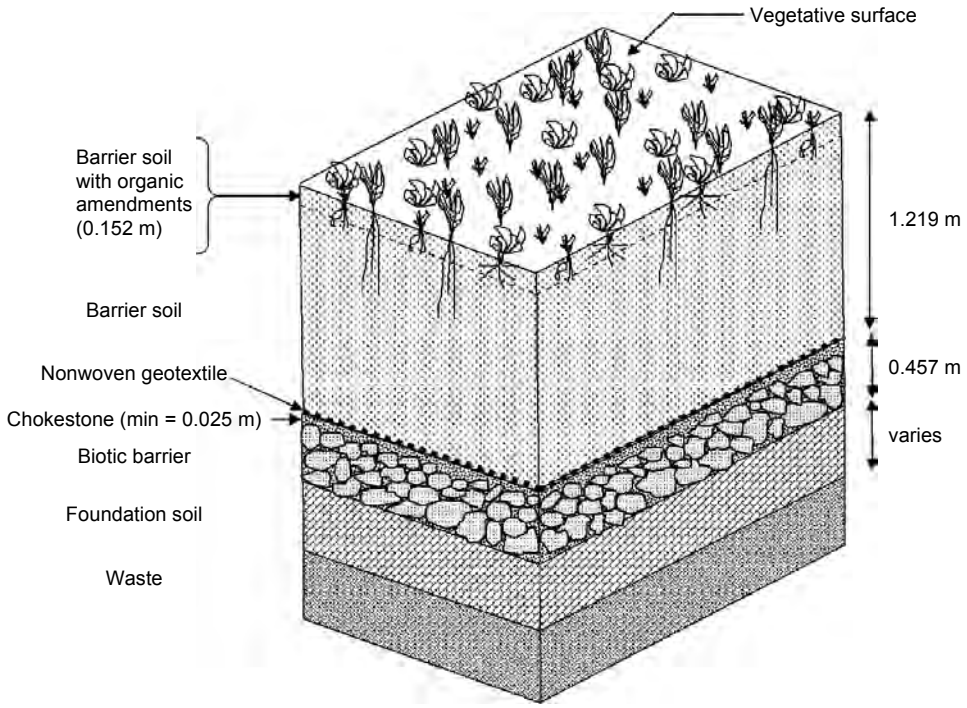

FIGURE 34.15 Final cover design at the Rocky Mountain Arsenal

to analyses described by Melchior (1997). This type of criterion was selected for its simplicity, as it sets a benchmark to be used in post-closure monitoring to demonstrate compliance, and is representative of the basal percolation for resistive covers.

The compliance demonstration at the Rocky Mountain Arsenal involved a field demonstration, which was complemented by comparative numerical analyses and a field demonstration (Kiel et al., 2002). Four evapotranspirative test covers were constructed on a rolling plain at the site in the summer of 1998. A plan view of the four test covers, referred to as covers A, B, C, and D, is shown in Figure 34.14a. The test covers were constructed using site-specific clays of low plasticity (CL), compacted atop large pan lysimeters (9.1 m by 15.2 m) placed on a 3% grade to allow gravity drainage to a collection tank. The geotechnical and hydraulic properties of the cover soils are summarized in Table 34.3. Figure 34.14b shows a schematic view of the monitoring layout used in the test covers. The instrumentation program involved monitoring of the basal percolation, precipitation, soil volumetric moisture content profile, and overland runoff in the four test covers. Basal percolation was collected in a gravity lysimeter, which consists of a geocomposite underlain by geomembrane. The lysimeters were constructed without sidewalls. Rain and snow were monitored using an all-season rain gauge. Surface water was collected in polyethylene geomembrane swales constructed around the cover perimeters. WCR probes were used to measure volumetric moisture content. Specifically, the covers were instrumented with nests of eight WCR probes. This included six WCR probes placed in a vertical nests of WCR probes and spaced evenly with depth. In addition, redundant WCR probes were placed at the same depth as the top and the bottom probes, approximately 1 foot aside from the vertical profile of WCR probes. Cover D was instrumented using three vertical profiles. Figure 34.14c shows an elevation view of the covers, indicating the depth of each cover. The covers are separated from each other by 2.4 m-wide buffer zones, and the entire area is vegetated with local grasses and shrubs.

The four test covers at the RMA were constructed to verify that the moisture flux through site-specific soils under local weather conditions remains below the MQPV of 1.3 mm/year (Kiel et al., 2002). The test plots at the Rocky Mountain Arsenal satisfied the quantitative percolation criterion over the period 1998 to 2003 of operation. That is, all four of the covers showed a yearly basal percolation rate below the MQPV despite having complemented the natural precipitation with irrigation. Although Cover D showed surface

depression, possibly due to the installation of moisture probes or burrowing animals, the collected basal percolation over this cover was still below the MQPV percolation threshold.

The monitoring results of the field demonstration program were used to develop the final cover design. As shown in Figure 34.15, the final cover design is a capillary barrier with a 1.067 m barrier layer, similar to that used in covers A and D. An additional 0.152 m of topsoil is used for vegetation. The specifications for the final cover soil are based on those for soil type I used in cover A. The final design includes a nonwoven geotextile over a chokestone layer (coarse gravel) to form a capillary break at the bottom interface of the barrier soil. The geotextile also helps prevent barrier soil particles from migrating into the chokestone layer. The chokestone is underlain by a biotic barrier consisting of crushed concrete from a demolition site. The biotic barrier is design to prevent plants and burrowing animals from reaching the waste. The final cover will be instrumented with gravity lysimeters placed within the final cover to measure basal percolation and WCR probes to measure moisture profiles within the barrier soil.

Glossary

Anisotropic barrier Evapotranspirative cover with a system of barrier and drainage layers placed on a slope so that water is removed from the cover by lateral drainage.

Basal percolation Water that passes through a cover system into the underlying waste.

Biota barrier Layer of gravel or crushed concrete beneath the cover used to prevent entry of plants or animals into the waste.

Capillary break cover Evapotranspirative cover that exploits the increased moisture storage arising from placing a fine-grained soil over a coarse-grained soil.

Degree of saturation Ratio of the volumetric moisture content and the porosity.

Evapotranspirative cover systems Class of alternative landfill cover systems that functions by storing water from precipitation until it may be removed by evapotranspiration.

Field capacity Moisture content at which water will drain from a soil by gravity.

Geocomposite Drainage material consisting of a geonet with high transmissivity sandwiched between two nonwoven geotextile filters.

Geomembrane Low permeability geosynthetic used in hydraulic barriers.

HDU Heat dissipation unit, a device used to measure soil suction.

Lysimeter Device used to measure the basal percolation through a saturated soil layer.

MCPR Maximum comparative percolation ratio, a percolation criterion relying on comparison of the performance of an evapotranspirative cover and a prescriptive cover.

Monolithic cover Evapotranspirative cover with a single layer of soil acting as a hydraulic barrier and vegetation substrate.

MPQV Maximum percolation quantitative value, a percolation criterion relying on comparison of the performance of an evapotranspirative cover with a selected basal percolation value.

Prescriptive cover Landfill cover prescribed by government regulations that limits percolation by maximizing overland runoff.

Richards' equation Governing equation for water flow through unsaturated porous media.

Suction Difference between the pore air pressure and pore water pressure.

TDR Time domain reflectometry, a device used to infer the soil volumetric moisture content.

Volumetric moisture content Volume of water in a soil divided by the total volume of the soil.

Porosity Ratio of the volume of voids and the total volume.

WCR Water content reflectometer, a device used to measure volumetric moisture content in the field based on TDR technology.

References

Albright, W.H. and Benson, C.H. (2002). *Alternative Cover Assessment Program 2002 Annual Report.* US EPA Publication No. 41182. 48 p.

Albright, W.H., Gee, G.W., Wilson, G.V., and Fayer, M. (2002). *Alternative Cover Assessment Program Phase 1 Report*. US EPA Publication 41183. 203 p.

Albright, W.H., Benson, C.H., Gee, G.W., Roesler, A.C., Abichou, T., Apiwantragoon, P., Lyles, B.F., and Rock, S.A. (2004). "Field water balance of landfill final covers." *Journal of Environmental Quality*. 33, 2317–2332.

Anderson, J.E., Nowak, R.S., Ratzlaff, T.D., and Markham, O.D. (1993). "Managing soil moisture on waste burial sites in arid regions." *Journal of Environmental Quality*. 22, 62–69.

Benson, C. and Gribb, M. (1997). "Measuring unsaturated hydraulic conductivity in the laboratory and field." In *Unsaturated Soil Engineering Practice*. Houston, S. and Wray, W. (eds). ASCE. Reston, VA. 113–168.

Benson, C., Abichou, T., Wang, X., Gee, G., and Albright, W. (1999). *Test section installation instructions — Alternative Cover Assessment Program*. Environmental Geotechnics Report 99-3, Department of Civil & Environmental Engineering, University of Wisconsin-Madison.

Benson, C., Abichou, T., Albright, W., Gee, G., and Roesler, A. (2001). "Field evaluation of alternative earthen final covers." *International Journal of Phytoremediation*. 3, 1–21.

Brooks, R.H. and Corey, A.T. (1964). "Hydraulic properties of porous medium." Colorado State University (Fort Collins). Hydrology Paper No. 3. March.

Burdine, N.T. (1953). "Relative permeability calculations from pore-size distribution data." *Petroleum Transactions of the American Institute of Mining and Metallurgical Engineering*. 198, 71–77.

Bussiere, B., Aubertin, M., and Chapuis, R. (2003). "The behavior of inclined covers used as oxygen barriers." *Canadian Geotechnical Journal*. 40, 512–535.

Cabral, A.R., Planchet, L., Marinho, F.A., and Lefebvre, G. (2004). "Determination of the soil water characteristic curve of compressible materials: Case study of de-inking residues." *ASTM Geotechnical Testing Journal*. 27(2): 154–162.

Campbell, G. (1974). "A simple method for determining unsaturated conductivity from moisture retention data." *Soil Science*. 117(6): 311–314.

Chandler, D.G., Seyfried, M., Murdock, M., and McNamara, J.P. (2004). "Field calibration of water content reflectometer." *Soil Science Society American Journal*. 68: 1501–1507.

Conca, J. and Wright, J. (1992). "Diffusion and flow in gravel, soil, and whole rock." *Applied Hydrogeology*. 1, 5–24.

Dell'Avanzi, E., Zornberg, J.G., and Cabral, A.R. (2004). "Suction profiles and scale factors for unsaturated flow under increased gravitational field." *Soils and Foundations*. 44, 1–11.

Dwyer, S.F. (1998). "Alternative landfill covers pass the test." *Civil Engineering*. ASCE. 68(9): 50–52.

Dwyer, S.F. (2003). *Water balance and computer simulations of landfill covers*. Doctoral thesis. The University of New Mexico. Albuquerque.

Fayer, M. and Jones, T.L. (1990). "UNSAT-H version 2.0: Unsaturated soil water and heat flow model." PNL-679, Pacific Northwest Laboratory, Richland, Washington.

Flint, A.L., Campbell, G.S., Ellet, K.M., and Calissendorff, C. (2002). "Calibration and temperature correction of heat dissipation matric potential densors." *Soil Science Society of America Journal*. 66, 1439–1445.

Forbes, P.L. (1994). "Simple and accurate methods for converting centrifuge data into drainage and imbibition capillary pressure curves." *The Log Analyst*. 35, 31–53.

Fredlund, D.G. and Xing, A. (1994). "Equations for the soil-water characteristic curve." *Canadian Geotechnical Journal*. 31, 521–532.

Gardner, R.A. (1937). "The method of measuring the capillary pressures in small core samples." *Soil Science*. 43, 277–283.

GeoSlope International Ltd. (2004). *Vadose/W Technical Overview*. Calgary, Canada.

Hassler, G.L. and Brunner, E. (1945). "Measurements of capillary pressure in small core samples." *Transactions of AIME*. 160, 114–123.

Hillel, D. (1998). *Environmental Soil Physics*. Academic Press. San Diego, CA.

Hutson, J.L. and Wagenet, R.J. (1992). "Leaching Estimation and Chemistry Model, LEACHM." New York State College of Agriculture and Life Sciences, Cornell University.

Kampf, M. and Holfelder, T. (1999). "Designing capillary barriers." *Seventh International Waste Management and Landfill Symposium.* CISA. Environmental Sanitary Engineering Centre, Sardinia. pp. 381–388.

Khire, M.V., Meerdink, J.S., Benson, C.H., and Bosscher, P.J. (1995). "Unsaturated hydraulic conductivity and water balance predictions for earthen landfill final covers." *Soil Suction Applications in Geotechnical Engineering Practice*, Geotechnical Special Publication No. 48. ASCE, 38–57.

Khire, M.V., Benson, C.H., and Bosscher, P.J. (1999). "Field data from a capillary barrier and model predictions with UNSAT-H." *Journal of Geotechnical and Geoenvironmental Engineering, ASCE*, 125, 518–527.

Khire, M., Benson, C., and Bosscher, P. (2000). "Capillary Barriers in Semi-Arid and Arid Climates: Design Variables and the Water Balance." *Journal of Geotechnical and Geoenvironmental Engineering, ASCE*, Vol. 126, No. 8, pp. 695–708.

Kiel, R.E., Chadwick, D.G., Lowrey, J., Mackey, C.V., and Greer, L.M. (2002). "Design of evapotranspirative (ET) covers at the Rocky Mountain Arsenal." *Proceedings: SWANA 6th Annual Landfill Symposium.*

Kim, K.C. and Benson, C.H. (2002), *Moisture Content Calibrations for Final Cover Soils*, University of Wisconsin-Madison Geotech. Eng. Report 02-12, Madison, WI, 122 p.

Klute, A. (1986). Water Retention: Laboratory Methods. *Methods of Soil Analysis, Part 1: Physical and Mineralogical Methods* SSSA. Madison, WI. 635–662.

Kool, J.B. and Parker, J.C. (1987). "Development and evaluation of closed-form expression for hysteretic soil hydraulic properties." *Water Resources Research*, 23, 105–114.

Lu, N. and Likos, W.J. (2005). *Unsaturated Soil Mechanics.* Wiley. New York. 584 p.

McCartney, J.S. and Zornberg, J.G. (2002). "Design and performance criteria for evapotranspirative cover systems." *Fourth International Congress on Environmental Geotechnics.* Rio de Janeiro, Brazil.

McCartney, J.S. and Zornberg, J.G. (2005a). "The Centrifuge Permeameter for Unsaturated Soils (CPUS)." *Proceedings of the International Symposium on Advanced Experimental Unsaturated Soil Mechanics, Experus 2005.* Trento, Italy, June 27–29, A.A. Balkema, pp. 299–304.

McCartney, J.S., Kuhn, J.A., and Zornberg J.G. (2005b). "Geosynthetic drainage layers in contact with unsaturated soils." *16th ISSMGE Conference: Geotechnical Engineering in Harmony with the Global Environment.* 12–16 September 2005. Osaka, Japan.

Meerdink, J.S., Benson, C.H., and Khire, M.V. (1996). "Unsaturated hydraulic conductivity of two compacted barrier soils." *Journal of Geotechnical and Geoenvironmental Engineering, ASCE*, 122, 565–576.

Melchior, S. (1997). "In-situ studies of the performance of landfill caps (Compacted clay liners, geomembranes, geosynthetic clay liner, capillary barriers)." *Land Contamination and Reclamation.* 5, 209–216.

Meyer, P.D. and Gee, G.W. (1999). "Flux-based estimation of field capacity." *Journal of Geotechnical and Geoenvironmental Engineering.* 125, 595–599.

Monteith, J.L. (1965) "Evaporation and environment." *Symposia of the Society for Experimental Biology.*

Morris, C.E. and Stormont, J.C. (1997). "Capillary barriers and Subtitle D covers: Estimating equivalency." *Journal of Environmental Engineering, ASCE*, 123, 3–10.

Nachabe, M.H. (1998). "Refining the definition of field capacity in the literature." *Journal of Irrigation and Drainage Engineering.* 124, 230–232.

Nichol, C., Smith, L., and Beckie, R. (2003). "Long-term measurement of matric suction using thermal conductivity sensors." *Can. Geotech. J.* 40: 587–597.

Nimmo, J.R., Rubin, J., and Hammermeister, D.P. (1987). "Unsaturated flow in a centrifugal field: Measurement of hydraulic conductivity and testing of Darcy's law." *Water Resources Research.* 23, 124–134.

O'Kane, M., Wilson, G.W., and Barbour, S.L. (1998). "Instrumentation and monitoring of an engineered soil cover system for mine waste rock." *Canadian Journal of Geotechnical Engineering.* 35, 828–846.

Olson, R.E. and Langfelder, L.J. (1965). "Pore water pressures in unsaturated soils." *Journal of the Soil Mechanical and Foundation Division* ASCE, 91, 127–151.

Parent, S.E. and Cabral, A.R. (2004). Procedure for the design of inclined covers with capillary barrier effect. *Proc. 57th Canadian Geotechnical Conference*, Québec, October, 24–28.

Ridley, A.M. and Burland, J.B. (1995). "A pore pressure probe for the in-situ measurement of soil suction". *Proceedings of Conference on Advances in Site Investigation Practice*. I.C.E.:London.

Scanlon, B.R. and Milly, P.C.D. (1994). "Water and heat fluxes in desert soils 2. Numerical simulations." *Water Resources Research*. 30, 721–733.

Schroeder, P.R., Dozier, T.S., Zappi, P.A., McEnroe, B.M., Sjostrom, J.W., and Peyton, R.L. (1994). "The Hydrologic Evaluation of Landfill Performance (HELP) Model: Engineering documentation for Version 3, EPA/600/R-94/168b." US EPA Risk Reduction Engineering Laboratory, Cincinnati, OH.

Shackelford, C.D., Chang, C.-K., and Chiu, T.-F. (1994). "The capillary barrier effect in unsaturated flow through soil barriers." *1st ICEG Conference*. Edmonton, CA, pp. 789–793.

Siddiqui, S.I., Drnevich, V.I., and Deschamps, R.J. (2000). "Time domain reflectometry development for use in geotechnical engineering," *Geotechnical Testing Journal*. 23, 9–20.

Simunek, J., Sejna, M., and van Genuchten, M. 1998. *HYDRUS-1D: Code for Simulating the One-Dimensional of Water, Heat, and Multiple Solutes in Variably Saturated Porous Media*. Version 2.02. International Groundwater Modeling Center. Colorado School of Mines. Golden, CO.

Sisson, J.B., Gee, G., Hubbell, J.M., Bratton, W.L., Ritter, J.C., Ward, A.L., and Caldwell, A.C. (2002). "Advances in tensiometry for long-term monitoring of soil water pressures." *Vadose Zone Hydrology*. 1, 310–315.

Stormont, J. (1995). "The effect of constant anisotropy on capillary barrier performance." *Water Resources Res*. 32, 783–785.

Stormont, J.C. and Anderson, C.E. (1999). "Capillary barrier effect from underlying coarser soil layer." *Journal of Geotechnical and Geoenvironmental Engineering*. 125, 641–648.

Stormont, J.C. and Morris, C.E. (2000). "Characterization of unsaturated nonwoven geotextiles." In *Advances in Unsaturated Geotechnics: Proceedings of Sessions of Geo-Denver 2000*. Chang, N.-Y., Houston, S.L., and Shackelford, C.D. (eds) August 5–8, 2000. Denver, Colorado. pp. 153–164.

Suwansuwat, S. and Benson C.H. (1999). "Cell size for water content-dielectric constant calibrations for time domain reflectometry." *Geotechnical Testing Journal*. 22, 3–12.

Tarantino, A. and Mongiovì, L. (2003). "Calibration of tensiometer for direct measurement of matric suction." *Géotechnique*. 53, 137–141.

Topp, G., Davis, J., and Annan, A. (1980). "Electromagnetic determination of soil water content: Measurement in coaxial transmission lines." *Water Resources Research*. 16, 574–582.

Topp, G.C. and Miller, E.E. (1966). "Hysteretic moisture characteristics and hydraulic conductivities for glass-bead media." *Soil Science Society of American Proceedings*. 30, 156–162.

van Genuchten, M. (1980). "A closed-form equation for predicting the hydraulic conductivity of unsaturated soils." *SSSA*. 44, 892–898.

Wang, X. and Benson, C.H. (2004). "Leak-free pressure plate extractor for the soil water characteristic curve." *Geotechnical Testing Journal*. 27, 1–10.

Watson, K.K. (1996). "An instantaneous profile method for determining the hydraulic conductivity of unsaturated porous materials." *Water Resour. Res.*, 2, 709–715.

Waugh, W.J., Petersen, K.L., Link, S.O., Bjornstad, B.N., and Gee, G.W. (1994). "Natural analogs of the long term performance of engineered covers." *In situ Remediation: Scientific Basis for Current and Future Technologies*, Gee, G.W. and Wing, N.R. (eds), Battelle Press, Richland Washington. pp. 379–409.

Williams, J.R., Jones, C.A., and Dyke, P.T. (1984). "The EPIC model and its application." *Proceeding of ICRISAT-IBSNAT-SYSS Symposium on Minimum Data Sets for Agrotechnology Transfer*. March 1993.

Zornberg, J.G. and McCartney, J.S. (2003). *Analysis of monitoring data from the evapotranspirative test covers at the Rocky Mountain Arsenal.* Geotechnical Research Report, US Environmental Protection Agency, Region 8, December 2003, 227 p.

Zornberg, J.G., Jernigan, B.L., Sanglerat, T.R., and Cooley, B.H. (1999). "Retention of free liquids in landfills undergoing vertical expansion." *Journal of Geotechnical and Geoenvironmental Engineering.* ASCE, 125, 583–594.

Zornberg, J.G., LaFountain, L., and Caldwell, J.C. (2003). "Analysis and design of evapotranspirative cover for hazardous waste landfill." *Journal of Geotechnical and Geoenvironmental Engineering.* ASCE. 129, 427–438.

Further Information

Further information on the hydraulic properties of unsaturated soils may be found in Lu and Likos (2005). Descriptions of common techniques used to determine the SWRC can be found in Wang and Benson (2004) and the proceedings of *Experus* (2005). Descriptions of common techniques used to determine the K-function can be found in Benson and Gribb (1997). The ACAP Phase 1 report provides a comparative analysis of available numerical models for evapotranspirative cover performance evaluation, while the 2002 ACAP Annual Report provides a summary of field monitoring programs for evapotranspirative covers. An overview of current research topics in monitoring and analysis of evapotranspirative covers can be found in ASCE Geotechnical Special Publication 142 "Waste Containment and Remediation," held at GeoFrontiers 2005 in Austin, TX.

Chapter 8

Internal and interface shear strength of geosynthetic clay liners

J.G. ZORNBERG
The University of Texas at Austin, Austin, TX, USA

J.S. McCARTNEY
University of Colorado at Boulder, Boulder,CO,USA

1 INTRODUCTION

Geosynthetic clay liners (GCLs) with geomembranes (GMs) placed on slopes as part of composite liner systems may be subject to a complex, time-dependent state of stresses. Stability is a major concern for side slopes in bottom liner or cover systems that include GCLs and GMs because of the wide range of commercially available GCL products, the change in behavior with exposure to water, variability in the quality of internal GCL reinforcement and GM texturing, and the low shear strength of hydrated sodium bentonite. Accordingly, proper project- and product-specific shear strength characterization is needed for the different materials and interfaces in composite liner systems.

A major concern when GCLs are placed in contact with GMs on steep slopes is the interface friction, which must be sufficiently high to transmit shear stresses generated during the lifetime of the facility. Shear stresses are typically generated in the field from static or seismic loads and waste decomposition. The need for a careful design of GCL-GM interfaces has been stressed by the failures generated by slip surfaces along liner interfaces, such as at the Kettleman Hills landfill (Byrne *et al.* 1992; Gilbert *et al.* 1998) and in the EPA test plots in Cincinnati, Ohio (Daniel *et al.* 1998). Another concern is the possibility of internal failure of GCLs (i.e. failure through the bentonite core), although failures have only been observed in unreinforced GCLs in the field, such as at the Mahoning landfill (Stark *et al.* 1998). The internal shear strength of GCLs should be characterized due to variations in shear strength due to moisture effects and manufacturing quality control. In addition, the use of GCLs in high normal stress applications such as heap-leach pads requires the identification of the internal and interface shear strength of GCLs.

Several studies have focused on experimental investigations of the different factors affecting the internal shear resistance of GCLs (Gilbert *et al.* 1996, 1997, Stark *et al.* 1996, Eid and Stark 1997, Fox *et al.* 1998, Eid *et al.* 1999; Chiu and Fox 2005; Zornberg *et al.* 2005) and the shear resistance of GCL-GM interfaces (Gilbert *et al.* 1996, 1997; Hewitt *et al.* 1997; Triplett and Fox 2001, McCartney *et al.* 2009). Some of these studies were used to guide the development of an ASTM standard for GCL internal and interface shear strength testing (ASTM D6243), which has been in effect since 1998. Several comprehensive reviews have already been compiled, including reviews on GCL internal and GCL-GM interface shear strength testing methods and representative shear strength values (Frobel 1996; Swan *et al.* 1999; Marr 2001; Bouazza *et al.* 2002; Fox and Stark 2004; McCartney *et al.* 2009), as well as evaluations of databases including internal and interface GCL shear strength results assembled from commercial testing laboratories (Chiu and Fox 2004; Zornberg *et al.* 2005; Koerner and Narejo 2005, McCartney *et al.* 2009). Recent research has focused on the shear strength of GCLs under dynamic loading (Fox and Olsta 2005). As a result of these studies, significant progress has been made in understanding and measuring GCL internal strength and GCL-GM interface strengths.

This chapter is geared toward providing practicing engineers a basic understanding of the variables that affect the GCL internal and GCL-GM interface shear strength determined via laboratory testing using a direct shear device with static loading. Specifically, the effects of GCL shear strength testing equipment and procedures, GCL reinforcement type, GM texturing and polymer type, normal stress, moisture conditioning, and shear displacement rate on the GCL internal and GCL-GM interface

(a)

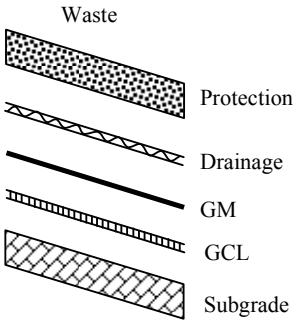

(b)

Figure 1: Composite liner system including a GCL: (a) Picture of GCL installation; (b) Components in a single composite liner system

shear strength are discussed. This chapter also includes a discussion of GCL shear strength variability, which may be significant compared with the variability in other engineering materials. Finally, a discussion of the relationship between field and laboratory shear strength values is included. Shear strength values from the literature and from a database of 414 GCL internal and 534 GCL-GM large-scale direct shear tests presented by Zornberg *et al.* (2005, 2006) and McCartney *et al.* (2009) are used to guide the discussion. The database was assembled from tests that were performed for commercial purposes between 1992 and 2003 by the Soil-Geosynthetic Interaction Laboratory of GeoSyntec Consultants, currently operated by SGI Testing Services (SGI). Test conditions reported for each series in the GCLSS database include specimen preparation and conditioning procedures, hydration time (t_h), consolidation time (t_c), normal stress during hydration (σ_h), normal stress during shearing (σ_n), and shear displacement rate (*SDR*).

2 MATERIALS

2.1 *GCL Reinforcement Types*

Several unique GCL products have been proposed to offer a compromise between the hydraulic conductivity and shear strength requirements of containment projects. These products can be broadly categorized into unreinforced and reinforced GCLs. Unreinforced GCLs typically consist of a layer of sodium bentonite that may be mixed with an adhesive and then affixed to geotextile or geomembrane backing components with additional adhesives (Bouazza 2002). The geotextile or geomembrane backing components of a GCL are typically referred to as the "carrier" geosynthetics. If hydrated, the strength of unreinforced GCLs is similar to that of the bentonite component (Gilbert *et al.* 1996). However, they are still useful for applications where slope stability is not a serious concern. For applications that require higher shear strength, reinforced GCLs transmit shear stresses to internal fiber reinforcements as tensile forces. The two predominant methods of GCL reinforcement are stitch-bonding and needle-punching (Bouazza 2002). Stitch-bonded GCLs consist of a layer of bentonite between two carrier geotextiles, sewn together with continuous fibers in parallel rows. Needle-punched GCLs consist of a layer of bentonite between two carrier geotextiles (woven or nonwoven), reinforced by pulling fibers from the nonwoven geotextile through the bentonite and woven geotextile using a needling board. The fiber reinforcements are typically left entangled on the surface of the top carrier geotextile. Since pullout of the needle-punched fibers from the top carrier geotextile may occur during shearing (Gilbert *et al.* 1996), some needle-punched GCL products are thermal-locked to minimize fiber pullout. Thermal-locking involves heating the GCL surface to induce bonding between individual reinforcing fibers as well as between the fibers and the carrier geotextiles (Lake and Rowe 2000). For simplicity, thermal-locked needle-punched GCLs are typically referred to simply as thermal-locked GCLs.

Nonwoven or woven carrier geotextiles are used in fiber reinforced GCLs to achieve different purposes. Nonwoven carrier geotextiles provide puncture protection to the bentonite layer of the GCL,

allow in-plane drainage and filtration, and provide interlocking capabilities with internal fiber reinforcements and textured geomembrane interfaces (McCartney *et al.* 2005). Woven carrier geotextiles provide tensile resistance to the GCL and allow bentonite migration, referred to as extrusion, which leads to improved hydraulic contact (Stark and Eid 1996). However, bentonite extrusion may lead to lubrication of interfaces between the GCL and the adjacent geomembrane, lowering the shear strength (Triplett and Fox 2001; McCartney *et al.* 2009).

2.2 *Geomembrane Texturing Types*

Geomembranes are flexible, polymeric sheets that have low hydraulic conductivity and are typically used as water or vapor barriers. Geomembranes come in a variety of polymer types, interface characteristics and thicknesses. High Density Polyethylene (HDPE) is the polymer predominantly used in geomembranes for landfill applications due to high chemical resistance and long-term durability. However, HDPE is relatively rigid, so more flexible polymers such as Low-Linear Density Polyethylene (LLDPE), Very-Low Density Polyethylene (VLDPE), and Polyvinyl Chloride (PVC) are often used for situations in which differential deformations are expected. During shearing, the flexibility of the geomembrane is related to the formation of ridges in the direction of shearing (plowing) which may help to increase the shear strength of geomembrane interfaces (Dove and Frost, 1999).

Geomembranes may have a smooth finish or textured finish. The textured features, typically referred to as asperities, are formed either by passing nitrogen gas through the polymer during formation (coextrusion), spraying of particles onto the geomembrane during formation (impingement), or by a physical structuring process (Koerner 2005). Asperities allow greater connection between the GM and GCL, which implies that the particular type of GCL fiber reinforcement can influence the interface strength. For instance, the interface of a needle-punched GCL with entangled fibers on the surface will likely have different behavior than a needle-punched GCL that has been thermal-locked. The effect of GM thickness on the shear strength of a GCL interface has not been investigated in detail, although McCartney *et al.* (2009) indicate that it may not be a significant factor.

3 GCL SHEAR STRENGTH TESTING EQUIPMENT

3.1 *Shear Strength Testing Alternatives*

Different aspects of shear testing conditions of GCLs must be thoroughly understood in order to reproduce representative field conditions in the laboratory. A number of devices have been developed to investigate the variables affecting GCL internal and interface shear strength, including the large-scale direct shear device, the ring shear device, and the tilt table (Marr 2001). The particular mechanisms of normal and shear load application, specimen size, and specimen confining method for a given device may have a significant impact on the GCL internal or GCL-GM interface shear strength.

The large-scale direct shear device is the testing approach most often used in industry, and it is recommended by the current testing standard for GCL internal and interface shear strength, ASTM D6243. The large-scale direct shear box is conceptually similar to the conventional direct shear test for soils (ASTM D3080) in that a horizontal, translational force is applied to a specimen to induce failure on a horizontal plane. However, larger shear boxes are used for GCL testing (300 mm by 300 mm in plan view) to reduce boundary effects from specimen confinement and allow a representative amount of internal reinforcements within the specimen. Figure 2 shows the picture of a direct shear device. Frobel (1996), Swan *et. al.* (1999), and Marr (2001) provide comprehensive summaries of issues pertinent to GCL internal and GCL-GM interface shear strength testing using a large-scale direct shear device. These studies identify the practical nature of using direct shear devices regarding ease of specimen preparation and availability.

Ring shear devices have been typically used for investigation of GCL shear strength at large displacements. In this device, ring shaped specimens of GCL are cut, and the top and bottom carrier geosynthetics are clamped onto ring-shaped platens. The top platen is then rotated about a central axis with respect to the bottom platen, inducing a shear stress in the specimen. This device is capa-

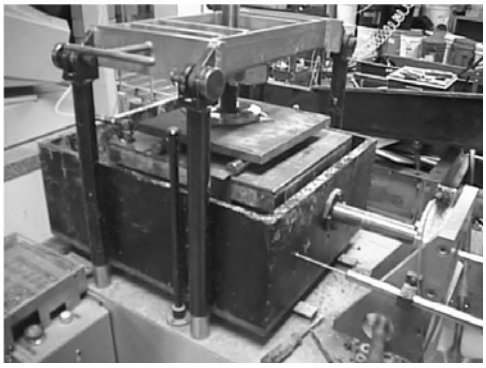

Figure 2: Large scale direct shear device

ble of applying large displacements in a single direction making it suitable for investigations of residual shear strength (Eid and Stark 1997). Additional benefits are that the contact area remains constant during shearing and the normal load moves with the top rotating rigid substrate. However, the rotational shearing mechanism may not be the same as that mobilized in the field. Ring shear devices have limitations related to specimen confinement and edge effects, testing difficulty, as well as possible lateral bentonite migration during loading (Eid and Stark 1997).

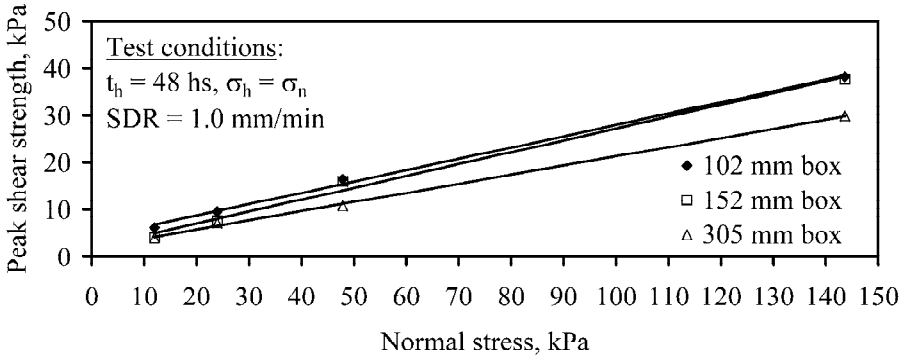

Figure 3: Effect of shear box size on GCL internal peak shear strength

The tilt table has been employed by some laboratories to test large specimens under field loading conditions (Marr 2001). In this test, a dead weight is placed above the specimen, and the entire system is tilted slowly from one side to induce a shear force. The angle of tilt and the displacements are measured. This test is a stress controlled test (*i.e.*, a constant shear force is applied throughout the specimen due to the inclination of the specimen and normal load), so it is not capable of measuring a post-peak shear strength loss. The tilt table can only be used for a limited range of normal stresses due to safety reasons.

3.2 *Specimen Size for the Direct Shear Device*

The standard large-scale direct shear device for GCLs consists of separate upper and lower boxes (or blocks) which have plan dimensions of at least 300 mm by 300 mm. This size has been selected as it provides a balance between the limitations of small boxes and large boxes. Small boxes typically give higher shear strength due to boundary effects from specimen confinement, and larger boxes have problems with uneven stress distribution and specimen hydration (Pavlik 1997). The results in Figure 3 show that testing of a 305 mm square specimen result in substantially lower shear strength than testing of a 102 mm square specimen.

Large-scale direct shear devices typically allow shear displacements of 50 to 75 mm, although the area during shearing may not be constant with shear displacement. For interface testing, the bottom box in the large-scale direct shear device is occasionally 50 to 60 mm longer (in the direction of shearing) than the top box, which provides a constant area during shearing. A longer bottom shear

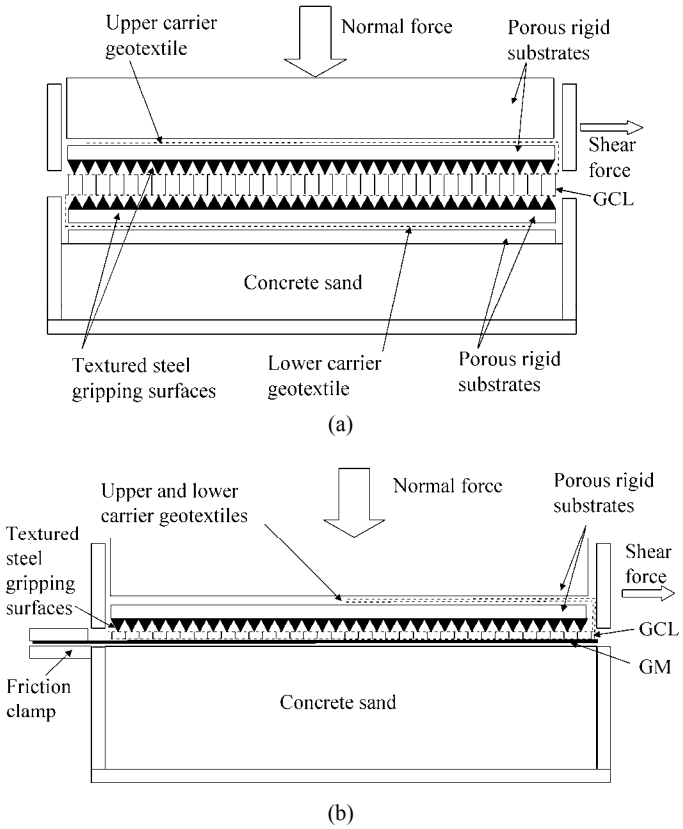

Figure 4: Large-scale direct shear device: (a) GCL internal detail; (b) GCL-GM interface detail

box is not recommended when shearing GCLs internally, as previously undisturbed and unconsolidated bentonite may enter the shear plane with further displacement. To further decrease the influence of the boundaries and allow greater shear displacements, Fox *et al.* (1997b) developed a larger direct shear device with dimensions of 405 mm by 1067 mm and maximum shear displacement of 203 mm.

3.3 *GCL Specimen Confinement for the Direct Shear Device*

The direct shear device configurations for internal GCL and GCL-GM interfaces are similar, differing only in specimen confinement. Swan *et al.* (1999) provides a review of issues relevant to the impact of specimen confinement on GCL internal and GCL-GM interface shear strength. Figure 4(a) shows the schematic view of a GCL confined within a direct shear box for internal shearing, while Figure 4(b) shows a GCL and GM confined within a direct shear box for interface shearing.

According to ASTM D6243, the GCL specimen should be confined between two porous rigid substrates (usually plywood, porous stone or porous metal) using textured steel gripping teeth, which are placed between the upper and lower boxes. The steel gripping teeth allow the shear force applied to the box to be transferred completely to the inner GCL interface. Slippage between the rigid substrate and the GCL should be minimized during shearing, as this may cause shear stress concentrations or tensile rupture of the carrier geosynthetics, which are not representative of field failure conditions. Figure 5 shows the picture of a specimen being manually trimmed to the dimensions of the rigid substrate. To speed the time of trimming GCL specimens for commercial testing, cutting dies have been developed to trim the GCL to the correct dimensions with minimal loss of bentonite. The steel gripping teeth shown in Figure 5 were constructed by adhering steel rasps (truss plates) to the rigid substrate. More intense gripping surfaces have recently been proposed to eliminate slippage problems under low confining pressures, which involve sharp teeth that enter into the carrier geotextile of the GCLs. The Geosynthetics Research Institute (GRI) is developing a new standard (GRI GCL3) that includes recommendations for GCL confinement.

The top or bottom carrier geosynthetics may be clamped into position by wrapping a flap of the GCL around the rigid substrate, and placing another rigid substrate onto the flap. Figure 6 shows a picture of a GCL-geotextile interface in which the specimens are wrapped around the rigid substrates. To provide confinement, a second rigid substrate is placed atop this assembly, which effectively clamps the top portion of the GCL into place. Gluing should not be used, as it may affect the behavior of the internal reinforcements.

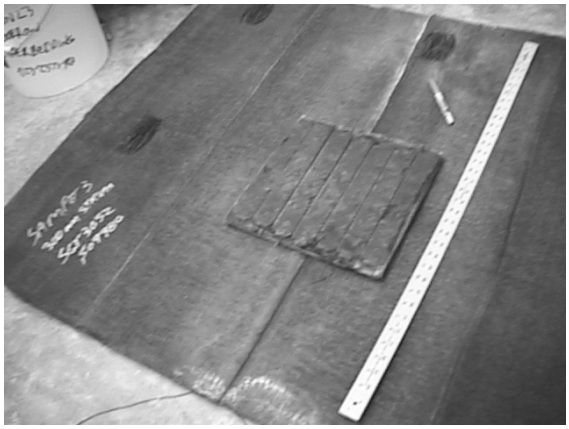

Figure 5: Specimen being trimmed to the dimension of the textured rigid substrate

Figure 6: Specimen confinement for GCL (top) and geotextile (bottom) interface testing

For GCL internal shear strength testing, the GCL is positioned in the direct shear device so that the top box is attached to the top carrier geosynthetic, and the bottom box is attached to the bottom carrier geosynthetic. The confined GCL specimen and the rigid substrates are placed atop a foundation of concrete sand, plywood or PVC plates in the bottom box, and the top box is placed so that it is in line with the top rigid substrate. The width of the gap between the boxes is adjusted to the mid-plane of the GCL.

For GCL-GM interface testing, the GCL is typically attached to the rigid substrate by wrapping extensions of the carrier geosynthetics around the textured rigid substrate in the direction of shear, then placing another rigid substrate above this to provide a frictional connection. As a GM is stiffer than a GCL and cannot be wrapped around the rigid substrate, it is typically placed atop a foundation of concrete sand (flush with the top of the bottom box). The GM is connected with a frictional clamp to the bottom box, on the opposite side to that of the shearing direction. As local slippage has been observed between the sand and GM in low normal stress tests, rigid substrates with gripping teeth have been proposed to enhance contact between the GM and the bottom box. The gap is then set to the height of the GCL-GM interface. Although the grip system forces failure at the GCL-GM interface, slack should remain in the carrier geosynthetics so that the initial shear stress distribution is not influenced by the grips.

The specimens may also be gripped so that failure occurs along the weakest interface (*e.g.*, either internally within the GCL or at the GCL-GM interface), in which case the extension of the lower GCL carrier geosynthetic is not wrapped around the rigid substrate. The gap setting should be wide enough to allow failure on the weakest plane.

GCL specimen sampling from different sections of the roll is not specifically addressed by ASTM D6243, although it is stated that specimens should not be chosen from near the edge of the GCL roll (a minimum distance of 1/10 the total width of the GCL roll). A specimen with a width of 305 mm and a length of twice the shear box (610 mm) should be trimmed from a bulk GCL specimen.

3.4 *Normal and Shear Load Application for the Direct Shear Device*

Figure 7 shows a schematic view of the load application configuration for a large-scale direct shear test. Direct shear devices can typically apply normal forces to the specimen ranging from 450 N (4.8 kPa for a 305 mm square specimen) to 140,000 N (1915 kPa for a 305 mm square specimen). Dead weights can be placed over the specimen in tests conducted under normal forces less than 500 kg, while an air bladder or hydraulic cylinder are used to apply higher forces between the specimen and a reaction frame, as shown in Figure 7. Dead weights are typically discouraged due to rotation of the top box during shear, which leads to an uneven normal stress distribution. The normal force is typically measured using a load cell placed under the cylinder, or using a system of load cells placed between a load distribution plate and the top rigid substrate. The latter option allows definition of the stress distribution during shearing. Although the top box remains stationary during testing, rollers are typically placed between the reaction frame and the load distribution plate to prevent moments induced during shearing, which may affect the shear force reading on the load cell. Most direct shear devices include an optional water bath for submerged testing. Uniform application of the normal stress over the area of the GCL is critical, as lateral migration of hydrated bentonite may occur (Stark 1998).

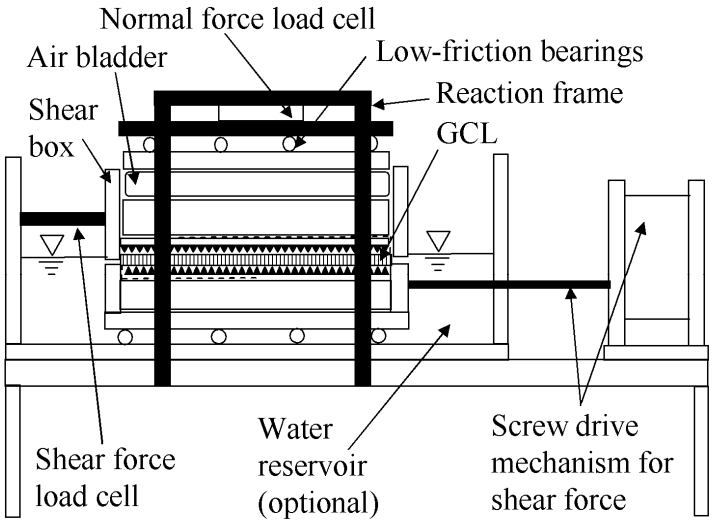

Figure 7: Load application configuration in the direct shear box (shearing occurs to the left)

For strain-controlled tests, a constant shear displacement rate is typically applied to the bottom box. As the normal load is applied to the stationary top box, translating the bottom box prevents the normal load from translating across the GCL specimen during shear. A guiding system of low friction bearings must be used to ensure that the movement between the boxes is in a single direction. The industry standard large scale direct shear device uses a mechanical screw drive mechanism to apply the constant shear displacement. The screw drive mechanism permits shear displacement rates ranging from 1.0 mm/min (time to failure of 75 minutes) to 0.0015 mm/min (time to failure of 35 days). The displacement rate is typically measured using linearly variable displacement transformers (LVDTs). For stress-controlled tests, a constant shear force is applied to the bottom box, and the resulting displacements are measured. The shear force is typically applied using a system of pulleys connected to a dead weight, or using an electric screw drive mechanism with a feedback system that regulates a constant pressure as displacement occurs. The shear force is increased incrementally to reach failure.

4 TESTING PROCEDURES

4.1 *Moisture Conditioning*

The bentonite clay in GCLs is initially in a powdered or granular form, with initial moisture content of approximately 12%. Moisture conditioning of GCL specimens for shear strength testing involves hydration and (in some cases) subsequent consolidation of the bentonite. During hydration, the bentonite absorbs water and increases in volume. Daniel *et al.* (1993) indicated that GCLs are typically expected to reach full hydration in the field unless encapsulated between two geomembranes. GCLs should be hydrated with a liquid that is representative of liquids found in the field. GCLs used in landfill liners may become hydrated before waste placement or after construction with waste leachate, while landfill covers may become hydrated from percolation through the vegetated cover or moisture in landfill gases (Gilbert *et al.* 1997; Bouazza 2002).

The hydration process typically used for GCLs is described by Fox *et al.* (1998). The specimen and rigid substrates are placed under a specified hydration normal stress (σ_h) outside the direct shear device and simultaneously submerged in a specified liquid, and allowed to hydrate during a specified hydration time (t_h). This assembly is then transferred to the direct shear device. Shearing commences immediately for specimens hydrated under the normal stress used during shearing. To simulate hydration of the GCL before loading occurs (*i.e.*, before waste placement or cover construction), the GCL is allowed to hydrated under a lower normal stress than that used during shearing. After this point, the GCL may or may not be consolidated before shearing. The GCL may not be consolidated to simulate situations where normal stress increases quickly in the field and drainage doesn't occur. When consolidating GCLs, the normal stress is increased in stages during a specified consolidation time (t_c), or until vertical displacement ceases.

Figure 8(a) shows the average moisture content of GCLs during hydration under different normal stresses. For low normal stresses, a significant increase in moisture content is observed, with constant moisture content observed after approximately 4 days. However, Gilbert *et al.* (1997) and Stark and Eid (1996) indicate that complete hydration typically requires 2 weeks. A percentage change in vertical swell of less than 5% can be obtained for unconfined GCLs in a period of 10 to 20 days, indicating full hydration (Gilbert *et al.* 1997). As the hydration normal stress increases, the moisture content only increases to 70%, and does not change significantly in water content with time.

Figure 8(b) shows the spatial distribution in moisture content in a needle-punched GCL specimen after different times of hydration. The specimen had an initial gravimetric moisture content of 12% and was hydrated under a normal stress of 9.6 kPa. Significant hydration occurs during 24 hs (moisture content change of 123%), although hydration continues after this time. The edge of the specimen has a greater increase in moisture content than the center, likely due to a rigid substrate with poor drainage. Pavlik (1997) and Fox *et al.* (1998) found that increased specimen size results in incomplete hydration at the center of GCL specimens as there is little lateral movement of water through the bentonite and carrier geotextiles. ASTM D6243 recommends using rigid substrates that are porous or have grooves to channel water during testing along with a time of hydration greater than 24 hs. Porous, textured, rigid substrates allow even hydration and better dissipation of pore water pressures during shear.

Figure 9(a) shows the vertical displacement during hydration for 4 needle-punched GCLs under different hydration normal stresses. Swelling occurs for GCLs with low hydration normal stress, and compression occurs during hydration for higher normal stress. The trend in vertical displacement with hydration normal stress is indicative of the swell pressure of the bentonite, which is defined as the hydration normal stress at which the GCL does not swell beyond its initial thickness. Petrov *et al.* (1997) reported swell pressures ranging from 100 to 160 kPa for a thermal-locked GCL, while lower values were reported by Stark (1997) for a needle-punched GCL. Zornberg *et al.* (2005) interpreted the internal peak shear strength of GCLs with different normal stresses, and shear displacement rates to infer that GCLs sheared internally will likely change in behavior above and below the swell pressure.

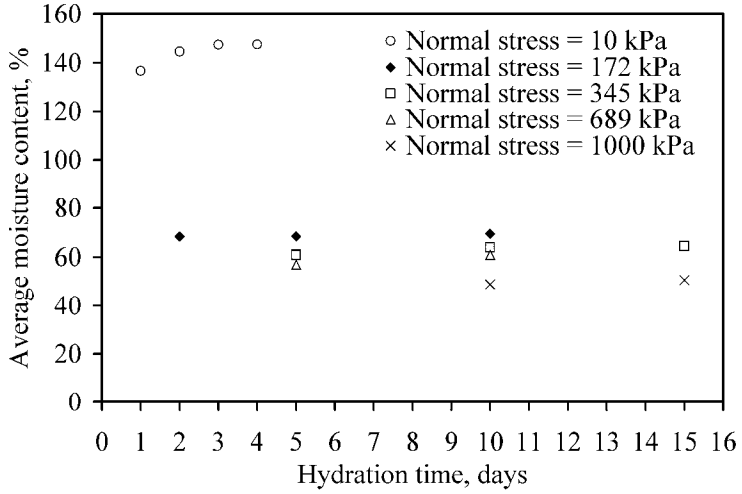

(a)

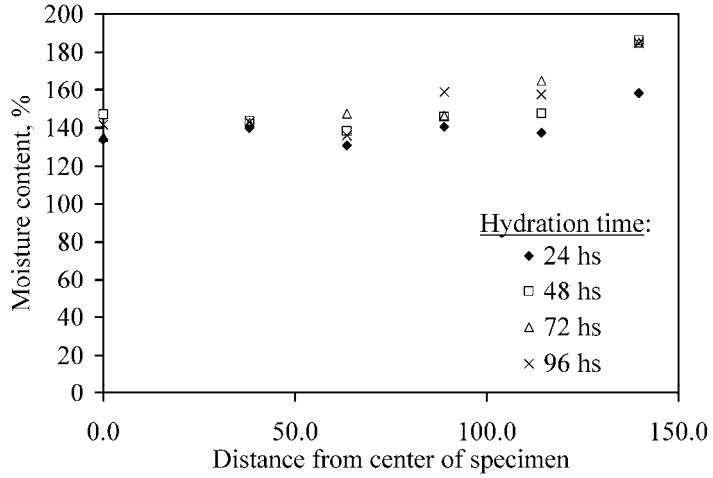

(b)

Figure 8: (a) Variation in bentonite moisture content with time during hydration under increasing σ_h; (b) Spatial variation in moisture content with time in a needle-punched GCL specimen

Figure 9(b) shows the vertical displacement of a GCL during hydration under a low normal stress and subsequently consolidated to a normal stress of 1000 kPa in stages over nearly two years. The specimen had an initial thickness of approximately 20 mm before hydration. Approximately 4 mm of vertical displacement was observed due to swelling during hydration, followed by 15 mm of settlement during consolidation. In practice, the normal load is applied in a single increment. This can lead to significant lateral movement of bentonite within the GCL, as well as extrusion through the carrier geotextiles. Lake and Rowe (2000) and Triplett and Fox (2001) observed extrusion of bentonite during moisture conditioning as well as during shearing. Bentonite extrusion may lead to lubrication of the GCL-GM interface, and may prevent drainage of water through the carrier geotextiles.

4.2 *Shearing Procedures*

Shearing is conducted after GCL conditioning by applying the shear load under a constant shear displacement rate. ASTM D6243 recommends using a shear displacement rate (SDR) consistent with the conditions expected in the field application. As it is not likely for pore pressures to be generated in the field for drained conditions such as those during staged construction of landfills (Gilbert *et al.* 1997; Marr 2001), an adequately low shear displacement rate should be used to allow dissipation of shear-induced pore water pressure. The approach used by Gibson and Henkel (1954) is typically used to define the shear displacement rate, as follows:

$$SDR = \frac{d_f}{50 t_{50} \eta} \tag{1}$$

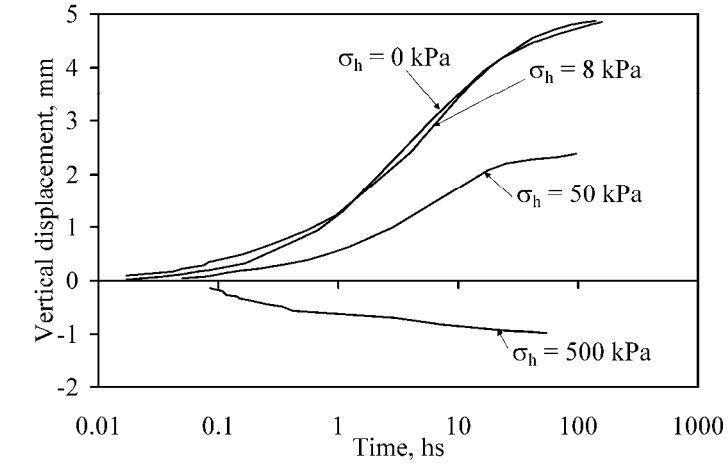

(a)

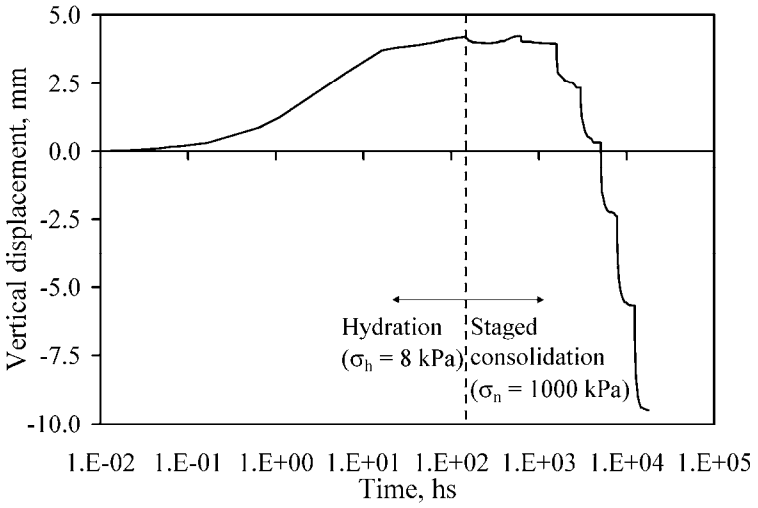

(b)

Figure 9: Conditioning of needle-punched GCLs: (a) Effect of hydration normal stress on vertical displacement during hydration; (b) Vertical displacement during hydration and consolidation

where d_f is the estimated horizontal displacement, t_{50} is the time required to reach 50% consolidation assuming drainage from the top and bottom of the specimen, and η is a factor used to account for drainage conditions. An appropriate value of t_{50} can be obtained using the vertical displacement measurements during hydration and consolidation for the GCL, shown in Figure 9(a). However, the determination of t_{50} may take several days, which may be prohibitive for commercial testing programs. In practice, engineers typically prescribe faster shear displacement rates to prevent long testing times and increased costs, despite the possible effects of shear-induced pore water pressure generation on the shear strength results. While relatively fast for guaranteeing drained conditions anticipated in the field, a *SDR* of 1.0 mm/min is typically used in engineering practice because of time and cost considerations. For d_f, ASTM D6243 requires a minimum of 50 mm of displacement when reporting the large-displacement shear strength of a GCL. ASTM D6243 defines the possible values of η to be 1 for internal shearing, 4 for shearing between the GCL and an impermeable interface, and 0.002 for shearing between the GCL and a permeable interface.

The shear displacement is typically measured using an LVDT or dial gauge, and the shear force measured using a load cell, are used to define the shear stress-displacement curve. Peak shear

strength is reported as the maximum shear stress experienced by the interface. The large-displacement shear strength is reported as the shear stress when there is constant deformation with no further change in shear stress, or the shear stress at a displacement of 50 to 70 mm. The large-displacement shear strength is the shear stress that remains after all fiber reinforcements (if any) in the failure plane rupture and the soil particles in the shear zone align into the direction of shear. Large-displacement shear strength is typically reported instead of residual shear strength because the shear displacement capability of the direct shear device is often not sufficient to mobilize GCL residual shear strength. The residual shear strength of a GCL may not be reached until displacements as large as 700 mm (Fox *et al.* 1998), although some testing facilities have observed residual conditions after approximately 300 mm.

5 GCL INTERNAL SHEAR STRENGTH

5.1 *Shear Stress-Displacement Behavior*

Figure 10(a) shows a typical set of shear stress-displacement curves for a needle-punched GCL tested under a wide range of normal stresses. A prominent peak value is observed at a shear displacement less than 25 mm, followed by a post-peak drop in shear strength. As normal stress increases, the secant modulus at 10 mm of displacement increases significantly, and the displacement at peak increases. For similar normal stress and conditioning procedures, Hewitt *et al.* (1997), Fox *et al.* (1998) and Zornberg *et al.* (2005) found that the needle-punched and thermal-locked GCLs have similar shaped shear-stress displacement curves with peak strength occurring at shear displacements ranging from 10 to 30 mm, while stitch-bonded GCLs have lower peak shear strength values occurring at a shear displacement ranging from 40 to 70 mm. Due to the greater amount of reinforcement in needle-punched GCLs than in stitch-bonded GCLs, needle-punched GCLs act in a more brittle manner than stitch-bonded.

Figure 10(b) shows typical vertical displacement vs. shear displacement curves for GCLs sheared internally under the same normal stress and conditioning procedures, but different shear displacement rates. The data in this figure indicate compressive deformations during shearing, which indicate consolidation of the GCL. Consolidation is likely occurring in these tests due to ongoing dissipation of excess pore water pressures from the increase in normal stress from 500 to 520 kPa, as well as due to dissipation of shear-induced positive pore water pressures. It should be noted that vertical displacement measurements in direct shear tests only measure the overall vertical displacement of the top box, which may be caused by GCL expansion/contraction during shear, continued consolidation of the GCL, and tilting of the top box from moments caused by the increase in horizontal stress. These changes may not be the same as those on the failure surface.

Inspection of the shear displacement curves may indicate the quality of the test. For example, testing problems such as slippage between the gripping system and GCL or plowing of the grip system into the GCL may manifest in the shear displacement curves. Slippage is typically indicated by a very rough shear displacement curve with erratic changes in shear load with increased displacement. Rapid application of the normal stress during consolidation may lead to excessive bentonite extrusion from the GCL, which may in turn cause interaction between the upper and lower grips during shear. Interaction between the grips is typically indicated by a constantly increasing shear stress, or a peak shear strength value that occurs at a displacement greater than 25 mm. A quality shear strength test will have a shear displacement curve with a peak occurring at less than 25 mm and a smooth post-peak reduction to a large-displacement shear strength resulting in a large-displacement friction angle of 8 to 13 degrees.

5.2 *Preliminary Shear Strength Overview*

Figure 11 shows GCL internal peak shear strength values τ_p reported in the literature. The wide range in shear strength reported by the different studies can be explained by differences in GCL reinforcement types, moisture conditioning procedures, shear displacement rates, as well as testing procedures and equipment used in the various studies, although significant variability is still apparent. Generally, reinforced GCLs show higher shear strength and greater variability than unreinforced GCLs.

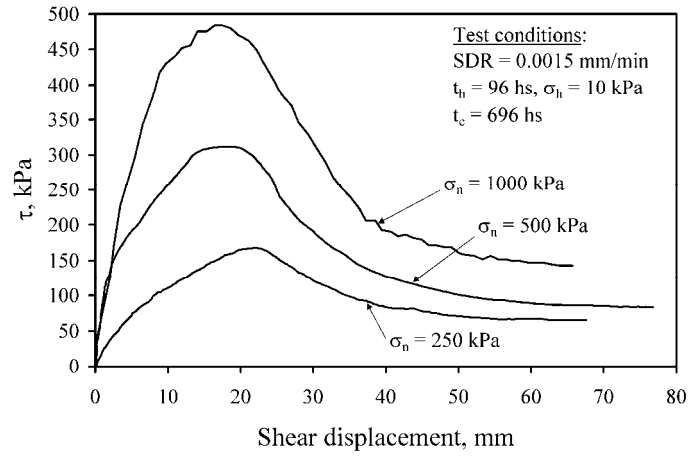

(a)

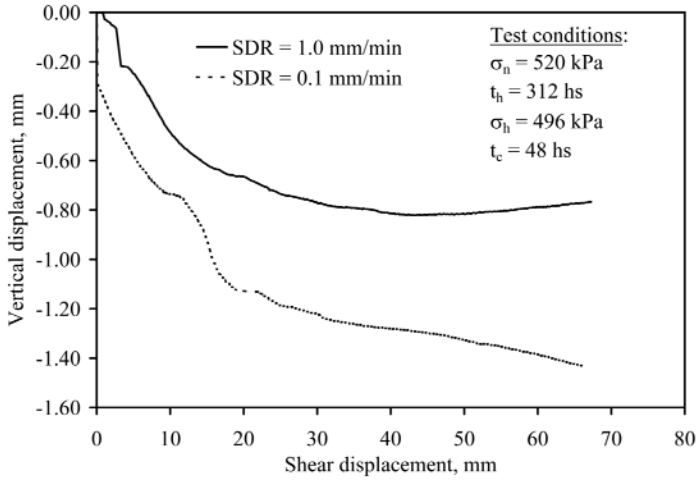

(b)

Figure 10: (a) Shear stress – shear displacement curves for needle-punched GCL sheared internally under different normal stresses; (b) Vertical displacement – Shear displacement curves

5.3 *Variables Affecting GCL Internal Shear Strength*

5.3.1 *Effect of Normal Stress*

GCLs are frictional materials, so their shear strength increases with normal stress. Also, the internal reinforcements give the GCL strength at low normal stress. Accordingly, the GCL internal peak shear strength for a set of tests with the same conditioning procedures and shear displacement rate is typically reported using the Mohr-Coulomb failure envelope, given by:

$$\tau_p = c_p + \phi_p \tan \sigma_n \qquad (2)$$

where τ_p is the peak shear strength, c_p is the cohesion intercept, σ_n is the normal stress and ϕ_p is the interface friction angle. ASTM D6243 requires a minimum of three points [(τ_{p1}, σ_{n1}), (τ_{p2}, σ_{n2}), (τ_{p3}, σ_{n3})] to define the peak or residual failure envelope for the given interface. Chiu and Fox (2004) and Zornberg *et al.* (2005) provide a range of internal peak shear strength parameters for different GCLs, hydration procedures, ranges of normal stresses, and shear displacement rates. Zornberg *et al.* (2005) also found that large-displacement shear strength was represented well by a linear failure envelope, although the cohesion intercept was typically negligible.

Most previous studies on GCL shear strength (Gilbert *et al.* 1996; Daniel and Shan 1993; Stark and Eid 1996; and Eid and Stark 1997, 1999) were for tests under low levels of normal stresses (typically below 200 kPa). Fox *et al.* (1998), Chiu and Fox (2004), and Zornberg *et al.* (2005) report shear

strength values for a wider range in normal stresses, and indicate that linear failure envelopes do not represent the change in shear strength with normal stress. Accordingly, multi-linear or nonlinear failure envelopes are recommended. Gilbert *et al.* (1996) and Fox *et al.* (1998) used the model presented by Duncan and Chang (1970) to represent nonlinear trends in shear strength with normal stress, as follows:

$$\tau_p = \sigma_n \left[\phi_0 - \Delta\phi \log\left(\frac{\sigma_n}{P_a} \right) \right] \tag{3}$$

where P_a is the atmospheric pressure, ϕ_0 is the secant friction angle at atmospheric pressure, and $\Delta\phi$ is the change in secant friction angle with the log of the normal stress normalized by P_a.

Figure 12 shows the trend in GCL internal peak shear strength with normal stress for different needle-punched GCLs. The results within each data set were obtained from direct shear tests with the same conditioning procedures and shear displacement rate. For tests under low normal stress (σ_n < 100 kPa), a significant increase in peak shear strength is observed with normal stress, while for tests under high normal stress (σ_n > 100 kPa), a less prominent increase in peak shear strength is observed.

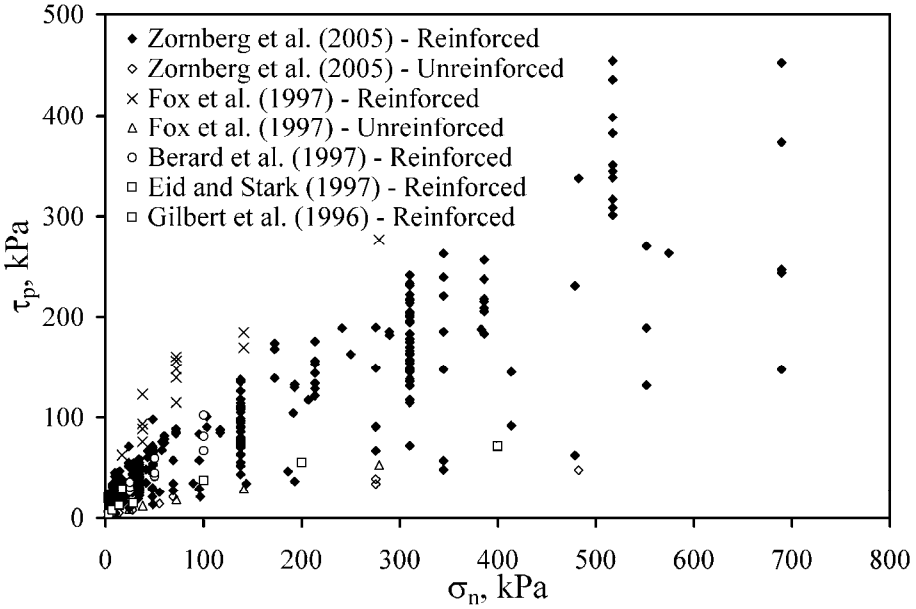

Figure 11: Overview of GCL internal peak shear strength values

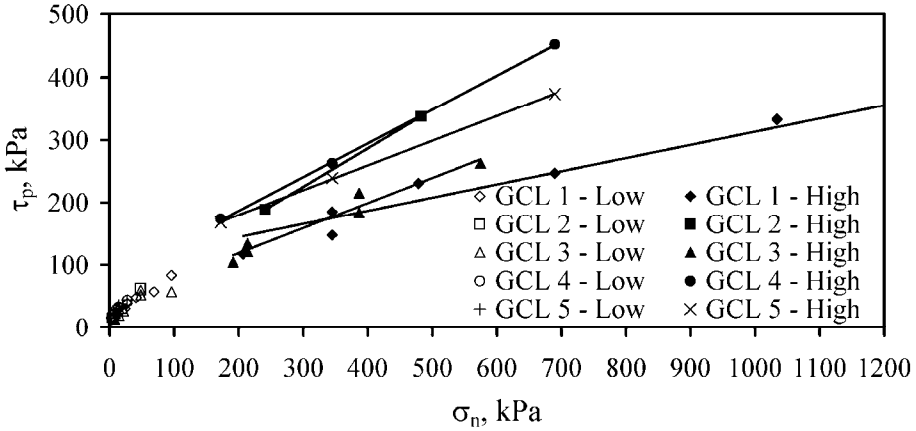

Figure 12: Normal stress effects on needle-punched GCL internal shear strength

The data in Figure 12 suggests that bilinear failure envelopes represent the data well for normal stresses under low normal stresses (< 100 kPa) and high normal stresses (>100 kPa). Zornberg *et al.* (2005) reported shear strength parameters for several bilinear failure envelopes. In addition, Chiu and Fox (2004) reported shear strength parameters for nonlinear failure envelopes. Both approaches tend to represent the shear strength of GCLs over a wide range in normal stress. The change in GCL shear strength behavior with normal stress is important to consider when specifying normal stresses to define a failure envelope, which should always be within the range expected in the application.

The normal stress applied to a GCL may affect the lateral transmissivity of the carrier geotextiles. Depending on if the carrier geotextile is woven or nonwoven and the carrier geotextile compressibility, high normal stresses may lead to decreased lateral transmissivity of the carrier geotextiles. Combined with bentonite extrusion, the carrier geotextiles may not aid the dissipation of shear-induced pore water pressures under high normal stresses. The normal stress may also affect the strength of GCL reinforcements. Gilbert *et al.* (1996) reported that the resistance of fiber reinforcements to pullout from the carrier geotextiles increased with normal stress because of the frictional nature of the connections.

5.3.2 *GCL Reinforcement*

Table 1 shows typical shear strength parameters for different sets of GCLs reported by Zornberg *et al.* (2005). The peak shear strength calculated at a normal stress of 50 kPa, τ_{50}, is also shown in Table 1 for comparison purposes. The peak internal shear strength of reinforced GCLs is significantly higher than that of unreinforced GCLs. The reinforced GCLs have a substantial intercept, while the unreinforced GCLs have a relatively low cohesion intercept and friction angle. The data in Table 1 indicates that needle-punched GCLs and thermally-locked GCLs have similar shear strength, while stitch-bonded GCLs have lower shear strength.

The difference between the needle-punched and thermal-locked GCLs may be explained by the pullout of reinforcements from the woven geotextile of the thermal-locked GCL during hydration and shearing (Lake and Rowe 2000). The fiber reinforcements in needle-punched GCLs are typically left entangled on the surface of the woven carrier geotextile, so significant swelling or shear displacement is required for pullout of the fibers from the carrier geotextile. On the other hand, the fibers in thermal-locked GCLs are melted together at the surfaces of the woven carrier geotextile. Stitch-bonded GCLs have less fiber reinforcement per unit area (stitches are typically at a 3-inch spacing), but the fiber reinforcements are continuous throughout the length of the GCL. Fox *et al.* (1998) and Zornberg *et al.* (2005) observed that the continuous fiber reinforcements in GCL *B* did not break during shearing, but instead the woven carrier geotextile ruptured at large shear displacements. The lower reinforcement density and mechanism of failure influences in the direct shear device leads to the low shear strength of these GCLs. Stitch-bonded GCLs are typically not used in practice. Table 1 also indicates that GCLs with nonwoven carrier geotextiles have similar shear strength at a normal stress of 50 kPa to woven carrier geotextiles. However, the greater friction angle of GCLs with woven carrier geotextiles leads to higher shear strength at high normal stresses for these GCLs.

Fox *et al.* (1998) found that the type of fiber reinforcement used in GCLs (needle-punched or stitch-bonded) has minor effect on the residual shear strength of GCL, although Zornberg *et al.* (2005) found that the type of fiber reinforcement still has an effect on the shear strength at a displacement of 75 mm.

Many studies have been conducted to investigate whether the internal shear strength of a needle-punched GCLs vary with the amount of needle punching per unit area of the GCL. Needle-punched GCLs are manufactured using a production line assembly which employs several threaded needles connected to a board (von Maubeuge and Ehrenberg 2000). As the lifetime of the needle-punching boards increases, more needles break and a lower density of fiber reinforcements may be apparent in the GCL with wear of the needle-punching board. The peel strength test (ASTM D6496) has been used as a manufacturing quality control test, as well as an index of the density (and possibly the contribution) of fiber reinforcements in needle-punched GCLs (Heerten *et al.* 1995, Eid and Stark 1999). Several studies have correlated the peak internal shear strength of needle-punched GCLs with peel strength (Berard 1997; Richardson 1997; Fox *et al.* 1998; Eid *et al.* 1999; Olsta and Crosson 1999; von Maubeuge and Lucas 2002; Zornberg *et al.* 2005). Figure 13 shows a comparison of the trends in peak shear strength of needle-punched GCLs with peel strength from several of these studies. An

increase in peak shear strength is apparent in some of these data sets, although only Zornberg *et al.* (2005) used the same GCL, same conditioning procedures, and shear displacement rate. Overall, no trend is observed in this data.

Stark and Eid (1996) performed shear strength tests on reinforced GCLs with and without a sodium bentonite component (filled and unfilled, respectively) to find the effect of the reinforcement of the shear strength of reinforced GCLs. They found that the peak shear strength of unfilled GCLs was higher than that of filled GCLs, which indicates that the shear resistances of the sodium bentonite and the reinforcements are not additive. This trend may be due to pullout of the fiber reinforcements due to swelling of the bentonite during hydration. The presence of reinforcement may cause an adhesive component in the shear strength failure envelope of the GCL, because the fiber reinforcements provide tensile resistance to the bentonite clay. The tensile strength of the fiber reinforcements provides confinement of the sodium bentonite portion of the GCL. Lake and Rowe (2000) found that reinforced GCLs provide additional confinement to the bentonite, which may prevent swelling of the bentonite during hydration.

Table 1: Shear strength parameters for GCL internal peak shear strength

GCLdescription	Peak envelope		τ_{50} (kPa)
	c_p (kPa)	ϕ_p (Degrees)	
Reinforced GCLs	40.9	18.0	57
Unreinforced GCLs	5.0	5.7	10
Needle-punched GCLs	40.5	19.5	61
Stitch-bonded GCLs	28.5	5.6	33
Thermal-locked GCLs	33.2	22.7	54
W-NW needle-punched GCLs	19.1	40.9	58
NW-NW needle-punched GCLs	35.0	24.5	58

5.3.3 *Moisture Conditioning*

Hydration of the bentonite layer has been reported to result in a decrease in shear strength (Gilbert *et al.* 1997; McCartney *et al.* 2004). Figure 13 shows a comparison between the internal peak shear strength at a normal stress of 50 kPa for a needle-punched GCL. Hydration of the GCL under the normal stress used during shearing during 48 hs led to a decrease in shear strength of about 40% from unhydrated conditions. Hydration of the GCL under a normal stress less than that used during shearing without allowing time for consolidation led to an even greater decrease in shear strength. Conversely, GCLs that were consolidated after hydration have shear strength closer to that of unhydrated GCLs.

Stark and Eid (1996) found that hydration of GCLs from a water content of approximately 10 to 20% to a water content of approximately 150 to 200% during 250 hours led to a reduction in the peak and residual friction angles by about 40%. However, GCLs do not lose shear strength at a rate proportional to the increase in specimen water content. Daniel and Shan (1993) found that partially hydrated GCL specimens have similar shear strength as fully hydrated GCL specimens for normal stress below 100 kPa. Their analysis showed that GCLs with a water contents between 50 and 80% (t_h < 24 hours) have similar shear strength to GCLs with water contents between 180 and 200% (t_h > 24 hours).

Hydration of GCLs under low hydration normal stresses leads to swelling of the sodium bentonite, which leads to an increase in the bentonite void ratio. Further, bentonite swelling leads to stretching or pullout of the fiber reinforcements. Conversely, high hydration normal stresses do not allow swelling of the bentonite. As consolidation occurs, the void ratio decreases during consolidation, leading to an increase in bentonite shear strength. However, consolidation does not lead to shear strength recovery in the case that fiber reinforcement pullout occurs during hydration. Further, the effective stress in the partially hydrated GCLs is higher due to negative pore pressures present before shearing occurs, while the effective stress in the GCLs hydrated under low normal stress and sheared at a

higher stress without allowing consolidation is higher due to positive pore pressures before shearing occurs.

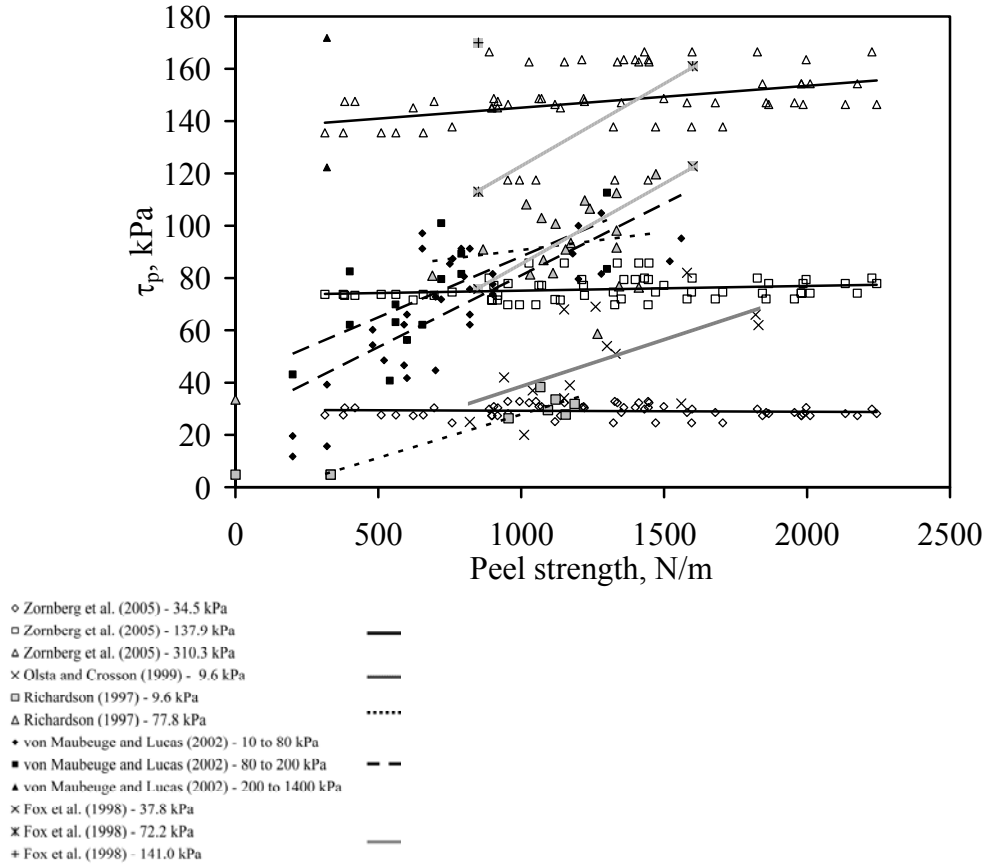

Figure 13: Relationship between GCL internal peak shear strength and GCL peel strength

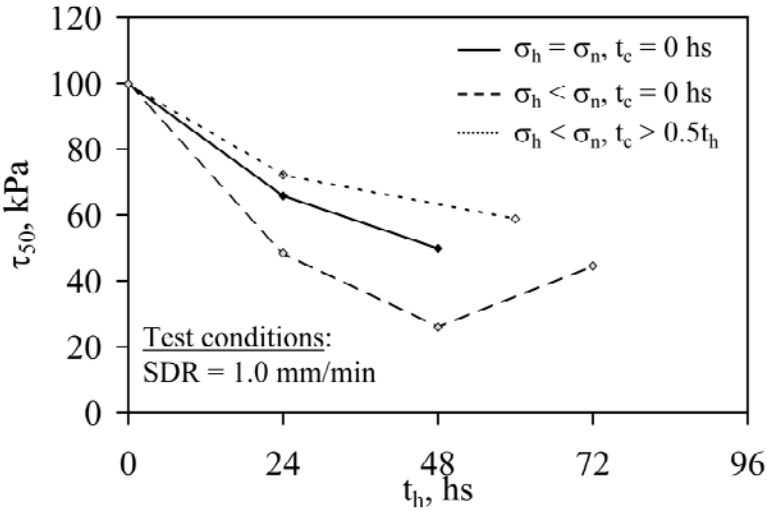

Figure 14: Effects of moisture conditioning on GCL internal peak shear strength

The liquid used in hydrating GCL test specimens may also yield varying shear strength results. Daniel and Shan (1993) tested the shear strength of GCLs with several different hydration liquids, including simulated leachate, and found that the use of distilled water leads to the lowest shear strength.

Gilbert *et al.* (1997) reported that the magnitude of sodium bentonite swell also depends on the hydration fluid, where distilled water induces the largest amount of swell, and inorganic and organic fluids cause the least. The data shown in Figure 13 is for GCLs hydrated with tap water, which has similar cation content to groundwater. Tap water provides a compromise between the effects of leachate and distilled water.

5.3.4 *Shear Displacement Rate*

The effect of SDR on the peak and large-displacement shear strength has been reported by Stark and Eid (1996), Gilbert *et al.* (1997), Eid and Stark (1997), Fox *et al.* (1998) and Eid *et al.* (1999). These studies, which primarily focused on the response of tests conducted under relatively low σ_n, reported increasing peak shear strength with increasing shear displacement rate. Gilbert *et al.* (1997) conducted direct shear tests at shear displacement rates ranging between 0.0005 and 1.0 mm/min on unreinforced GCLs with normal stresses of 17 kPa and 170 kPa. Eid *et al.* (1999) conducted ring shear tests at shear displacement rates ranging between 0.015 mm/min and 36.5 mm/min for needle-punched GCLs sheared at normal stresses between 17 and 400 kPa. Figure 15 shows the effect of shear displacement rate on the internal peak shear strength of reinforced and unreinforced GCLs sheared under a range of normal stresses. The data reported by Zornberg *et al.* (2005) and McCartney *et al.* (2002) included specimens that were trimmed from the center of the same roll to prevent variations in reinforcement density that may occur with the width. The data in Figure 15 follows an increasing trend in peak shear strength with shear displacement rate for tests conducted under low normal stresses (< 100 kPa), and a decrease in shear strength for tests conducted under high normal stresses (> 100 kPa).

Explanations proposed to justify the trend of increasing peak shear strength with increasing *SDR* observed in other studies, conducted under relatively low σ_n, have included shear-induced pore water pressures, secondary creep, undrained frictional resistance of bentonite at low water content, and rate-dependent pullout of fiber reinforcements during shearing. However, the results obtained from tests conducted under both low and high σ_n suggest that the observed trends are consistent with generation of shear-induced pore water pressures. Further, longer tests allow additional time for hydration and consolidation of the GCL, which may have an additional effect on the shear strength of the GCL. The GCLs tested under low normal stress may tend to swell during hydration, so longer testing times may lead to lower shear strength. Conversely, the GCLs tested under high normal stress may tend to consolidate during hydration, so longer testing times will lead to specimens with lower void ratio and higher shear strength.

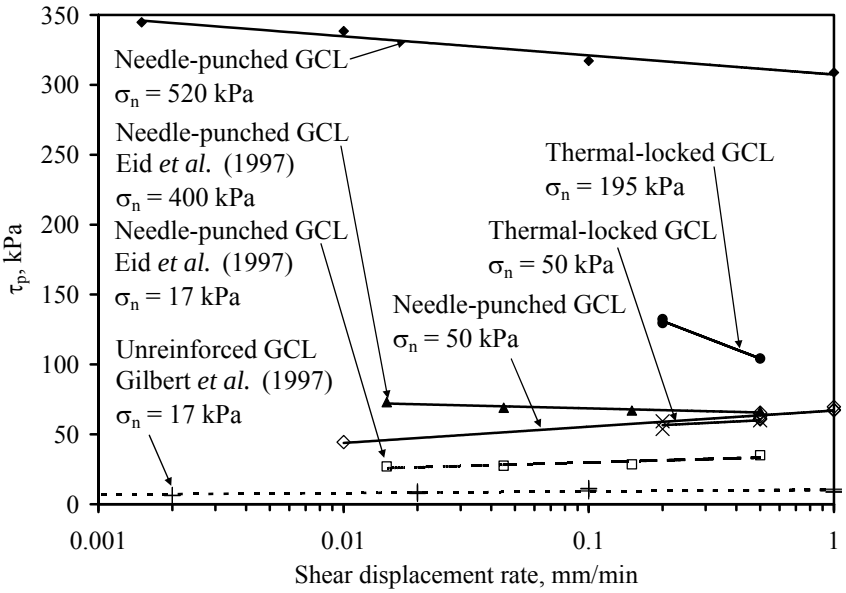

Figure 15: Effects of shear displacement rate on GCL internal peak shear strength

The shear-induced pore pressure response of the sodium bentonite may indicate its positive or negative contribution to the shear strength of the GCL. Shear-induced pore water pressures are expected to be negative in tests conducted under low σ_n (*i.e.,* below the swell pressure of GCLs). Consequently, increasing the shear displacement rate will lead to increasingly negative pore water pressures and higher peak shear strength. On the other hand, shear-induced pore water pressures are expected to be positive in tests conducted under high σ_n (*i.e.,* above the swell pressure of GCLs). In this case, increasing SDR will lead to increasingly positive pore water pressures and thus lower peak shear strength.

Gilbert *et al.* (1997) reported a pore water pressure dissipation time analysis using a model proposed by Gibson and Henkel (1954). This model predicts that shear displacement rates less than 0.001 mm/min result in constant peak shear strength for unreinforced GCLs. Gilbert *et al.* (1997) suggested that slow shear displacement rates could result in creep, as it is a rate-dependent mechanism. This may explain the decreasing trend in shear strength with decreasing shear displacement rate.

Kovacevic Zelic *et al.* (2002) reported that the peak and large-displacement shear strength of an unreinforced GCLs increase with increasing shear displacement rates for normal stresses of between 50 and 200 kPa. This was postulated to be a result of changing effective stress (*i.e.*, generation of positive pore water pressure) on the failure plane or rate effects such as creep. However, when the vertical displacement during shearing was measured, inconsistent findings were apparent. Swelling occurred during shearing for slow shear displacement rates, and settlement occurred during shearing for fast shear displacement rates. Swelling is associated to negative pore water pressure generation, which should yield higher shear strength, which was the opposite observed. The authors were inconclusive with respect to the effect of the shear displacement rate on pore water pressure generation. Vertical displacements measured in the direct shear box are typically not representative of the displacements along the shear plane due to principal stress rotation during shear, tilting of the top platen, and uneven distribution of pore water pressures (or strains) throughout the bentonite thickness.

Stark and Eid (1996) observed that the peak shear strength increased with increasing shear displacement rates for GCLs with the sodium bentonite component removed (*i.e.*, the interface between two geotextiles, needle-punched together). This phenomenon was postulated to arise from tensile rupture of the fiber reinforcements at high shear displacement rates, and gradual pullout of the fiber reinforcements at slow shear displacement rates. For filled GCLs, the peak shear strength was constant below 0.4 mm/min, then increased with increasing shear rate up to about 1.5 mm/min, and then decreased for greater shear displacement rates. Stark and Eid (1996) hypothesized several mechanisms that explained these phenomena. Although pore water pressures may have been generated in the GCL at shear displacement rates between 0.4 mm/min and 1.5 mm/min, the increased shear strength was associated with rapid rupture of the fiber reinforcements. The decrease in strength associated with excess pore water pressures in the sodium bentonite dominated at shear displacement rates above 1.5 mm/min. At shear displacement rates below 0.4 mm/min, no excess pore water pressures generated, and gradual pullout failure of the fiber reinforcements may have led to the minimum peak shear strength. Stark and Eid (1996) recommended that shear displacement rates less that 0.4 mm/min be used for shearing of needle-punched GCLs. Eid and Stark (1999) reported a decrease in final water content at high normal stresses as a result of consolidation during shear.

Stark and Eid (1996) and McCartney *et al.* (2002) found that the large-displacement shear strength of reinforced GCLs remains constant with decreasing shear rate. The shear-induced pore pressures are expected to fully dissipate upon reaching residual shear strength.

5.4 *GCL Internal Shear Strength Variability*

The data shown in Figure 11 indicate that GCL internal shear strength is an inherently variable property. Zornberg *et al.* (2005) indicated that potential sources of GCL internal shear strength variability include: (*i*) differences in material types (type of GCL reinforcement, carrier geosynthetic), (*ii*) variation in test results from the same laboratory (repeatability), and (*iii*) overall material variability. In turn, the overall material variability includes more specific sources such as: (*iii-a*) inherent variability of fiber reinforcements, and (*iii-b*) inherent variability of the shear strength of sodium bentonite. This study found that the most significant source of shear strength variability was due to

inherent material variability. Figure 16 shows the peak shear strength of GCLs with the same conditioning procedures and shear displacement rate. The spread in peak shear strength values about the mean trend line, represented by the probability density functions, increases with normal stress. In particular, a mean shear strength of 177 kPa is observed at a normal stress of 310 kPa, but the shear strength varies from approximately 115 kPa to 230 kPa. Chiu and Fox (2004) also provide measures of shear strength variability, and McCartney *et al.* (2004) presented an application of GCL shear strength variability in stability design.

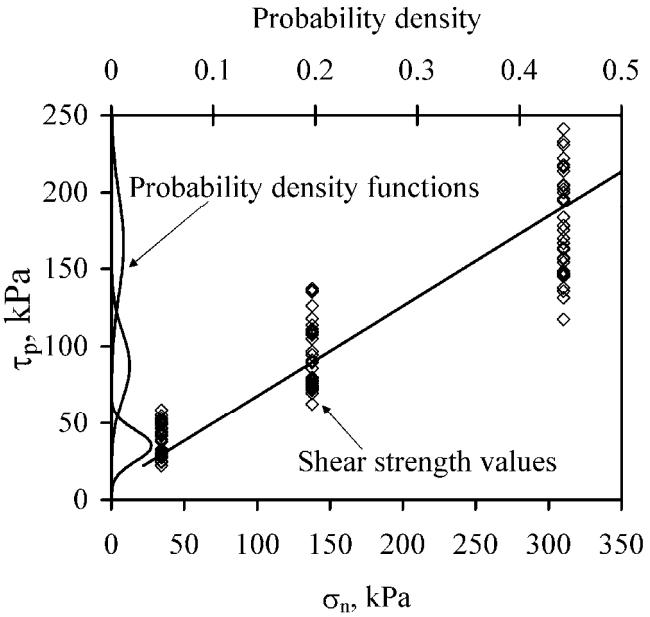

Figure 16: Variability in GCL internal peak shear strength for constant moisture conditioning (t_h = 168 hs, σ_h = 20.7 kPa, t_c = 48 hs, SDR = 1.0 mm/min) with mean failure envelope

6 GCL-GM INTERFACE SHEAR STRENGTH

6.1 *Shear Stress-Displacement Behavior*

Figure 17 shows typical shear stress-displacement curves for interfaces between the woven carrier geotextile side of a needle-punched GCL-textured HDPE GM with the same conditioning procedures and sheared under a slow shear displacement rate under different normal stresses. Similar to the GCL curves, the secant modulus tends to increase with normal stress, but the displacement at peak tends to increase with normal stress from 10 to 20 mm.

The relatively short displacement required to reach peak shear strength, combined with the large post-peak shear strength loss are important factors to consider when designing for static and dynamic design loads. The displacement at peak shear strength for the GCL-textured GM interface is slightly less than that measured for internal GCLs. The peak strength of textured GM interfaces is usually developed at 7 to 20 mm when the interlocking connections between the GCL and the textured geomembrane rupture. However, the peak shear strength of smooth geomembranes is typically developed at shear displacements less than 3 mm (Triplett and Fox 2001; McCartney *et al.* 2009). Hewitt *et al.* (1997) observed that the shear stress-displacement curves of different GCLs with different interfaces follow similar behavior to the GCL internal shear stress-displacement curves, especially for stitch-bonded GCLs. Little post-peak shear strength loss is observed for smooth geomembrane interfaces.

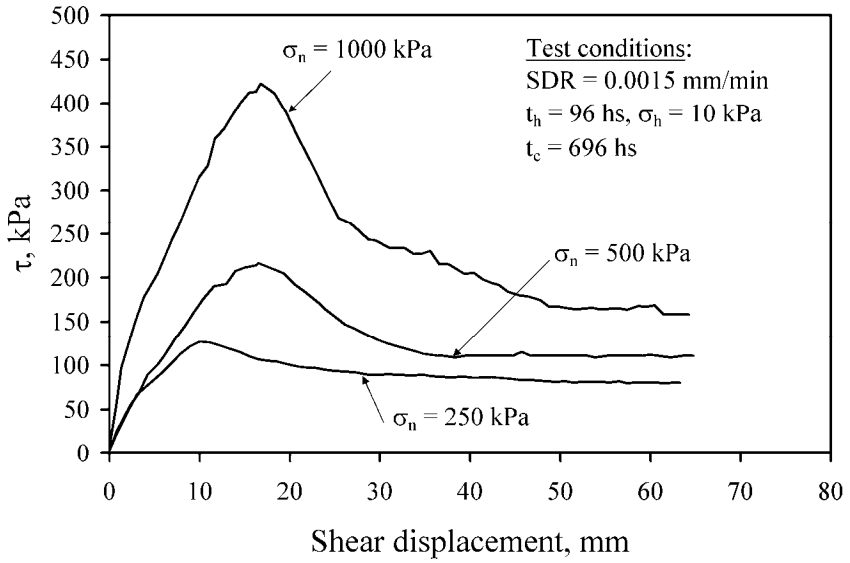

Figure 17: Shear stress – displacement curves for interface shearing of the woven carrier geotextile side of a needle-punche GM under different normal stresses

Triplett and Fox (2001) and McCartney *et al.* (2009) observed that textured HDPE geomembrane interfaces experience a greater post-peak shear strength loss than smooth HDPE geomembranes. In fact, smooth GM interfaces rarely experience any post-peak shear strength reduction. Accordingly, the difference between peak and residual shear strengths was greater for textured GM interfaces. This is most likely due to the fact that at the peak shear strength, the interlocking capabilities of the geotextile and fiber reinforcements with the geomembrane asperities rupture, resulting in a large loss of strength.

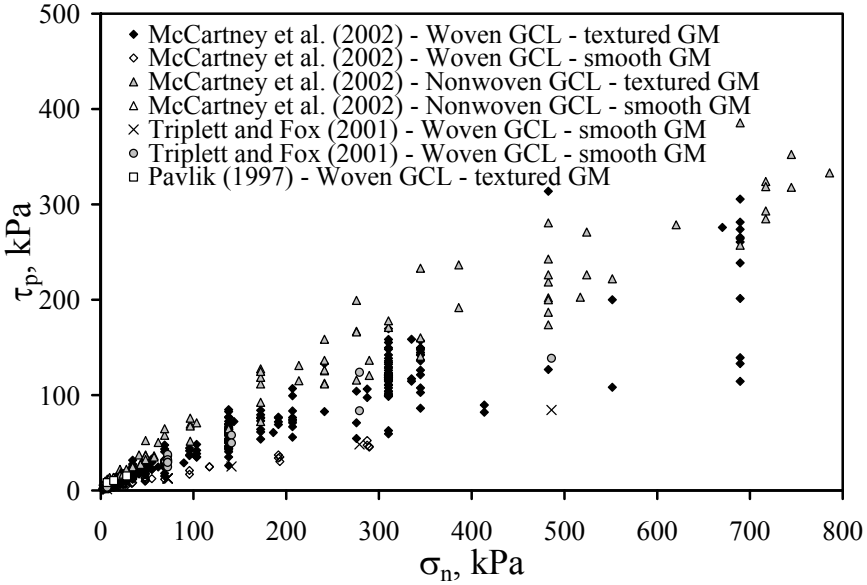

Figure 18: Overview of GCL-GM interface shear strength values

6.2 *Preliminary GCL-GM Interface Shear Strength Overview*

Figure 18 shows the range of peak shear strength values obtained from several studies on GCL-GM interfaces. Good agreement is observed between the results from the different studies, although significant variability is observed. The textured GM interfaces are significantly stronger than the

smooth GM interfaces. In general, the nonwoven carrier geotextile side of the GCL has higher interface shear strength than the woven carrier geotextile side. Different from the data for GCL internal shear strength shown in Figure 11, the GCL-GM interface shear strength does not show a strong cohesion intercept.

6.3 *Variables Affecting GCL Internal Shear Strength*

6.3.1 *Normal Stress Effects*

The GCL-GM interface behaves in a frictional manner with an increase in shear strength, but it does not have a significant cohesion intercept. Accordingly, the GCL-GM interface shear strength is well represented using a Mohr-Coulomb failure envelope with a zero intercept, or a nonlinear envelope. GCL-GM interface shear strength has less pronounced nonlinearity in shear strength with normal stress than GCL internal shear strength, but the peak shear strength is best represented by the Duncan and Chang (1970) model shown in Equation (3).

Eid and Stark (1997) found that for interface tests between a GM and an unreinforced GCL involving a layer of sodium bentonite adhered to a GM, an adhesive failure occurs between the two components at high normal stresses. At lower normal stresses, the GCL failed at the expected sodium bentonite-geomembrane interface. Eid and Stark (1997) also found that the peak shear strength failure envelope for this interface is slightly non-linear.

The critical interface in a layered system may change with normal stress due to the difference in the friction angles of the internal and interface GCL failure envelopes (Stark and Eid 1996). The failure envelopes may cross at a certain normal stress, above which the interface shear strength may be the critical interface (Gilbert *et al.* 1996). As the normal stress may vary along the length of a slope (*i.e.,* in a mounded layer of waste), the critical interface may change along the length of the slope if the failure envelopes cross at the normal stress on the interface.

6.3.2 *Effects of GCL Reinforcement Type and GM Polymer*

Table 2 shows a summary of the shear strength parameters for different sets of GCL-GM shear strength data using the Duncan and Chang (1970) approach shown in Equation (3). Consistent with the data in Figure 18, the nonwoven carrier geotextiles interfaces of a GCL are typically stronger than the woven carrier geotextiles interfaces, for both textured and smooth GMs.

Table 2: Shear strength parameters for GCL-GM interface peak shear strength

Interface description	Peak envelope		τ_{50} (kPa)
	ϕ_p (degrees)	$\Delta\phi_p$ (degrees)	
Woven GCL - textured GM interfaces	23.8	7.7	25
Nonwoven GCL - textured GM interfaces	33.1	11.4	37
Woven GCL - smooth GM interfaces	11.5	7.1	12
Nonwoven GCL - smooth GM interfaces	13.7	5.0	14
GCL-textured HDPE GM interfaces	23.4	6.2	24
GCL-textured VLDPE GM interfaces	22.3	19.5	27
GCL-textured LLDPE GM interfaces	28.0	4.2	28
Needle-punched, woven GCL - textured HDPE GM interfaces	24.2	5.9	24
Stitch-bonded, woven GCL - textured HDPE GM interfaces	16.0	10.3	17
Thermal-locked, woven GCL - textured HDPE GM interfaces	23.0	5.2	23

The data in Table 2 also indicates that GMs with more flexible polymers may have higher peak shear strength than stiffer GMs. The GMs with LLDPE and VLDPE polymers generally have higher shear strength than HDPE GMs. For smooth GMs, McCartney *et al.* (2009) indicated that the flexible PVC GMs tended to have the highest interface shear strength of the smooth GM interfaces. The data in Table 2 indicates that needle-punched GCL interfaces have slightly higher shear strength than thermal-locked GCL interfaces and greater shear strength than stitch-bonded GCL interfaces.

Triplett and Fox (2001), Stark and Eid (1998), Gilbert *et al.* (1996) and Hewitt *et al.* (1997) identified that interface shear strength of GCL-textured GM interface shear strength arises from: (*i*) frictional resistance to shearing between the un-textured portions of the GM and the woven carrier geo-

textile of the GCL, (*ii*) interlocking between the woven carrier geotextile and the textured GM asperities, and (*iii*) interlocking between the fiber reinforcements of the GCL on the surface of the woven carrier geotextile and the GM asperities. The difference between smooth and textured GM interface shear strength shown in Table 2 indicate the impact of the first two mechanisms. The difference between the shear strength of the different GCL types shown in Table 2 indicates the effect of the third mechanism. In needle-punched GCLs, the fiber reinforcements formed small bundles (not thermal-locked) or asperities (thermal-locked) on the surface of the woven carrier geotextile, which generally flattened during shearing (Gilbert *et al.* 1996).

The observations of Lake and Rowe (2000) indicate that the difference between the interface shear strength of GCLs with different reinforcement types may be related to moisture conditioning Specifically, during hydration of the bentonite, the needle-punched fiber reinforcements typically pullout from the carrier geotextile while thermal-locked fiber reinforcements resist swelling of the bentonite. This implies that more bentonite extrusion will occur from thermal-locked and stitch-bonded GCLs as the bentonite is rigidly confined between the carrier geotextiles. Hewitt *et al.* (1997) confirmed that the least amount of bentonite extrusion occurs in needle-punched GCLs. Triplett and Fox (2001) found that less bentonite was extruded from the GCLs when a smooth geomembrane was used, likely due to less interaction between the GCL and GM during shearing.

6.3.3 *Effect of GM Texturing*

GM texturing is often used to increase the peak shear strength of GCL-GM interfaces, and recent studies have found that it leads to an increase in the shear interaction between the GCL and the GM using asperity heights (Ivy 2003; McCartney *et al.* 2005) and post-failure examination (Triplett and Fox 2001). Triplett and Fox (2001) and McCartney *et al.* (2005) found that GM texturing leads to an improvement in the peak and large-displacement shear strength of GCL-GM interfaces. Different texturing approaches have not been shown to influence GCL-GM interface shear strength. Ivy (2003) and McCartney *et al.* (2005) found that GM asperity heights, despite being highly variable, were a good indicator of the peak shear strength of GCL-GM interfaces and clay-GM interfaces. McCartney *et al.* (2005) found that GM asperity height is an inconsistent indicator of GCL-GM large-displacement shear strength, most likely due to rupture of asperities-GCL connections during shearing.

6.3.4 *Moisture Conditioning*

Hydration of the GCL has been reported to result in extrusion of bentonite from the GCL, and impregnation of the carrier geotextiles with sodium bentonite. Figure 18 shows a comparison between the interface peak shear strength of the woven and nonwoven carrier geotextiles of a needle-punched GCL and a textured HDPE GM at a normal stress of 50 kPa. Hydration of the woven GCL interfaces under the normal stress used during shearing led to a decrease in shear strength of about 30% from unhydrated conditions, but little impact is observed for nonwoven GCL interfaces, except for a hydration time longer than 72 hs. Hydration of the nonwoven and woven GCL interfaces under a normal stress less than that used during shearing without allowing time for consolidation led to similar to slightly lower shear strength. Unlike the trend observed for GCL interfaces, both woven and nonwoven GCL interfaces consolidated after hydration under low normal stress have the lowest shear strength.

As mentioned, the sodium bentonite component of GCLs swells during hydration, which leads to extrusion and impregnation of bentonite in the carrier geotextiles. The extruded bentonite lubricates the connections between the fiber reinforcements and the woven or nonwoven carrier geotextiles. The nonwoven carrier geotextile of needle-punched GCLs is generally thicker than the woven carrier geotextile, so more extrusion is expected from the woven carrier geotextiles. The data shown in Figure 19 indicates that moisture conditioning does not have a significant impact on the shear strength of nonwoven GCL carrier geotextile interfaces. However, moisture conditioning has a greater effect on the woven GCL carrier geotextile interface. Consolidation of the interface after hydration does not remove the lubrication effect of the hydrated bentonite. Impregnation of woven carrier geotextiles

with sodium bentonite has been shown to lead to lower shear strength than clean woven geotextile-GM interfaces (Lake and Rowe 2000).

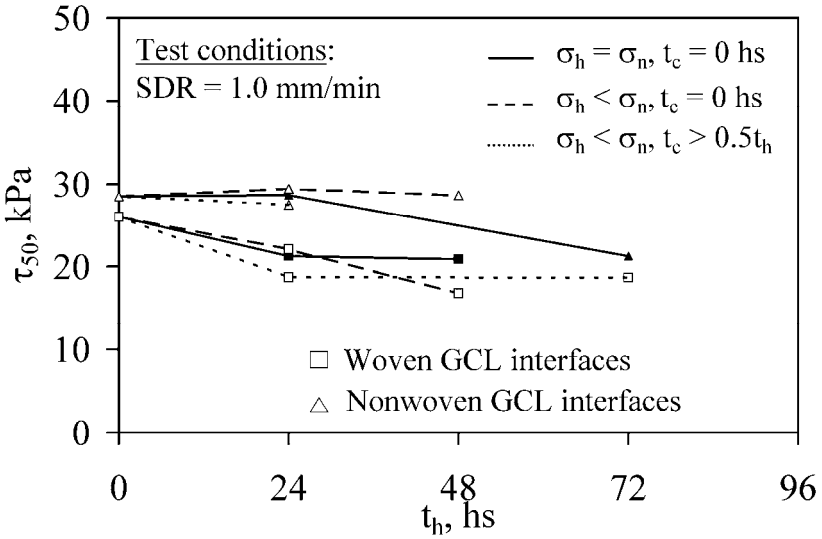

Figure 19: Effects of moisture conditioning on GCL-GM interface peak shear strength

6.3.5 *Shear Displacement Rate*

The available literature on GCL-GM interface shear strength indicates that there is not a significant effect of SDR on the peak shear strength value (Triplett and Fox 2001; McCartney *et al.* 2009). Eid *et. al.* (1999) found that the shear displacement required to reach peak strength conditions does not vary with shear displacement rate. This finding is consistent with results for geotextile-GM interfaces (Stark *et al.* 1996). The lack of a trend indicates that shear displacement effects for GCL internal shear strength are likely due to the contribution of the fiber reinforcements and bentonite. The lack of trend also implies that faster shear displacement rates may be used in practice to replicate field conditions.

6.4 *GCL Internal Shear Strength Variability*

The spread in the data shown in Figure 18 indicates that GCL-GM interface shear strength is as variable as GCL internal shear strength. The variability in GCL internal and GCL-GM interface shear strength values may have implications on the weakest plane in a liner system. Figure 20 shows a comparison between the variability in GCL internal and GCL-GM interface shear strength for tests with the same conditioning procedures and shear displacement rate. The mean failure envelopes for the sets of data indicate that the GCL internal shear strength is significantly above the GCL-GM interface shear strength. However, due to variability, a zone of overlap is observed. In this zone, the GCL internal shear strength may be less than the GCL-GM interface shear strength. The data shown in Figure 20 indicate that design of composite liner systems on a slope will be governed by GCL-GM interface shear strength except in the overlap zone delineated by the two failure envelopes. In this zone, either the GCL internal or GCL-GM interface shear strength may be the lower strength.

The GCL and GM specimens with shear strength shown in Figure 20 were obtained from the center of different manufacturing lots (*i.e.*, a set of rolls manufactured in a given batch). Zornberg *et al.* (2005) found that the variability in peak shear strength of GCLs sampled from the same manufacturing lot is less than the variability within different rolls due to manufacturing differences over time. Because the direct shear test provides the shear strength of a relatively small specimen with respect to the area of the roll, the variability in shear strength within a given roll is expected to average out over the length of a slope. However, McCartney *et al.* (2005) observed that variability in shear strength between rolls from different lots used at a given job site may not average out over the area of the

landfill, leading to zones that have lower shear strength than others. This observation emphasizes the need to conduct project-specific and product-specific shear strength testing.

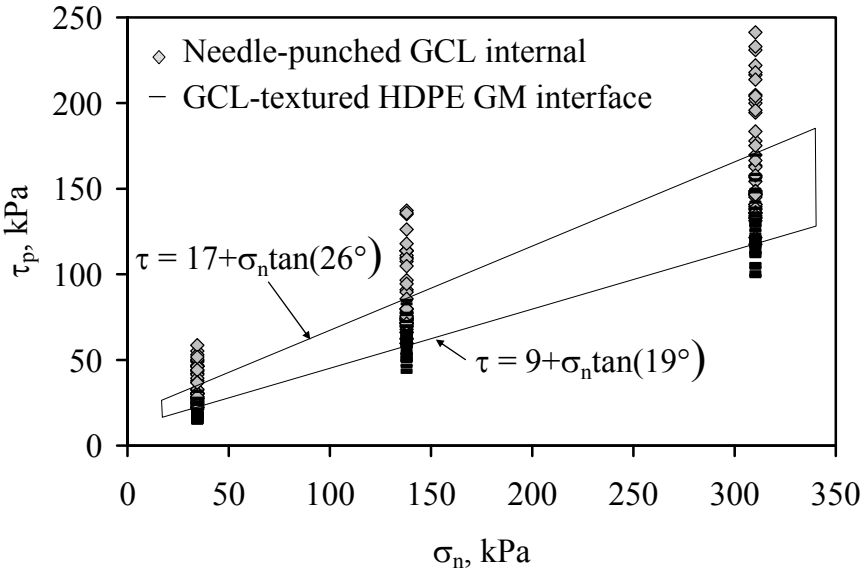

Figure 20: Internal and interface shear strength for tests with the same conditioning procedures

7 LABORATORY AND FIELD SHEAR STRENGTH COMPARISONS

Although analyses of slope failures involving GCLs are not widely published, the slope failures at the Mahoning landfill site (Stark *et al.* 1998) and the US Environmental Protection Agency (EPA) GCL test section in Cincinnati, Ohio (Daniel *et al.* 1998; Stark and Eid 1996) provide excellent opportunities to verify the results of different test devices for GCLs. Stark *et al.* (1998) observed that failure of the Mahoning landfill occurred along an unreinforced, geomembrane-backed GCL located in the landfill base liner. Further, settlement of the overlying waste caused down-drag on the liner system, resulting in large shear displacements. To simulate field conditions, the investigation included a study of the loading procedures and the hydration process for the GCL. The results of ring shear tests on hydrated GCL internal and GCL-GM interfaces were consistent with the shear strength of the soil back-calculated using two-dimensional limit equilibrium analysis.

Stark and Eid (1996) present a comparison of the results of a three-dimensional back-analysis of failures at the EPA GCL test sections with direct shear and a ring shear test results on the same GCLs and GMs. Daniel *et al.* (1998) observed failure at the interfaces between the woven geotextiles of a needle-punched GCL and a textured HDPE GM, as well as between a stitch-bonded GCL and a textured HDPE geomembrane lying on a slope of about 23.5° (Daniel *et al.* 1998). The failures occurred 20 and 50 days after construction, respectively. For the interface failures between the GCLs and GMs, the mobilized interface friction angle was approximately 21.5°. Ring and direct shear tests were conducted on the same materials under fully hydrated conditions, and it was found that the ring shear test obtained a peak friction angle of 22.5°, and the direct shear test obtained a peak friction angle of 23.8°. Both test methods obtained friction angles slightly above the actual back-calculated three dimensional friction angles, so the difference in actual and experimental friction angles may be attributed to three dimensional effects, such as the strength contribution of the vertical failure surfaces at the edges of the veneer failure or differences in scale. In addition, further differences in the shear strength measured in the laboratory and the shear strength back-calculated from forensic studies may arise from the tensile forces that may develop in the carrier geotextiles of the GCL. This phenomenon may increase the back-calculated shear strength of the GCL as the tensile forces provide additional resistance to down-slope deformations.

8 CONCLUSIONS

This chapter uses shear strength data from the literature and commercial databases to indicate the basic concepts behind geosynthetic clay liner (GCL) internal and interface shear strength values obtained from laboratory testing. The information in this chapter can be used guide the design of a site-specific shear strength testing program. The effects of different variables on the GCL and GCL-geomembrane interface shear strength are quantified. Specifically, the effects of normal stress, GCL reinforcement, geomembrane texturing and polymer type, moisture conditioning, shear displacement rate, and normal stress are assessed.

9 REFERENCES

American Society of Testing and Materials, 1998. Standard Test Method for Determining the Internal and Interface Shear Resistance of Geosynthetic Clay Liner by the Direct Shear Method. *ASTM D6243*. West Conshohocken, Pennsylvania.

American Society of Testing and Materials, 1999. Standard Test Method for Determining Average Bonding Peel Strength between the Top and Bottom Layers of Needle-Punched Geosynthetic Clay Liners." *ASTM D6496*. West Conshohocken, Pennsylvania.

Berard, J. F. 1997. Evaluation of Needle-Punched Geosynthetic Clay Liners Internal Friction. *Geosyn. '97*, St. Paul, MI. pp. 351-362.

Bouazza, A., Zornberg, J.G., and Adam, D. 2002. Geosynthetics in Waste Containments: Recent Advances. *Proc. 7th Int. Conf. on Geosynthetics*, Nice, France. vol. 2, pp. 445-507.

Byrne, R.J., Kendall, J., and Brown, S. (992. Cause and Mechanism of Failure, Kettleman Hills landfill B-19, Unit IA. *Proc. ASCE Spec. Conf. On Performance and Stability of Slopes and Embankments*, Vol. 2, ASCE. pp. 1188-1215.

Daniel, D. E., and Shan, H. Y. 1991. Results of Direct Shear Tests on Hydrated Bentonitic Blankets." Geotechnical Engineering Center, University of Texas at Austin, Austin, TX.

Daniel, D. E., Shan, H. Y., and Anderson, J. D. 1993. Effects of Partial Wetting on the Performance of the Bentonite Component of a Geosynthetic Clay Liner. *Geosyn. '97*, St. Paul, MN.

Daniel, D. E., Carson, D. A., Bonaparte, R., Koerner, R. M., and Scranton, H. B. 1998. Slope Stability of Geosynthetic Clay Liner Test Plots. *Journal of Geot.and Geoenv. Eng.*, ASCE, 124(7), 628-637.

Dove, J. E., and Frost, J. D. 1999. Peak Friction Behavior of Smooth GM-Particle Interfaces. *Journal of Geot. and Geoenv. Engineering*, ASCE, 125(7), 544-555.

Duncan, J. M. & Chang, C.-Y. 1970. Nonlinear Analysis of Stress and Strain in Soils. *Journal of the Soil Mechanics and Foundations Division*. ASCE. 96(SM5), 1629–1653.

Eid, H. T., and Stark, T. D. 1997. Shear Behavior of an Unreinforced Geosynthetic Clay Liner. *Geosyn. Int.* IFAI, 4(6), 645-659.

Eid, H. T., Stark, T. D., and Doerfler, C. K. 1999. Effect of Shear Displacement Rate on Internal Shear Strength of a Reinforced Geosynthetic Clay Liner. *Geosyn. Int.* IFAI, 6(3), 219-239.

Fox, P. J., Rowland, M. G., and Scheithe, J. R. 1998. Internal Shear Strength of Three Geosynthetic Clay Liners. *Journal of Geot. and Geoenv. Eng.*, ASCE, 124(10), 933-944.

Fox, P.J., Rowland, M.G., Scheithe, J.R., Davis, K.L., Supple, M.R., and Crow, C.C. 1997. Design and Evaluation of a Large Direct Shear Machine for Geosynthetic Clay Liners. *Geotechnical Testing Journal*. 10(3).

Fox, P.J., and Olsta, J. 2005. Current Research on Dynamic Shear Behavior of Geosynthetic Clay Liners. *Proceedings of Geo-Frontiers 2005*. ASCE.

Gibson, R.E., and D.J. Henkel. 1954. Influence of Duration of Tests at Constant Rate of Strain on Measured Drained Strength. *Geotechnique*. 4, 6-15.

Gilbert, R. B., Fernandez, F. F., and Horsfield, D. 1996. Shear Strength of a Reinforced Clay Liner. *Journal of Geot. and Geoenv. Engineering*, ASCE, 122(4), 259-266.

Gilbert, R. B., Scranton, H. B., and Daniel, D. E. 1997. Shear Strength Testing for Geosynthetic Clay Liners. *Testing and Acceptance Criteria for Geosynthetic Clay Liners*, L. Well, ed., American Society for Testing and Materials, Philadelphia, 121-138.

Heerten, G., Saathoff, F., Scheu, C., von Maubeuge, K. P. 1995. On the Long-Term Shear Behavior of Geosynthetic Clay Liners (GCLs) in Capping Sealing Systems. *Proceedings of the International Symposium "Geosynthetic Clay Liners".* Nuremberg, 141-150.

Helsel, D.R. and Hirsh, R.M. 1991. *Statistical Methods in Water Resources*. United States Geologic Survey.

Hewitt, R. D., Soydemir, C., Stulgis, R. P., and Coombs, M. T. 1997. Effect of Normal Stress During Hydration and Shear on the Shear Strength of GCL/Textured Geomembrane Interfaces. *Testing and Acceptance Criteria for Geosynthetic Clay Liners*, L. Well, ed., American Society for Testing and Materials, Philadelphia, 55-71.

Koerner, G.R. and Narejo, D. Direct Shear Database of Geosynthetic-to-Geosynthetic and Geosynthetic-to-Soil Interfaces. GRI Report #30. Folsom, PA. 106 pp.

Kovacevic Zelic, B., Znidarcic, D., and Kovacic, D. 2002. Shear Strength Testing on Claymax 200R. *7th International Conference on Geosynthetics*. Nice, France.

Lake, C. G., and Rowe, R. K. 2000. Swelling Characteristics of Needle-Punched, Thermal Treated Geosynthetic Clay Liners. *Geotextiles and Geomembranes*, 18, 77-101.

Marr, W. A. 2001. Interface and Internal Shear Testing Procedures to Obtain Peak and Residual Values." *15th GRI Conference: Hot Topics in Geosynthetics (Peak/Residual; RECMs; Installation; Concerns)*. Houston, TX, pp. 1-27.

McCartney, J.S. and Zornberg, J.G. 2005. Effect of Geomembrane Texturing on Geosynthetic Clay Liner - Geomembrane Interface Shear Strength. *ASCE GeoFrontiers 2005*. Austin, TX January 27-29, 2005.

McCartney, J.S., Zornberg, J.G., Swan, Jr., R.H., and Gilbert, R.B. 2004. Reliability-Based Stability Analysis Considering GCL Shear Strength Variability. *Geosyn. Int.*. 11(3), 212-232.

McCartney, J.S. and Zornberg, J.G. 2004. Effect of Specimen Conditioning on GCL Shear Strength." *GeoAsia 2004: 3rd Asian Regional Conference on Geosynthetics*. Eds. Shim, J.G., Yoo, C., and Jeon, H-Y. Seoul, Korea. pp. 631-643

McCartney, J.S., Zornberg, J.G., and Swan, R. 2002. *Internal and Interface Shear Strength of Geosynthetic Clay Liners (GCLs)*. Geotechnical Research Report, Department of Civil, Environmental and Architectural Engineering, University of Colorado at Boulder, 471 p.

McCartney, J.S., Zornberg, J.G., and Swan, R.H. 2009. Analysis of a Large Database of GCL-Geomembrane Interface Shear Strength Results. *Journal of Geotechnical and Geotechnical Engineering, ASCE*, 134(2), 209-223.

Olsta, J. and L. Crosson 1999. Geosynthetic clay liner peel index test correlation to direct shear. *Proceedings Sardinia 99, Seventh International Waste Management and Landfill Symposium.* S. Margherita di Pula, Cagliari, Italy. 4-8 October 1999.

Pavlik, K. L. 1997. U.S. Army Corps of Engineers GCL Interface Testing Program. Geosynthetics '97, St. Paul, MN, 877-884.

Petrov, R. J., Rowe, R. K., and Quigley, R. M. 1997. Selected Factors Influencing GCL Hydraulic Conductivity. *Journal of Geot. and Geoenv. Eng. ASCE*, 123(8), 683-695.

Richardson, G. N. 1997. GCL Internal Shear Strength Requirements. *Geosyn. Fabric Report*, March, 20-25.

Stark, T. D., and Eid, H. T. 1996. Shear Behavior of a Reinforced Geosynthetic Clay Liner. *Geosyn. Int.* IFA. 3(6), 771-785.

Stark, T. D. 1997. Effect of Swell Pressure on GCL Cover Stability. *Testing and Acceptance Criteria for Geosynthetic Clay Liners*, ASTM STP 1308, L. W. Well, Ed., ASTM, 30-44.

Stark, T. D., Arellano, D., Evans, W. D., Wilson, V. L., and Gonda, J. M. 1998. Unreinforced Geosynthetic Clay Liner Case History. *Geosynthetics International*, IFAI, 5(5), 521-544.

Swan Jr., R. H., Yuan, Z., and Bachus, R. C. 1996. Factors Influencing Laboratory Measurement of the Internal and Interface Shear Strength of GCLs. *ASTM Symposium on Testing and Acceptance Criteria for Geosynthetic Clay Liners*, Atlanta, GA.

Swan Jr., R. H., Yuan, Z., and Bachus, R. C. 1999. Key Factors Influencing Laboratory Measurement of the Internal and Interface Shear Strength of GCLs. *ASTM on Grips, Clamps, Clamping Techniques and Strain Measurement for Testing Geosynthetics*, Memphis, TN.

Triplett, E. J., and Fox, P. J. 2001. Shear Strength of HDPE Geomembrane/Geosynthetic Clay Liner Interfaces. *Journal of Geot. and Geoenv. Engineering*, ASCE, 127(6), 543-552.

von Maubeuge, K. P., and Ehrenberg, H. 2000. Comparison of Peel Bond and Shear Tensile Test Methods for Needle-Punched Geosynthetic Clay Liners. *Geot. and Geomem.*, 18, 203-214.

von Maubeuge, K. P. and Lucas, S. N. 2002. Peel and shear test comparison and geosynthetic clay liner shear strength correlation. *Clay Geosynthetic Barriers*. H. Zanzinger, R. M. Koerner, and E. Gartung, eds. Swets & Zeitlinger. Lisse, the Netherlands. 105-110.

Zornberg, J.G., McCartney, J.S., and Swan, R.H. 2005. Analysis of a Large Database of GCL Internal Shear Strength Results. *Journal of Geotechnical and Geotechnical Engineering, ASCE*, 131(3), 367-380.

Zornberg, J.G., McCartney, J.S., and Swan, R.H. 2006. Analysis of a Large Database of GCL Internal Shear Strength Results. Closure, *Journal of Geotechnical and Geotechnical Engineering*, ASCE, 132(10), 1376-1379.